PLANAR ARRAY STRUCTURES FOR TWO-DIMENSIONAL DIRECTION-OF-ARRIVAL ESTIMATION

A THESIS SUBMITTED TO
THE GRADUATE SCHOOL OF NATURAL AND APPLIED SCIENCES
OF
MIDDLE EAST TECHNICAL UNIVERSITY

BY

TANSU FİLİK

IN PARTIAL FULFILLMENT OF THE REQUIREMENTS
FOR
THE DEGREE OF PHILOSOPHY OF DOCTORATE
IN
ELECTRICAL AND ELECTRONICS ENGINEERING

APRIL 2010

Approval of the thesis:

PLANAR ARRAY STRUCTURES FOR TWO-DIMENSIONAL DIRECTION-OF-ARRIVAL ESTIMATION

submitted by **TANSU FİLİK** in partial fulfillment of the requirements for the degree of **Philosophy of Doctorate in Electrical and Electronics Engineering Department, Middle East Technical University** by,

Prof. Dr. Canan Özgen _____
Dean, Graduate School of **Natural and Applied Sciences**

Prof. Dr. İsmet Erkmen _____
Head of Department, **Electrical and Electronics Engineering**

Prof. Dr. T. Engin Tuncer _____
Supervisor, **Electrical and Electronics Engineering Department**

Examining Committee Members:

Prof. Dr. Kemal Leblebicioğlu
Electrical and Electronics Engineering, METU _____

Prof. Dr. T. Engin Tuncer
Electrical and Electronics Engineering, METU _____

Assist. Prof. Dr. Yakup Özkazanç
Electrical and Electronics Engineering, Hacettepe University _____

Assist. Prof. Dr. Cağatay Candan
Electrical and Electronics Engineering, METU _____

Dr. Arzu Tuncay Koç
Electrical and Electronics Engineering, METU _____

Date: _____

I hereby declare that all information in this document has been obtained and presented in accordance with academic rules and ethical conduct. I also declare that, as required by these rules and conduct, I have fully cited and referenced all material and results that are not original to this work.

Name, Last Name: TANSU FİLİK

Signature :

ABSTRACT

PLANAR ARRAY STRUCTURES FOR TWO-DIMENSIONAL
DIRECTION-OF-ARRIVAL ESTIMATION

Filik, Tansu
Ph.D., Department of Electrical and Electronics Engineering
Supervisor : Prof. Dr. T. Engin Tuncer

April 2010, 111 pages

In this thesis, two-dimensional (2-D) direction-of-arrival (DOA) estimation problem is considered. Usually, DOA estimation is considered in one dimension assuming a fixed elevation angle. While this assumption simplifies the problem, both the azimuth and elevation angles, namely, the 2-D DOA estimates are required in practical scenarios. In this thesis, planar array structures are considered for 2-D DOA estimation. In this context, V-shaped arrays are discussed and some of the important features of these arrays are outlined. A new method for the design of V-shaped arrays is presented for both isotropic and directional beam patterns. The design procedure is simple and can be applied for both uniform and nonuniform V-shaped sensor arrays. Closed form expressions are presented for the V-angle in order to obtain isotropic angle performance. While circular arrays have the isotropic characteristics, V-shaped arrays present certain advantages due to their large aperture for the same number of sensors and inter-sensor distance. The comparison of circular and V-shaped arrays is done by considering the azimuth and elevation Cramer-Rao Bounds (CRB). It is shown that V-shaped and circular arrays have similar characteristics for the sensor position errors while the uniform isotropic (UI) V-array performs better when there is mutual coupling and the sources are correlated.

In the literature, there are several techniques for 2-D DOA estimation. Usually, fast algorithms are desired for this purpose since a search in two dimensions is a costly process. These algorithms have a major problem, namely, the pairing of the azimuth-elevation couples for multiple sources. In this thesis, a new fast and effective technique for this purpose is proposed. In this technique, a virtual array output is generated such that when the ESPRIT algorithm is used, the eigenvalues of the rotational transformation matrix have the 2-D angle information in both magnitude and phase. This idea is applied in different scenarios and three methods are presented for these cases. In one case, given an arbitrary array structure, array interpolation is used to generate the appropriate virtual arrays. When the antenna mutual coupling is taken into account, a special type of array structure, such as circular, should be used in order to apply the array interpolation. In general, the array mutual coupling matrix (MCM) should have a symmetric Toeplitz form. It is shown that the 2-D DOA performance of the proposed method approaches to the CRB by using minimum number of antennas in case of mutual coupling. This method does not require the estimation of the mutual coupling coefficients. While this technique is effective, it has problems especially when the number of sources increases. In order to improve the performance, MCM is estimated in the third approach. This new approach performs better, but it cannot be used satisfactorily in case of multipath signals. In this thesis, the proposed idea for fast 2-D DOA estimation is further developed in order to solve the problem when mutual coupling and multipath signals jointly exist. In this case, real arrays with some auxiliary sensors are used to generate a structured mutual coupling matrix. It is shown that the problem can be effectively solved when the array structure has a special form. Specifically, parallel uniform linear arrays (PULA) are employed for this purpose. When auxiliary sensors are used, a symmetric banded Toeplitz MCM is obtained for the PULA. This allows the application of spatial smoothing and ESPRIT algorithm for 2-D DOA estimation. The proposed algorithm uses triplets and presents closed form paired 2-D DOA estimates in case of unknown mutual coupling and multipath signals. Several simulations are done and it is shown that the proposed array structure and the method effectively solve the problem.

Keywords: direction-of-arrival estimation, V-shaped arrays, 2-D array interpolation, mutual coupling, multipath, angle pairing

ÖZ

İKİ BOYUTLU VARIŞ AÇISI KESTİRİMİ İÇİN DÜZLEMSEL DİZİ YAPILARI

Filik, Tansu
Doktora, Elektrik ve Elektronik Mühendisligi Bölümü
Tez Yöneticisi : Prof. Dr. T. Engin Tuncer

Nisan 2010, 111 sayfa

Bu tezde, varış-açısı (DOA) kestirimi problemi ele alınmıştır. Genellikle DOA kestirimi kaynakların yükseklik açılarını sabit kabul ederek, bir boyutlu çözülür. Bu varsayım problemi basitleştirmesine rağmen, pratik senaryolarda hem yanca hem de yükseklik, yani iki-boyutlu (2-B), açı bilgisi gerekmektedir. Bu tezde, 2-B DOA kestirimi için düzlemsel dizi yapıları ele alınmıştır. Bu bağlamda, V-şekilli dizilere değinilmiş ve detaylı bir tartışma yapılmıştır. Literatürde V-şekilli anten dizileri için sınırlı çalışma olmasına rağmen, bu diziler birçok avantaj sunmaktadır. Bu tezde, hem yön bağımsız hem de yönlü ışıma örüntüsü için V-şekilli dizi tasarımı sunulmuştur. Bu tasarım, V-yapı üzerine düzenli ve düzensiz yerleştirilmiş sensörlere uygulanabilmektedir. Yön bağımsız açı performansı sağlayan V-açısını veren kapalı formadaki ifadeler bulunmuştur. Çembersel diziler yön bağımsız açı performansına sahip olmasına rağmen, V-şekilli diziler aynı sayıda sensör ve sensörler arası uzaklık için daha büyük bir açıklığa sahiptir. Bu durum bazı avantajlar sağlamaktadır. Çembersel ve V-şekilli dizilerin karşılaştırması yanca ve yükseklik açıları için olan Cramer-Rao sınır (CRB) değerlerine göre yapılmıştır. V-şekilli ve çembersel dizileri pozisyon hataları için benzer bir karakteristiğe sahip olduğu ve düzenli yön bağımsız V-dizilerin antenler arası karşılıklı bağlaşım ve kaynakların ilintili olduğu durumlarda daha iyi olduğu gösterilmiştir. Literatürde, 2-B DOA kestirimi için birçok teknik mevcuttur. Genellikle, 2-B taramanın maliyetinden dolayı hızlı

algoritmalar tercih edilmektedir. Hızlı 2-B DOA kestirimde en temel sorun çok kaynak durumunda yanca ve yükseklik açılarının eşleştirilmesi problemidir. Bu tezde, bu amaçla yeni ve etkin bir teknik sunulmuştur. Bu teknikte, sanal bir dizi çıktısı üretilmiştir. Öyle ki ESPRIT algoritması uygulandığında, rotasyonel dönüşüm matrisinin özdeğerleri 2-B açı bilgisini genlik ve fazda taşırlar. Bu fikir değişik platformlara uygulanmıştır. Bu platformlardan birisi rastgele düzlemsel dizilerdir ve dizilim ara değerleme kullanılarak 2-B DOA kestirimi için uygun sanal dizilimler üretilebilmektedir. Antenler arası bağlaşım hesaba katıldığında, dizilim ara değerlemeyi uygulayabilmek için çembersel dizilim gibi özel bir dizi yapısı kullanılmalıdır. Dizi bağlaşım matrisi (DBM) simetrik Toeplitz formda olmalıdır. Önerilen yöntem antenler arası bağlaşım varken uygulandığında 2-B DOA performansı CRB seviyesinde olmaktadır ve en az sayıda anten kullanılarak yapılmaktadır. Metot bağlaşım katsayılarının bulunmasına gerek duymamaktadır. Bu teknik çok etkin olmasına rağmen, özellikte kaynak sayısı arttığında sorunları vardır. Çok kaynak durumundaki performans bozulmasını düzeltmek için, bağlaşım katsayıları bulunarak dizilim ara değerlemede kullanılabilir. Bu yeni yaklaşım daha iyi performans sağlamasına ve önemli avantajlara sahip olmasına rağmen, çok yollu yansımış sinyallerin olduğu ortamlarda başarılı değildir. Bu tezde, hızlı 2-B DOA kestirimi için önerilen fikir antenler arası bağlaşım ve çok yollu yansımış sinyallerin aynı anda olduğu durumlar için uygulanmıştır. Bu amaçla, yapısal DBM oluşturmak için kullanılan yardımcı sensörlerin bulunduğu diziler kullanılmıştır. Bu problemin çözümünde kullanılan düzenli dikdörtgen (URA) gibi büyük diziler yerine, daha etkin dizi kullanımı hedeflenmiştir. Bunu için paralel düzenli doğrusal (PULA) yapı kullanılmıştır. Yardımcı ilave sensörler kullanıldığında, PULA simetrik ve Toeplitz bağlaşım matrisine sahip olmaktadır. Böylece uzaysal düzleme ve ESPRIT algoritmasını kullanarak bilinmeyen bağlaşım ve çok yollu sinyallerin olduğu durumda kapalı formda ve eşlenmiş 2-B DOA kestirimi mümkün olur. Bu dizilim yapısı DOA performansını daha da iyileştirmeye olanak tanımaktadır. Değişik simülasyonlar yapılarak önerilen yöntemin ve dizilim yapısının problemi etkin bir şekilde çözdüğü gösterilmiştir.

Anahtar Kelimeler: varış açısı kestirimi, V-şekilli diziler, 2-B dizi aradeğerleme, antenler arası bağlaşım, çok yollu yansıma, açı eşleme

To my wife Ümmühan
and to
my parents

ACKNOWLEDGMENTS

I am heartily thankful to my supervisor, Prof. Dr. T. Engin Tuncer, whose encouragement, guidance and support from the initial to the final level enabled me to present this thesis. He is the best teacher I have ever met. He showed me different ways to approach a research problem and the need to be persistent to accomplish any goal.

I would like to thank Associate Prof. Çağatay Candan and Associate Prof. Yakup Özkazanç for their valuable suggestions during the whole period and for their time during the Progress Committee meetings. I also want thank Dr. Arzu Tuncay Koç and Prof. Kemal Leblebicioğlu for their comments and suggestions in order to improve the quality of the thesis.

I would like to thank to Dr. Serkan Karakütük, Metin Aktaş and M. Onur Özeç of METU Sensor Array and Multi-channel Signal Processing (SAM) Group and Yılmaz Kalkan, M. Fatih Bayramoğlu and Erhan Örümlü for their support and friendship during my thesis work.

Finally, I want to thank to my family and my lovely wife Ümmühan Başaran Filik for their support and love that keep me eager and hopeful to accomplish this.

TABLE OF CONTENTS

ABSTRACT iv

ÖZ vi

DEDICATON viii

ACKNOWLEDGMENTS ix

TABLE OF CONTENTS x

LIST OF TABLES xiii

LIST OF FIGURES xiv

CHAPTERS

1 INTRODUCTION 1

1.1 Motivation and Objectives 1

1.2 Literature Overview 2

1.3 Contributions 3

1.4 Organization of the Thesis 4

2 DIRECTION-OF-ARRIVAL (DOA) ESTIMATION 6

2.1 Introduction 6

2.2 Array Data Model 8

2.3 Modeling Errors 11

2.3.1 Mutual Coupling 11

2.3.2 Gain/Phase Mismatch 12

2.3.3 Position Errors 12

2.3.4 Multipath Sources 12

2.4 Array Interpolation 13

2.4.1 2-D Array Interpolation 14

2.4.2 Iterative Improvement 15
3 UNIFORM AND NONUNIFORM V-SHAPED PLANAR ARRAYS 17
3.1 Introduction 17
3.2 Problem Formulation 19
3.2.1 Data Model 19
3.2.2 CRB for 2-D DOA Estimation 20
3.2.2.1 Conditions for Uncoupled 2-D DOA Angle Estimation 22
3.3 Isotropic Planar Array 22
3.3.1 Isotropic Uniform V-shaped Array 22
3.3.2 Isotropic Nonuniform V-shaped Array 23
3.4 Directional V-shaped Planar Array Design 24
3.4.1 Design Procedure 25
3.5 Analysis of Mutual Coupling Effects 27
3.6 Simulation Results 31
3.6.1 Simulations for Uniform Isotropic V-shaped Arrays 31
3.6.2 Simulations for Nonuniform Isotropic V-shaped Arrays . . 35
3.6.3 Simulations for Directional Uniform V-shaped Arrays . . . 35
3.7 Conclusion 38
4 FAST AND AUTOMATICALLY PAIRED 2-D DOA ESTIMATION 40
4.1 Introduction 40
4.2 Problem Formulation 43
4.3 2-D Paired DOA Estimation with Array Interpolation 44
4.3.1 2-D Paired DOA Estimation For No-Coupling 44
4.3.1.1 Automatically Pairing the Azimuth and Elevation Angles 44
4.3.1.2 2-D Paired Interpolated ESPRIT (PIE) Algorithm 46
4.3.1.3 Uniform Circular Array (UCA) 48
4.3.1.4 Two Parallel Uniform Linear Array (PULA) . 49
4.4 2-D Paired DOA Estimation with Unknown Mutual Coupling 51

4.4.1 2-D DOA Estimation Without Estimating the Coupling Coefficients . . . 52
4.4.2 2-D DOA Estimation by Estimating the Coupling Coefficients . . . 54
4.5 Simulation Results . . . 56
4.5.1 No mutual coupling . . . 57
4.5.1.1 UCA . . . 57
4.5.1.2 PULA . . . 62
4.5.2 Mutual coupling . . . 66
4.6 Discussions . . . 71
4.7 Conclusion . . . 72
5 2-D DOA ESTIMATION IN CASE OF UNKNOWN MUTUAL COUPLING FOR MULTIPATH SIGNALS . . . 74
5.1 Introduction . . . 74
5.2 Problem Formulation . . . 75
5.3 Closed form 2-D Paired DOA Estimation . . . 77
5.3.1 Spatial Smoothing of the Combined Measurements . . . 81
5.3.2 Algorithm for PULA-1 . . . 82
5.3.3 Selecting Different Subarrays within PULA and the PULA-2 Algorithm . . . 83
5.4 Simulations . . . 88
5.5 Conclusion . . . 93
6 CONCLUSION . . . 94
6.1 Future Works . . . 97
REFERENCES . . . 98
APPENDICES
A Isotropic V-angle for Uniform V-shaped Arrays . . . 103
B Isotropic V-angle for Nonuniform V-shaped Arrays . . . 105
C The MCM Structure of PULA . . . 107
CURRICULUM VITAE . . . 109

LIST OF TABLES

TABLES

Table 3.1 Distance between sensors for 9 elements UCA in terms of λ. 29

Table 3.2 Distance between sensors for 9 elements UI V-shaped array in terms of λ. . 29

Table 3.3 Mutual coupling matrix for 9 elements UCA. 29

Table 3.4 Mutual coupling matrix for 9 elements UI V-shaped array. 30

Table 3.5 Mutual Coupling Coefficients of UCA and UI V-shaped array. 30

Table 3.6 Isotropic nonuniform V-shaped design examples for $M_1 = M_2$ and $M_1 \neq M_2$. 35

LIST OF FIGURES

FIGURES

Figure 2.1 Spherical coordinate system for a point source in three-dimensional space. 7

Figure 2.2 Illustration of a practical mobile communication scenario. 7

Figure 2.3 Coordinate system and planar array structure for 2-D angle estimation. . . 9

Figure 2.4 Illustration of sensor position errors for arbitrary planar arrays. 13

Figure 2.5 The 2-D angular sector for array interpolation. 14

Figure 2.6 The 2-D narrow angular sectors in the neighborhood of the DOA estimates. 15

Figure 3.1 Coordinate system for 2-D angle estimation and V-shaped array. 20

Figure 3.2 Uniform V-shaped array geometry. 23

Figure 3.3 Nonuniform V-shaped array geometry. 25

Figure 3.4 DOA performance of 9 elements V-shaped arrays with different γ angles for a single source which is swept between all azimuth angles with 256 snapshots and 20 dB SNR. 26

Figure 3.5 The design regions and parameters for V-shaped planar array geometry. . . 26

Figure 3.6 The best and worst performance levels of the azimuth CRB versus V-angle, γ, when α_1 and α_2 are 90 degrees. 28

Figure 3.7 Azimuth DOA performance for three sources at 60, 100 and 120 degrees, respectively, when UI V-shaped array and UCA are used without and with sensor position errors (2%, 1%, 0.2%). 32

Figure 3.8 Azimuth CRB DOA performance of 9 elements UI V-array and UCA for two sources when the sources are correlated with the correlation coefficient ρ. Sources are at 80 and 85 degrees and elevations are fixed at 90 degrees. SNR = 15 dB. 33

Figure 3.9 CRB DOA performance with and without unknown mutual coupling of UI V-shaped array and UCA for two sources when one source is swept between 0 and 360 degrees while the other two sources are at 161 and 180 degrees. Elevation angles are fixed to 90 degrees. 34

Figure 3.10 CRB DOA performance with and without unknown mutual coupling for three sources at 60, 100 and 120 degrees, respectively, when UI V-array and UCA are used. Elevation angles are fixed to 90 degrees. 34

Figure 3.11 CRB DOA performance of nonuniform isotropic (NUI) V-array and UCA for a single source is swept between 0 and 360 degrees when $M = 7$, $M = 10$ and elevation angles are fixed to $\theta = 90^\circ$ and SNR = 20 dB. 36

Figure 3.12 CRB DOA performance for two sources at $\phi_1 = 81^\circ$, $\phi_2 = 98^\circ$, respectively, when DU V-array and UCA are used (elevation angles are fixed to $\theta = 90^\circ$). 37

Figure 3.13 The elevation CRB for DU V-array and UCA with different azimuth angles (for ϕ_1). 37

Figure 3.14 CRB DOA performance of DU V-array and UCA for three sources when one source is swept between 0 and 360 degrees while the other sources are at 83 and 99 degrees. Elevation angles are fixed to 90 degrees. 38

Figure 4.1 Positioning of the virtual arrays for 2-D paired DOA estimation. Virtual array-1 is obtained from the real array with a shift by (d_x, d_y). Virtual array-2 is obtained with a shift by $(-d_x, d_y)$. 45

Figure 4.2 Virtual arrays positioned accordingly for UCA when $d_x = d_y = \lambda/5$. 48

Figure 4.3 Positioning of the real PULA. ULA-2 is obtained from the ULA-1 with a shift by (d_x, d_y). ULA-3 is obtained with a shift by $(-d_x, d_y)$. 49

Figure 4.4 Positioning of the virtual PULA. Virtual ULA-2 and ULA-3 are obtained from the base array with array interpolation. ULA-1 is available in the base array. 50

Figure 4.5 2-D paired DOA performance for a single source. SNR is 15 dB. There is no mutual coupling between antennas. (a) Azimuth performance (b) Elevation performance. 58

Figure 4.6 2-D paired DOA performance for two sources for PIE algorithm. SNR is 15 dB. There is no mutual coupling between antennas. (a) Azimuth performance (b) Elevation performance. 60

Figure 4.7 2-D paired DOA performance for closely spaced sources for the PIE algorithm. SNR is 15 dB. (a) Azimuth performance (b) Elevation performance. 61

Figure 4.8 The progress in DOA estimation during iterations for the resolution of out-of-sector sources. SNR is 15 dB and there are four iterations. (a) Single source, (b) Two sources. 63

Figure 4.9 2-D paired DOA performance for PIE when there is no-coupling between antennas and there are two sources. (a) Azimuth performance (b) Elevation performance. 64

Figure 4.10 2-D paired azimuth and elevation DOA performance for different SNR levels when there are two sources. 65

Figure 4.11 2-D paired azimuth and elevation DOA estimates when there are two sources and SNR=15dB. 65

Figure 4.12 2-D DOA distribution when there are two closely located sources and SNR=15dB. (a) Real PULA (b) Virtual PULA. 66

Figure 4.13 2-D DOA distribution when there are four sources and SNR=15dB. 67

Figure 4.14 2-D paired DOA performance for BPIE for a single source. SNR is 15 dB. There is unknown mutual coupling between antennas. (a) Azimuth performance (b) Elevation performance. 68

Figure 4.15 2-D paired DOA performance for two sources for BPIE and PIECE algorithms. SNR is 15 dB. There is unknown mutual coupling between antennas. (a) Azimuth performance (b) Elevation performance. 69

Figure 4.16 2-D paired DOA performance for BPIE and PIECE algorithms when there is unknown mutual coupling between antennas and there are two sources. (a) Azimuth performance (b) Elevation performance. 70

Figure 4.17 Mutual coupling coefficient estimation performance. 72

Figure 5.1 ULA structures in a triplet. 76

Figure 5.2 Two subarrays within PULA for x-axis shift. 84

Figure 5.3 Two subarrays within PULA for y-axis shift. 84

Figure 5.4 2-D paired azimuth DOA performance for different SNR levels when there are three sources. 89

Figure 5.5 2-D paired elevation DOA performance for different SNR levels when there are three sources. 89

Figure 5.6 2-D paired azimuth and elevation DOA estimates for different number of snapshots when there are three sources and SNR=15dB. 90

Figure 5.7 2-D DOA distribution of PULA-1 when there are three coherent sources and SNR=15dB. 91

Figure 5.8 2-D DOA distribution of PULA-2 when there are three coherent sources and SNR=15dB. 91

Figure 5.9 2-D paired azimuth DOA performance for two coherent sources for PULA-1 and PULA-2. SNR is 15 dB. There is unknown mutual coupling between antennas. 92

Figure 5.10 2-D paired elevation DOA performance for two coherent sources for PULA-1 and PULA-2. SNR is 15 dB. There is unknown mutual coupling between antennas. 92

CHAPTER 1

INTRODUCTION

1.1 Motivation and Objectives

Radio Direction finding (DF) is nearly as old as radio itself. In 1903, the first DF system (radio goniometry) was developed by Bellini and Tosi [1]. Thereafter the importance of the radio and DF technologies increased steadily especially with the World War I and II [2], [3]. Most of the developed techniques at that time assume presence of a single radiation source. The direction-of-arrival (DOA) angle accuracy of the DF techniques is restricted with the deficiency of the analog systems. Fortunately, at the end of 1970s the digital systems (the fast A/D converters, processors) and digital signal processing techniques come to the scene. The requirement for obtaining high-accuracy DOA information of the multiple sources forced the researchers to new techniques such as subspace based methods [4]. The subspace idea has opened the ways of many parametric estimators. This new approach for DOA estimation is usually studied as a part of array signal processing. The main driving force behind the research in array signal processing in the 1980s, was the military applications such as radar, sonar and target tracking [5], [6], [7]. In the middle of the 1990s the field of personal wireless communications has emerged and the applications of array signal processing to communication systems have become a new driving force. Some other important applications of this area are in navigations, rescue, radio astronomy, seismology and ionosphere research [8]-[11]. Nowadays this area is still evolving and is a quite active field of research. The motivation for this thesis comes from the need for practical array structures and fast DOA estimation techniques for two dimensional (2-D), namely, azimuth and elevation angle estimation under some practical distortions such as mutual coupling, multipath, and sensor position errors.

The main objective of the thesis is to examine novel planar array structures and direction finding techniques in order to improve the 2-D DOA estimation performance. The planar array structure is the fundamental factor which determines the 2-D DOA performance. So the first main objective is to propose a simple and efficient planar array structure which has some favorable properties compared to some well known array geometries. The designed array structures should be compared with the known array structures by considering the position errors for the array elements and the mutual coupling between elements.

In practical applications, both azimuth and elevation angles of source signals are desired. When there are multiple sources, a pairing problem is observed where azimuth-elevation angles for each source should be paired. The other objective is to find a fast and effective technique to solve the pairing problem. In practice, mutual coupling between antennas and multipath signals cause major problems for 2-D DOA estimation. In this thesis, these problems are also considered for the development of an algorithm for fast 2-D DOA estimation.

1.2 Literature Overview

The majority of the works about the DOA angle estimation of propagating waves are focused on one dimensional (1-D), azimuth-only angle estimation. The most effective array structures and algorithms are proposed for the 1-D DOA angle estimation. In this context, uniform and nonuniform linear arrays (ULA and NLA) are widely studied for 1-D DOA estimation [12],[13] and the optimization of these array structures for the best DOA performance is also studied in [14]. Some of the effective algorithms such as Root-MUSIC [15], spatial smoothing [16], etc. are also proposed for linear arrays.

In practical scenarios both the azimuth and elevation (2-D) angles are required to be estimated. For the 2-D DOA estimation, sensor array geometry has to be planar or volumetric. In order to design best array structure, some desired performance criteria and constraints are defined in the literature such as in [17], [18]. In [17] the objective is to design isotropic array geometries which provide the same DOA performance for all azimuth angles. In [18], directional arrays are designed for the best DOA performance for an angular sector. In another study, [19], some of the basic array geometries such as circular, Y, X, L and (cross) shaped arrays are compared. L-shaped array is the extended version of the ULA to the planar array structure and has some

favorable advantages which are addressed in the literature [20], [21]. On the other hand, there are limited discussions on the V-shaped arrays in the literature [22], although it has better performance than other array structures. In addition, while designing array structures and techniques for 2-D DOA estimation, the mutual coupling effect between array elements are also considered in some studies such as [23], [24], [25].

There are several algorithms for 2-D DOA estimation and the simplest method is to search the sources in both azimuth and elevation simultaneously as in [26]. But this is a slow and computationally costly way in practical applications. Hence, fast algorithms are usually desired. It is found out that when the fast algorithms for 1-D angle estimation are applied for 2-D case, the angle pairing problem is observed. In the literature, several techniques are proposed to overcome this problem [27]-[33]. However, these methods can fail when solving multiple 2-D angles especially at low signal-to-noise ratio (SNR). Closed form automatically paired 2-D DOA estimation methods are proposed for different array structures [34]- [37]. But these methods use some special array structures and mutual coupling between array elements and multipath are not considered.

1.3 Contributions

The contributions of the thesis can be summarized in two parts as follows:

- A design methodology for uniform and nonuniform V-shaped arrays is presented in Chapter 3. Closed form expressions for isotropic response are also given.
  - Closed form expressions for the isotropic uniform and non-uniform V-shaped planar arrays are presented. These expressions are unique in the literature and allows one to design the isotropic V-shaped array easily [44], [46].
  - The performance of V-shaped arrays, including uniform isotropic and nonuniform arrays, is analyzed for different cases. These involve correlated signals, mutual coupling, and sensor position errors. It is shown that V-shaped arrays perform better than the UCA for different types of error sources which is not well known in the literature [46].
  - A design procedure is presented for uniform directional V-arrays which allows one to trade off the isotropic characteristics for the better DOA performance for a

given angular sector [45], [46].

- Closed form paired 2-D DOA estimation techniques are proposed for different array structures which can perform well in case of mutual coupling and multipath signals. In Chapter 4, the interpolated planar array structures are used:
  - A novel technique for fast and paired azimuth and elevation (2-D) DOA estimation is proposed for arbitrary arrays which is called paired interpolated ESPRIT (PIE). Efficient use of antenna elements is achieved by integrating the proposed method with the array interpolation [57], [61].
  - Two blind methods (BPIE and PIECE) are proposed for fast and paired 2-D DOA estimation in case of unknown mutual coupling between antenna array elements. These two methods can be applied for the array geometries which have mutual coupling matrices with a symmetric Toeplitz structure [61].
  - The proposed idea on the closed form, fast and paired 2-D DOA estimation is employed in a special array structure, parallel uniform linear array (PULA), when unknown mutual coupling and multipath signals jointly exist. Auxiliary sensors are used so that the entire mutual coupling matrix (MCM) for the selected array outputs has a banded Toeplitz structure. The required formulation and detailed analytical analysis of the method is given in Chapter 5. To our knowledge, there is no previous work where the closed form paired 2-D DOA estimates are given when there is unknown mutual coupling and in case of multipath signals [62].

1.4 Organization of the Thesis

In this section the organization and an overview of the contents of the subsequent chapters of the thesis are given.

In Chapter 2, some of the basics of the array signal processing for 2-D DOA estimation are reviewed. The fundamental assumptions, model and mathematical tools used throughout the thesis are given. Some of the main problems of the practical DOA estimation systems due to mutual coupling, multipath and sensor position errors are discussed.

In Chapter 3, isotropic and directional uniform and nonuniform V-shaped planar array structures are considered for 2-D DOA estimation. First, the uniform and nonuniform isotropic

V-shaped arrays are investigated and closed form expressions are presented. Then a new design method for the directional V-shaped arrays is proposed. Finally the performance of the V-arrays are simulated and analyzed for correlated signals, mutual coupling, and sensor position errors.

In Chapter 4, a fast and automatically paired 2-D DOA estimation algorithm is proposed for arbitrary planar arrays, which is integrated with 2-D array interpolation for efficient use of the antenna elements. Then two blind approaches are proposed for fast and paired 2-D DOA estimation in case of unknown mutual coupling. The performances of the proposed methods are compared with the CRB.

In Chapter 5, the proposed algorithm (given in Chapter 4) is applied to a special array geometry, namely, two parallel uniform linear arrays (PULA) for closed form 2-D DOA estimation in the presence of unknown mutual coupling and multipath signals. The mutual coupling structure of the PULA is formulated.

In Chapter 6, the conclusion of the thesis is given.

In some chapters (3, 4 and 5), the employed data models and other assumptions are restated at the beginning of the chapters to make the chapters more self contained.

CHAPTER 2

DIRECTION-OF-ARRIVAL (DOA) ESTIMATION

In this chapter, the basic background of array signal processing for DOA estimation is reviewed. First the narrowband array data model is discussed. Then the sources of error for the array data model due to the mutual coupling, gain/phase mismatch, sensor position error and multipath sources are investigated. Finally the 2-D array interpolation (mapping) which is used in the following chapters is considered. The iterated version of the array interpolation, which improves the DOA performance, is given.

2.1 Introduction

Array signal processing deals with the space-time signals which are collected by an array of sensors. These multichannel signals can be processed to enhance the signal-to-interference-plus-noise ratio (SINR) or to determine the number of emitting sources, the locations of these sources, etc., [7] - [11]. In this thesis we focus on 2-D DOA estimation of multiple sources. In order to determine the direction of an emitting source in space we need two parameters, the elevation angle (θ) of that source from a fixed plane and the azimuth angle (ϕ) of its orthogonal projection on that plane as in Figure 2.1. In addition to these two parameters, another parameter is the radial distance from a fixed origin (r) which specifies the exact location of the source.

The 2-D DOA estimation problem has received much attention over the last several decades from the practical point of view. For instance, a practical mobile communications system is shown in Figure 2.2. In this scenario, base station should estimate the 2-D DOA angles of multiple sources for better communication quality and capacity. In order to estimate 2-

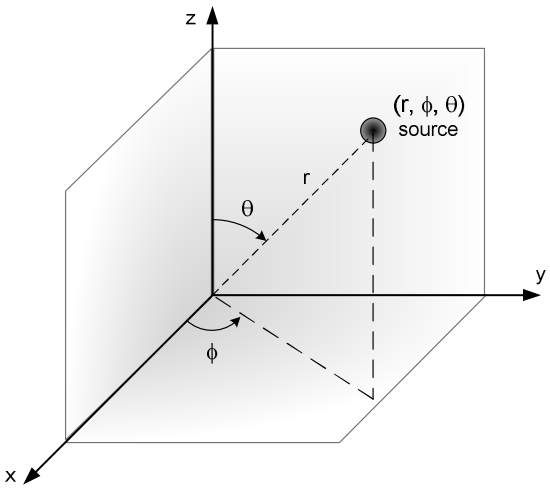

Figure 2.1: Spherical coordinate system for a point source in three-dimensional space.

D DOA angles accurately, we need to study two important problems; array geometry and DOA estimation method. The first problem is to design of the array geometry for the best 2-D DOA estimation performance which is one of the objectives of this thesis. The other important problem is the DOA estimation method which can be parametric or nonparametric. Parametric methods assume an array data model and promise better DOA performance for multiple sources. But when the fast (search-free) algorithms are used for 2-D DOA angle estimation, a parameter pairing problem is observed which is the topic of this thesis. However

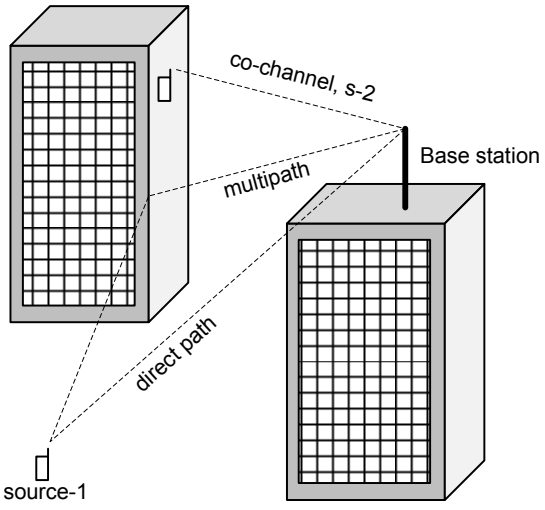

Figure 2.2: Illustration of a practical mobile communication scenario.

in practical applications, there are some distortions on the theoretical array model. These

distortions are due to mutual coupling, gain/phase mismatch between array elements, sensor position errors and multipath sources. The effects of these distortions on the array model should be taken into account for better DOA performance.

2.2 Array Data Model

In this part, the array mathematical model is derived for arbitrary array geometry and multiple two-dimensional source signals. In order to obtain a simplified mathematical model, first we have to make two reasonable assumptions:

- Far-field assumption: The signal wavefronts are planar when impinging on the array.
- Narrow-Band (NB) assumption: This means that signals have bandpass characteristics around a carrier frequency.

Let the complex narrow-band signal waveform be s(t) and given by

$$s(t) = \alpha(t)e^{jw_c t} \tag{2.1}$$

where ω_c is the carrier angular frequency. The narrowband assumption implies that the amplitude or the envelope α(t) varies much slower than s(t). Hence, for small time delays, τ,

$$s(t-\tau) = \alpha(t-\tau)e^{jw_c(t-\tau)} \approx \alpha(t)e^{jw_c t}e^{-jw_c\tau} = s(t)e^{-jw_c\tau}. \tag{2.2}$$

Consider an array of M sensors located at the positions $[x_i, y_i, z_i]$, $i = 1, \ldots, M$ as shown in Figure 2.3. The signal at the i^{th} sensor output is,

$$y_i(t) = P_i(\Theta)s(t-\tau_i) + n_i(t) \tag{2.3}$$

where $P()$ is the sensor pattern, Θ=[ϕ,θ] is the source DOA, τ_i is the propagation delay and $n_i(t)$ is an additive noise term at the i^{th} sensor. We can express all sensor outputs in vector form as

$$\mathbf{y}(t) = \begin{bmatrix} y_1(t) \\ y_2(t) \\ \vdots \\ y_M(t) \end{bmatrix}_{M\times 1} = \begin{bmatrix} P_1(\Theta)s(t-\tau_1) \\ P_2(\Theta)s(t-\tau_2) \\ \vdots \\ P_M(\Theta)s(t-\tau_M) \end{bmatrix}_{M\times 1} + \begin{bmatrix} n_1(t) \\ n_2(t) \\ \vdots \\ n_M(t) \end{bmatrix}_{M\times 1} \tag{2.4}$$

where

$$\tau_i = \frac{\mathbf{u}^T \mathbf{p}_i}{c} \tag{2.5}$$

and c is the velocity of propogation in the medium and $\mathbf{u}$ is a unit vector which can be expressed as

$$\mathbf{u} = \begin{bmatrix} -\sin(\theta)\cos(\phi) \\ -\sin(\theta)\sin(\phi) \\ -\cos(\theta) \end{bmatrix}. \tag{2.6}$$

$\mathbf{p}_i$ is the position vector of the i^{th} sensor. We assume that the source signal is narrowband,

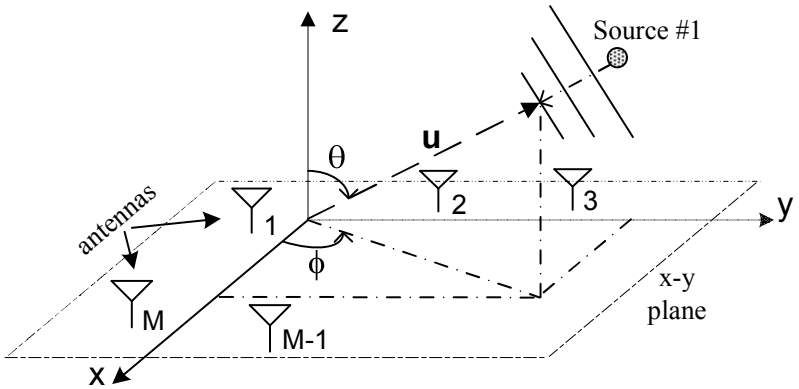

Figure 2.3: Coordinate system and planar array structure for 2-D angle estimation.

(2.2), and the sensors are identical omnidirectional (isotropic) which means $P_i(\Theta)$=1 for $i = 1, \ldots, M$. In this case, $\mathbf{y}(t)$ can be rewritten as,

$$\mathbf{y}(t) = \begin{bmatrix} s(t)e^{-jw_0\tau_1} \\ \vdots \\ s(t)e^{-jw_0\tau_M} \end{bmatrix}_{M\times 1} + \begin{bmatrix} n_1(t) \\ \vdots \\ n_M(t) \end{bmatrix}_{M\times 1}. \tag{2.7}$$

In case of multiple sources, we assume that there are D, ($D < M$), narrowband signals impinging on the array from the directions $\Theta_d = [\phi_d, \theta_d]$, $d = 1, \ldots, D$. For multiple sources, the equation (2.5) can be modified as,

$$\tau_{id} = \frac{\mathbf{u}_d^T \mathbf{p}_i}{c}, \tag{2.8}$$

so the sensor outputs for multiple sources can be rewritten as,

$$\mathbf{y}(t) = \begin{bmatrix} e^{-jw_0\tau_{11}} & e^{-jw_0\tau_{12}} & \dots & e^{-jw_0\tau_{1D}} \\ e^{-jw_0\tau_{21}} & e^{-jw_0\tau_{22}} & \dots & e^{-jw_0\tau_{2D}} \\ \vdots & & & \\ e^{-jw_0\tau_{M1}} & e^{-jw_0\tau_{M2}} & \dots & e^{-jw_0\tau_{MD}} \end{bmatrix} \begin{bmatrix} s_1(t) \\ s_2(t) \\ \vdots \\ s_D(t) \end{bmatrix} + \begin{bmatrix} n_1(t) \\ n_2(t) \\ \vdots \\ n_M(t) \end{bmatrix}. \tag{2.9}$$

In general the array output can be written as,

$$\mathbf{y}(t) = \mathbf{A}(\Theta)\mathbf{s}(t) + \mathbf{n}(t), \quad t = 1, \dots, N \tag{2.10}$$

where N is the number of the snapshots and $\mathbf{s}(t)$ is a $D \times 1$ signal vector which represents a wide sense stationary, zero-mean random process uncorrelated with noise. It is assumed that the noise, $\mathbf{n}(t)$, is both spatially and temporally white with variance σ_n^2. $\mathbf{A}(\Theta)$ is the $M \times D$ steering matrix. The idth component of the $\mathbf{A}(\Theta)$ matrix is

$$a_i(\phi_d, \theta_d) = e^{-j2\pi f_0 \tau_{id}} \tag{2.11}$$

and if we put (2.8) into (2.11) we get $a_i(\phi_d, \theta_d) = e^{-j2\pi \frac{f_0}{c} \mathbf{u}_d^T \mathbf{p}_i}$ where $\frac{f_0}{c}$ is the $\frac{1}{\lambda}$ and we define the wavenumber $\mathbf{k}$ of the d^{th} source as,

$$\mathbf{k}_d = \frac{2\pi}{\lambda}\mathbf{u}_d = \frac{2\pi}{\lambda} \begin{bmatrix} -\sin(\theta_d)\cos(\phi_d) \\ -\sin(\theta_d)\sin(\phi_d) \\ -\cos(\theta_d) \end{bmatrix}. \tag{2.12}$$

So for an arbitrary array geometry array steering vector can be defined as,

$$\mathbf{a}(\Theta_d) = \begin{bmatrix} e^{-j\mathbf{k}_d^T \mathbf{p}_1} \\ e^{-j\mathbf{k}_d^T \mathbf{p}_2} \\ \dots \\ e^{-j\mathbf{k}_d^T \mathbf{p}_M} \end{bmatrix}. \tag{2.13}$$

and the steering matrix is $\mathbf{A}(\mathbf{\Theta})$=[$\mathbf{a}(\Theta_1)$ $\mathbf{a}(\Theta_2)$ $\dots$ $\mathbf{a}(\Theta_D)$]. The problem is to find DOA angles, $\mathbf{\Theta}$, given the array output (2.10). Since the DOA angle, Θ, is a spatial parameter we need spatial covariance matrix between sensors. The output covariance matrix, $\mathbf{R}$, is

$$E\{\mathbf{y}(t)\mathbf{y}(t)^H\} = \mathbf{R} = \mathbf{A}(\mathbf{\Theta})\mathbf{R}_s\mathbf{A}(\mathbf{\Theta})^H + \sigma^2\mathbf{I}, \tag{2.14}$$

where $(.)^H$ denotes the conjugate transpose of a matrix, $\mathbf{R}_s$ is the source correlation matrix and $\mathbf{I}$ is the identity matrix.

2.3 Modeling Errors

In practical DF system there are various external factors which can cause some distortions on the above mathematical array model. The DOA performance of the model based methods is significantly degraded when there are unknown distortions on the model due to mutual coupling or gain and phase mismatch between the array elements. The mathematical array model can be rewritten as,

$$\mathbf{y}(t) = \mathbf{C}\boldsymbol{\Gamma}\mathbf{A}(\boldsymbol{\Theta})\mathbf{s}(t) + \mathbf{n}(t), \quad t = 1, \ldots, N \tag{2.15}$$

where $\mathbf{C}$ and $\boldsymbol{\Gamma}$ matrices stand for mutual coupling and gain/phase mismatch matrices between array elements, respectively. These two matrices can be seen as distortion matrices. In this section, we briefly investigate these distortions and their effects on DOA estimation performance.

2.3.1 Mutual Coupling

In practical arrays, array elements are located close to each other and this causes mutual coupling between array elements. Mutual coupling between array elements distorts the theoretical array steering vector. This distortion can be modeled as,

$$\tilde{\mathbf{a}}(\Theta) = \mathbf{C}(\Theta)\mathbf{a}(\Theta) \tag{2.16}$$

where $\mathbf{C}(\Theta)$, $M \times M$, is the mutual coupling matrix (MCM). The distortion matrix, MCM, is generally considered to be independent of DOA angle. The mutual coupling between two array elements depends on the distance between elements. As the distance increases, the magnitude of the coupling coefficient decreases. The MCM, $\mathbf{C}$ is in the form,

$$\mathbf{C} = \begin{bmatrix} 1 & c_{12} & \ldots & c_{1M} \\ c_{21} & 1 & \ldots & c_{2M} \\ \vdots & \vdots & \ddots & \vdots \\ c_{M1} & \ldots & \ldots & 1 \end{bmatrix} \tag{2.17}$$

where $c_{ij} \in \mathbb{C}$, for $i = 1, \ldots, M$ and $j = 1, \ldots, M$. These complex coefficients are called the mutual coupling coefficients of the MCM. It is assumed that the main diagonal of the MCM is normalized to unity. In order to make an accurate DOA estimation, the effects of the MCM have to be taken into account. In this thesis, we propose novel approaches to compensate this effect.

2.3.2 Gain/Phase Mismatch

In the theoretical model, it is assumed that the cables, antennas and receivers are identical which is not possible in practical systems. So there is no gain and phase match between channels. This effect can be included into model with $\mathbf{\Gamma}$, $M \times M$, diagonal matrix,

$$\mathbf{\Gamma} = \begin{bmatrix} g_1 & 0 & \dots & 0 \\ 0 & g_2 & \dots & 0 \\ \vdots & \vdots & \ddots & 0 \\ 0 & \dots & 0 & g_m \end{bmatrix} \tag{2.18}$$

where $g_i \in \mathbb{C}$, for $i = 1, \dots, M$. These complex numbers distort the steering matrix. It is required to calibrate the array elements for better DOA performance.

2.3.3 Position Errors

In array data model, the sensor locations of the planar array, (x_i, y_i) for $i = 1, \dots, M$, are assumed to be known. In practical arrays, sensors can deviate from their known positions. This error on sensor positions can be illustrated as in Figure 2.4. We can denote the amount of this error by p_e. p_e is an error with respect to the intersensor distance, $d = \frac{\lambda}{2}$ where λ is the wavelength. Therefore 2% position error corresponds to $\frac{|p_e|}{d} = 0.02$. Error displacement is on a circle with radius $|p_e|$ and the circle center is at the true sensor position. So the p_e can be expressed as $p_e = |p_e| \exp^{j\xi}$ where angle, ξ, is uniformly distributed between $(0, 2\pi]$ and radius $|p_e|$ is the distance from the nominal position.

In this thesis, the effects of sensor position error on DOA performance are compared for proposed V-shaped arrays and UCAs with different position errors. These position errors can be modeled as the random phase distortions on the steering vectors which degrade DOA angle estimation accuracy significantly.

2.3.4 Multipath Sources

The multipath propagation is a common situation in wireless communications. In this case, the signals impinging on the array from different angles, are highly or fully correlated versions

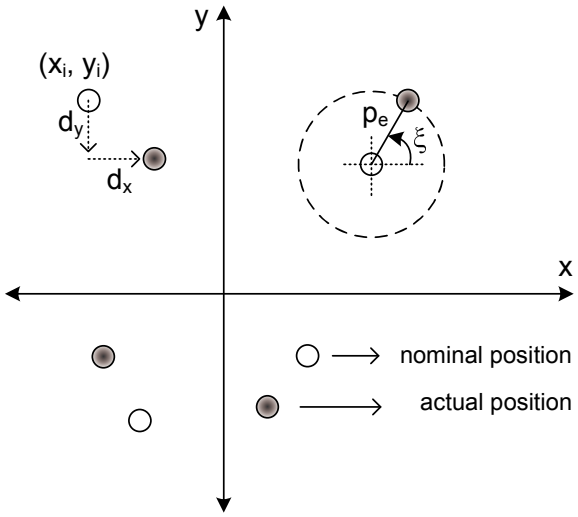

Figure 2.4: Illustration of sensor position errors for arbitrary planar arrays.

of one signal such as in Figure 2.2. This causes signal covariance matrix, $\mathbf{R}_s$ in (2.14) to became a singular matrix. So the rank of signal subspace of $\mathbf{R}$ is less than the number of DOA angles, and the noise subspace is not orthogonal to the columns of $\mathbf{A}(\Theta)$, which implies the failure of the eigenstructure-based techniques when the covariance matrix $\mathbf{R}$ is used.

In order to find 2-D DOA angles, we need to take into account of this fact. In this thesis, we proposed a spatial smoothing based array structure and paired 2-D DOA estimation method.

2.4 Array Interpolation

Array interpolation is a well known technique in DOA estimation [38], [39], [40]. It is used to map a real array to a virtual array. Usually an initial angular sector is chosen and array interpolation matrix is computed offline. Sector by sector processing is applied to cover all azimuth angles (360 degrees). Array interpolation is often used to extent the root-MUSIC algorithm to arbitrary array geometries for 1-D angle estimation [39]. Therefore the interpolated (virtual) arrays are usually selected as linear arrays. In this thesis, array interpolation concept is used as a tool in order to propose the closed form 2-D paired DOA estimation algorithm. Hence 2-D array interpolation is defined and Wiener formulation is applied to find the mapping matrices.

2.4.1 2-D Array Interpolation

2-D array interpolation is implemented by considering a two dimensional interpolation sector for the azimuth and elevation angles. This two dimensional angular sector is defined as $\{\tilde{\Theta}=(\tilde{\phi},\tilde{\theta}) \mid \phi_s \leq \tilde{\phi} \leq \phi_f, \theta_s \leq \tilde{\theta} \leq \theta_f\}$ as in Figure 2.5. Let $\mathbf{A}_1(\tilde{\Theta})$ and $\mathbf{A}_2(\tilde{\Theta})$ be the steering matrices for the real and virtual array, respectively. It is desired to find a mapping matrix $\mathbf{B}_{12}$ such that $\mathbf{B}_{12}\mathbf{A}_1(\tilde{\Theta})=\mathbf{A}_2(\tilde{\Theta})$. In general, the steering matrices are constructed by using finite number of calibration angles, i.e., $\tilde{\phi}_j=\phi_s+(j-1)\Delta\phi,\ j=1,\ldots,N_\phi$ where $N_\phi=\lfloor\frac{\phi_f-\phi_s}{\Delta\phi}\rfloor$ is the number of the azimuth angles and $\Delta\phi$ is the step size of the azimuth angles. Similarly, $\tilde{\theta}_m=\theta_s+(m-1)\Delta\theta, m=1,\ldots,N_\theta$ where $N_\theta=\lfloor\frac{\theta_f-\theta_s}{\Delta\theta}\rfloor$ is the number of the elevation angles, $\Delta\theta$ is the step size of the elevation angles and $\lfloor\rfloor$ takes the integer part. The mapping matrix for the conventional array interpolation, $\mathbf{B}_{12}$, is given as,

$$\mathbf{B}_{12}=\mathbf{A}_2(\tilde{\Theta})\mathbf{A}_1(\tilde{\Theta})^H\left(\mathbf{A}_1(\tilde{\Theta})\mathbf{A}_1(\tilde{\Theta})^H\right)^{-1} \tag{2.19}$$

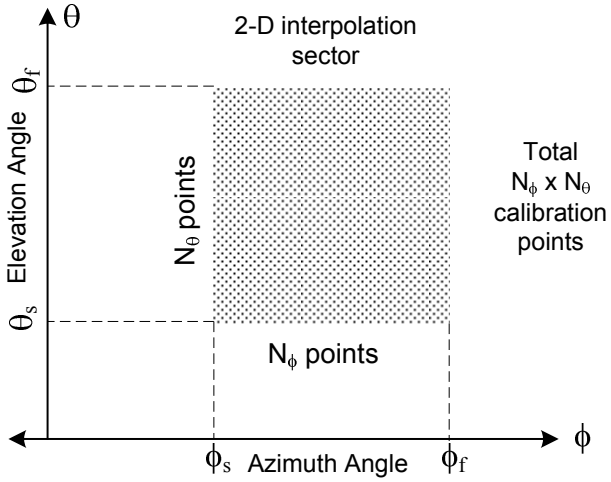

Figure 2.5: The 2-D angular sector for array interpolation.

In [13], [41], Wiener array interpolation is proposed to improve the performance of conventional array interpolation especially at low SNR. The mapping matrix for Wiener array interpolation is given as,

$$\mathbf{B}_{12}=\mathbf{A}_2(\tilde{\Theta})\mathbf{R}_s\mathbf{A}_1(\tilde{\Theta})^H\left(\mathbf{A}_1(\tilde{\Theta})\mathbf{R}_s\mathbf{A}_1(\tilde{\Theta})^H+\mathbf{R}_n\right)^{-1} \tag{2.20}$$

If we assume $\mathbf{R}_n=\sigma_n^2\mathbf{I}$ and $\mathbf{R}_s=\sigma_s^2\mathbf{I}$ for uncorrelated source signals, we have,

$$\mathbf{B}_{12}=\sigma_s^2\mathbf{A}_2(\tilde{\Theta})\mathbf{A}_1(\tilde{\Theta})^H\left(\sigma_s^2\mathbf{A}_1(\tilde{\Theta})\mathbf{A}_1(\tilde{\Theta})^H+\sigma_n^2\mathbf{I}\right)^{-1} \tag{2.21}$$

Wiener array interpolation and the technique in [41] allows one to choose a larger interpolation sector compared to the alternative approaches. In this paper, Wiener array interpolation is used for the proposed 2-D paired DOA estimation algorithms and SNR is assumed to be known. The signal-to-noise ratio can be estimated as in [13] and [42].

2.4.2 Iterative Improvement

If an initial DOA estimate, $\hat{\mathbf{\Theta}}$=$[(\hat{\phi}_1, \hat{\theta}_1), \ldots, (\hat{\phi}_D, \hat{\theta}_D)]$ is available, array interpolation error can be decreased by selecting a narrow sector in the neighborhood of the initial estimate. This is illustrated in Figure 2.6.

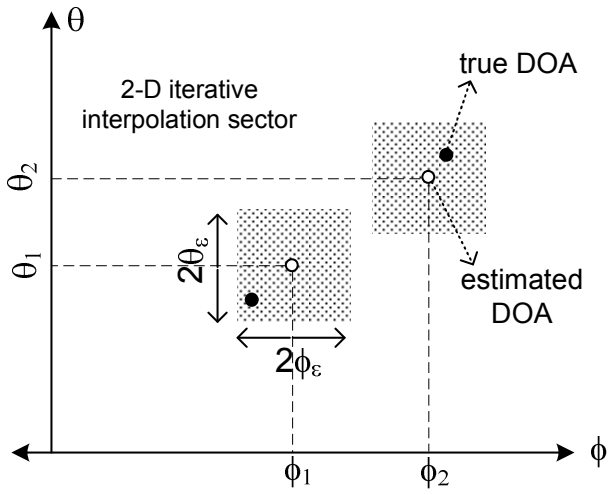

Figure 2.6: The 2-D narrow angular sectors in the neighborhood of the DOA estimates.

Note that the estimate can be obtained by first considering a large sector as in the conventional array interpolation. $\mathbf{B}_{12}$ can be constructed by considering narrow sectors in the neighborhood of each azimuth and elevation angle. In this case, the calibration angles in these sectors can be defined as $\tilde{\phi}_{i,j} \in [\hat{\phi}_i - \phi_\epsilon, \hat{\phi}_i + \phi_\epsilon]$, $\tilde{\phi}_{i,j}$=$\hat{\phi}_i - \phi_\epsilon + j\Delta\phi$ and $\tilde{\theta}_{i,m} \in [\hat{\theta}_i - \theta_\epsilon, \hat{\theta}_i + \theta_\epsilon]$, $\tilde{\theta}_{i,m}$=$\hat{\theta}_i - \theta_\epsilon + m\Delta\theta$. ϕ_ϵ and θ_ϵ are the sector sizes for the azimuth and elevation angles, respectively. $\tilde{\Theta}$ is a collection of the azimuth and elevation angle pairs in the interpolation sectors corresponding to each initial DOA estimate, i.e.,

$$\tilde{\Theta} = [\tilde{\Theta}_1, \tilde{\Theta}_2, \ldots, \tilde{\Theta}_D] \tag{2.22}$$

where $\tilde{\Theta}_i$=[$(\tilde{\phi}_{i1}, \tilde{\theta}_{i1})$, ..., $(\tilde{\phi}_{ij}, \tilde{\theta}_{im})$, ..., $(\tilde{\phi}_{iN_\phi}, \tilde{\theta}_{iN_\theta})$] for $j = 0, 1, \cdots, N_\phi = \lfloor \frac{2\phi_\epsilon}{\Delta\phi} \rfloor$ and $m = 0, 1, \cdots, N_\theta = \lfloor \frac{2\theta_\epsilon}{\Delta\theta} \rfloor$. By using the definition of $\tilde{\Theta}$, $\mathbf{A}_1(\tilde{\Theta})$ and $\mathbf{A}_2(\tilde{\Theta})$ are found as in (2.12) and (2.13). Then the interpolation matrix is found from (2.21). As the DOA estimation is iterated, it is possible to decrease the sector size. While a monotonic convergence and improvement is not guaranteed, iterations result better estimates with high probability [41]. The proposed method does not have any a priori information except the assumption that the source signals reside in an angular sector. The array interpolation accuracy depends on how large this angular sector. As the sector size decreases, array interpolation accuracy improves. The proposed technique obtains an initial DOA estimate by using a large angular sector. Once the initial DOA angles are available, the angular sector is decreased in the neighborhood of the initial estimates. This improves the accuracy of the array interpolation and a better DOA estimate is obtained. The iterations improve the performance significantly. The fact is, convergence is not guaranteed if the iterations are continued. In this respect, the number of iterations is kept small since most of the gain in performance is obtained within a couple of iterations.

CHAPTER 3

UNIFORM AND NONUNIFORM V-SHAPED PLANAR ARRAYS

3.1 Introduction

The performance of the direction finding (DF) system is significantly dependent to sensor array geometry. Therefore, the design of optimum array geometry for the best two-dimensional (2-D) DOA estimation performance is an important problem. This problem is investigated in previous works for the most general parameter settings. In these works, CRB on error variance is used as the performance measure and objective functions for the desired performance are minimized. The desired performance can change according to the application. In [17], the goal is to find planar and volumetric arrays for uniform DOA performance in all directions. In [18], DOA of interest is an angular sector and the goal is to find optimum array geometry for this scenario. It is seen that optimum array geometry for DOA estimation depends on many parameters including the number of sensors, number of sources and their DOA angles [14]. Furthermore it is not easy to find a single optimum geometry since the cost function changes depending on the number of sources and DOA's.

In this study, the array geometry is fixed as V-shaped in order to simplify the design and use certain advantages of V-shaped arrays which are not well known in the literature. V-shaped planar arrays can be designed for good directional DOA performance. It can also be designed for isotropic response such that the DOA performance is uniform for all directions. When the array intersensor distance is fixed to half of the wavelength, V-shaped array has a larger aperture than circular array. The number of sensors in V-shaped arrays can be decreased when the sensors are placed nonuniformly for each sub-array. Furthermore, it is possible to apply

forward-backward spatial smoothing [43] for each sub-array in order to deal with multipath signals. Fast algorithms can be applied for these subarrays and the results can be combined as in [20]. It is also shown that joint accuracy of two subarray's is better than each subarray's accuracy [21].

V-shaped arrays are not fully investigated in the literature. In [22], V-shaped arrays are considered with limited scope. Statistical angle coupling between the azimuth and elevation angle estimation is ignored and V-angle for uniform DOA performance is determined only for infinite number of sensors. Until now there is no known method and expression for finding the isotropic V-angle. Furthermore the directional characteristic of the V-shaped arrays is not fully exploited.

In this study, closed form expressions are presented for the V-angle in order to obtain isotropic DOA response. The UI V-shaped array and UCA are compared for the same number of sensors and intersensor distances. The comparison is done in terms of sensor position errors, source signal correlation, and mutual coupling between antennas. It is shown that the DOA accuracy of the UI V-shaped array is better than UCA. V-shaped arrays and UCA have similar robustness for the sensor position errors. The effect of source signal correlation is similar for both arrays while the performance of UI V-array gets better as the correlation increases. A similar observation is done for the mutual coupling. The performance of UI V-array is better than UCA in case of multiple sources. Different nonuniform V-shaped isotropic arrays are considered where the numbers of sensors at each subarray can be different. It is shown that the DOA performance can be improved significantly when the isotropic nonuniform V-shaped arrays are used. A design procedure for the directional uniform V-shaped arrays is presented. The directional V-shaped arrays are also compared with UCA for different DOA scenarios.

The contribution of this part for 2-D DOA estimation with V-shaped planar array geometry can be summarized as follows: Closed form expressions for the isotropic V-angle are presented. The expressions are given for both uniform and nonuniform V-shaped planar arrays [44]. The performances of V-shaped arrays, including uniform isotropic and nonuniform arrays, are analyzed for different cases. These involve correlated signals, mutual coupling, and sensor position errors. It is shown that V-shaped arrays perform better than the UCA for different types of error sources which is not well known in the literature. A design procedure is presented for uniform directional V-arrays which allows one to trade off the isotropic char-

acteristics for better DOA performance for a given angular sector. The optimization of the V-angle is done by defining a cost function over the CRB on DOA error variance which takes into account the coupling effect of azimuth and elevation angles. The proposed design considers two regions, namely, focused and unfocused region. The limits of the regions determine the angular accuracy and the performance of the V-array. It is shown that optimum V-angle can be found easily with only a limited search due to the monotonic characteristics of the cost function for the worst and best levels specified in the design parameters of the regions. This design procedure can also find the V-angle for isotropic DOA performance numerically [45], [46].

This chapter is organized as follows: In section 3.2, we describe the model of the array signals and CRB expressions are presented for 2-D DOA estimation. In section 3.3, closed form expressions for uniform and nonuniform V-shaped arrays for isotropic azimuth response are given. We present the directional V-shaped planar array design procedure in section 3.4. In section 3.5, the effect of mutual coupling between array elements is considered. The performances of the designed V-shaped arrays and UCA are presented in section 3.6.

3.2 Problem Formulation

3.2.1 Data Model

In this section, the array data model which is derived in Section 2.2, is restated to make the chapter more facilitate for the reader.

We consider an array of M sensors located at the positions $[x_l, y_l]$, $l = 1, \ldots, M$. We assume that there are L ($L < M$) narrowband signals impinging on the array from the directions $\Theta_i = [\phi_i, \theta_i]$ $i = 1, \ldots, L$, where ϕ and θ are the azimuth and elevation angles respectively as shown in Figure 3.1. If the sensors are identical omnidirectional and far-field assumption is made, the sensor output, $\mathbf{y}(t)$, can be written as,

$$\mathbf{y}(t) = \mathbf{A}(\Theta)\mathbf{s}(t) + \mathbf{n}(t), \quad t = 1, \ldots, N \tag{3.1}$$

where N is the number of snapshots. It is assumed that the noise, $\mathbf{n}(t)$, is both spatially and temporally white with variance σ^2. It is also uncorrelated with the source signals. $\mathbf{A}(\Theta) = [\mathbf{a}(\phi_1, \theta_1) \ldots \mathbf{a}(\phi_L, \theta_L)]$ is the $M \times L$ steering matrix for the planar array and the vectors $\mathbf{a}(\phi, \theta)$

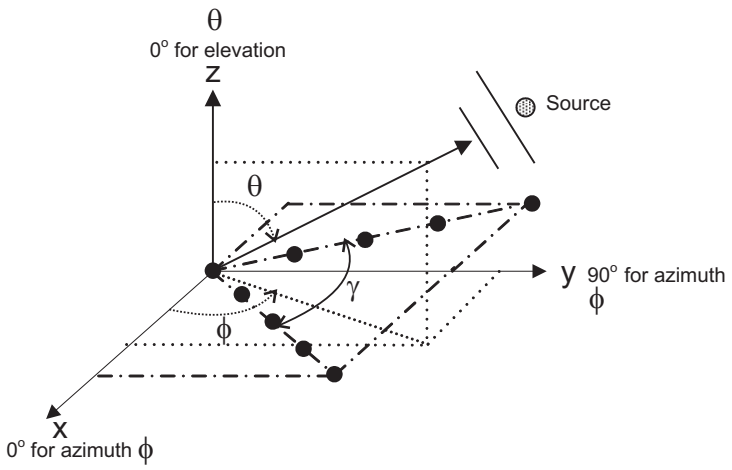

Figure 3.1: Coordinate system for 2-D angle estimation and V-shaped array.

are given as,

$$\mathbf{a}(\phi,\theta) = \left[e^{\{j\frac{2\pi}{\lambda}(x_1 \cos\phi \sin\theta + y_1 \sin\phi \sin\theta)\}} \dots e^{\{j\frac{2\pi}{\lambda}(x_M \cos\phi \sin\theta + y_M \sin\phi \sin\theta)\}} \right]^T . \tag{3.2}$$

The output covariance matrix, $\mathbf{R}$, is

$$E\{\mathbf{y}(t)\mathbf{y}(t)^H\} = \mathbf{R} = \mathbf{A}\mathbf{R}_s\mathbf{A}^H + \sigma^2\mathbf{I}, \tag{3.3}$$

where $(.)^H$ denotes the conjugate transpose of a matrix, $\mathbf{R}_s$ is the source correlation matrix and $\mathbf{I}$ is the identity matrix.

3.2.2 CRB for 2-D DOA Estimation

CRB shows the ultimate performance of an unbiased estimate for a given array geometry. When 2-D DOA estimation is considered, there is statistical coupling between the azimuth and elevation DOA performances in general. The existence of coupling depends on array geometry. Some of the array geometries like circular arrays are uncoupled. V-shaped arrays show coupling effects and therefore coupling should be taken into account for the CRB. The proposed V-shaped array design method uses the CRB in the cost function. Therefore, a review of the angle coupling effect for the CRB is considered in this section. The inequality for the variance of the parameters is given as,

$$var(\hat{\theta}_m) \geq [\mathbf{F}^{-1}]_{mm}, \tag{3.4}$$

where the mn^{th} element of the Fisher information matrix, $\mathbf{F}$, is given in [47] as

$$\mathbf{F}_{mn} = N \times tr\{\mathbf{R}^{-1}\frac{\partial \mathbf{R}}{\partial p_m}\mathbf{R}^{-1}\frac{\partial \mathbf{R}}{\partial p_n}\}, \tag{3.5}$$

For 2-D angle estimation, the unknown parameter vector is defined by $\mathbf{p} = [\phi, \theta]$. Fisher information matrix (FIM) is given by

$$\mathbf{F} = \begin{bmatrix} \mathbf{F}_{\phi\phi} & \mathbf{F}_{\phi\theta} \\ \mathbf{F}_{\theta\phi} & \mathbf{F}_{\theta\theta} \end{bmatrix} \tag{3.6}$$

where

$$\mathbf{F}_{\phi\phi} = 2NRe\{(\mathbf{R}_s\mathbf{A}^H\mathbf{R}^{-1}\mathbf{A}\mathbf{R}_s) \times (\dot{\mathbf{A}}_\phi^H\mathbf{P}_A^\perp\mathbf{R}^{-1}\dot{\mathbf{A}}_\phi)^T\} \tag{3.7}$$

$$\mathbf{F}_{\phi\theta} = 2NRe\{(\mathbf{R}_s\mathbf{A}^H\mathbf{R}^{-1}\mathbf{A}\mathbf{R}_s) \times (\dot{\mathbf{A}}_\phi^H\mathbf{P}_A^\perp\mathbf{R}^{-1}\dot{\mathbf{A}}_\theta)^T\} \tag{3.8}$$

$\mathbf{F}_{\theta\theta}$, can be written similar to (3.7). $\mathbf{F}_{\phi\theta} = \mathbf{F}_{\theta\phi}$ and

$$\mathbf{P}_A^\perp = \mathbf{I} - \mathbf{A}(\mathbf{A}^H\mathbf{A})^{-1}\mathbf{A}^H, \quad \dot{\mathbf{A}}_\phi = \sum_{n=1}^{L}\frac{\partial \mathbf{A}}{\partial \phi_n}. \tag{3.9}$$

If the off-diagonal term, $\mathbf{F}_{\phi\theta}$ is zero, the estimates of the azimuth and elevation angles are uncoupled. But for arbitrary array geometries, this off-diagonal term, $\mathbf{F}_{\phi\theta}$, is nonzero. For 2-D angle estimation, the CRB defined in [48] and [49] takes the coupling effect into account and the CRB for the azimuth and elevation angles are given as,

$$CRB_\phi = \frac{1}{\mathbf{F}_{\phi\phi}}\left[\frac{1}{1-\rho^2}\right] \tag{3.10}$$

$$CRB_\theta = \frac{1}{\mathbf{F}_{\theta\theta}}\left[\frac{1}{1-\rho^2}\right] \tag{3.11}$$

where

$$0 \leq \rho^2 = \frac{\mathbf{F}_{\phi\theta}^2}{\mathbf{F}_{\phi\phi}\mathbf{F}_{\theta\theta}} \leq 1. \tag{3.12}$$

If $\rho^2 = 1$, the estimates are said to be perfectly coupled and the unknown parameters (ϕ, θ) cannot be estimated simultaneously. If $\rho^2 \neq 0$, uncertainty in one parameter degrades the other parameter's accuracy. $\rho^2 = 0$ is required for uncoupled 2-D DOA estimation. Therefore it is important to consider the coupling effect when 2-D DOA estimation is done. The constraints on array sensor locations for uncoupled DOA angle estimation are reviewed in the following part.

3.2.2.1 Conditions for Uncoupled 2-D DOA Angle Estimation

In order to have 2-D uncoupled DOA angle estimation, the off-diagonal terms of FIM must be zero, i.e, $F_{\phi\theta} = 0$. The required conditions for uncoupled DOA estimation according to the array sensor locations are derived in [49] as,

$$P_{xx} = P_{yy} \quad and \quad P_{xy} = 0 \tag{3.13}$$

where P_{xx}, P_{yy} and P_{xy} depend on the sensor coordinates,

$$P_{xx} = \sum_{l=1}^{M} (x_l - x_c)^2 \ , \ P_{yy} = \sum_{l=1}^{M} (y_l - y_c)^2 \tag{3.14}$$

$$P_{xy} = \sum_{l=1}^{M} (x_l - x_c)(y_l - y_c) \tag{3.15}$$

and x_c, y_c given as,

$$x_c = \frac{1}{M} \sum_{l=1}^{M} x_l \ , \ y_c = \frac{1}{M} \sum_{l=1}^{M} y_l \tag{3.16}$$

(x_l, y_l) is the l^{th} sensor position and (x_c, y_c) are array center of gravity. Therefore (3.13) should be satisfied in order to have uncoupled DOA angle estimation for a planar array.

3.3 Isotropic Planar Array

CRB for an isotropic planar array in case of a single source is uniform for all azimuth DOA angles. In [17] and [22], it is shown that the conditions for an isotropic array are the same as the conditions for an array to have uncoupled azimuth and elevation estimation which is given in the previous part.

In the following part, we present the closed form expressions which return the V-angle for uniform and nonuniform V-shaped isotropic planar arrays.

3.3.1 Isotropic Uniform V-shaped Array

Let M be an odd number for simplicity and $k = \frac{M+1}{2}$ is the index of the reference sensor at the origin. The sensor positions for uniform V-shaped array in Figure 3.2 can be expressed as,

$$\begin{aligned} x_l &= (l-k)d \sin(\frac{\gamma}{2}), \quad l = 1, \ldots, M \\ y_l &= |l-k|d \cos(\frac{\gamma}{2}), \quad l = 1, \ldots, M. \end{aligned} \tag{3.17}$$

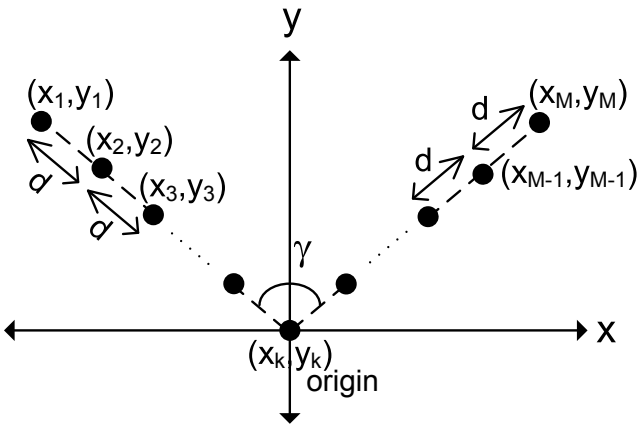

Figure 3.2: Uniform V-shaped array geometry.

It is assumed that the sensor positions are symmetric according to the y axis and sensors are separated with a distance which is an integer multiple of a distance d. In order to design an isotropic uniform V-shaped array, equation (3.13) should be satisfied. Since the sensor positions are uniform and symmetric according to the y axis, $x_c = 0$ and $P_{xy} = 0$ for all γ angles. The condition $P_{xx} = P_{yy}$ should be satisfied for the isotropic angle γ_{iso}. The derivation of γ_{iso} formulation is presented in Appendix A. The closed form expression for γ_{iso} for a uniform V-shaped array is given as,

$$\gamma_{iso} = 2 \times \arctan\left(\sqrt{\frac{M^2+3}{4M^2}}\right). \tag{3.18}$$

3.3.2 Isotropic Nonuniform V-shaped Array

In this case, the distance from the reference sensor is nonuniform for the sensors in the array as shown in Figure 3.3. It is known that nonuniform arrays can perform better than the same number of element uniform linear array (ULA), in a variety of cases [41]. There are M_1 sensors at the left nonuniform linear sub-array and M_2 sensors at the right nonuniform linear sub-array and a reference sensor at the origin. We can express the sensor positions for the

nonuniform V-shaped array as,

$$\begin{aligned} x_l &= -d_l \sin(\frac{\gamma}{2}), \\ y_l &= d_l \cos(\frac{\gamma}{2}) \ \ for \ \ l = 1, \ldots, M_1 \\ x_l &= d_l \sin(\frac{\gamma}{2}), \\ y_l &= d_l \cos(\frac{\gamma}{2}) \ \ for \ \ l = M_1 + 2, \ldots, M \\ x_{M_1+1} &= 0, \ \ y_{M_1+1} = 0 \end{aligned} \tag{3.19}$$

where d_l is a real positive number. We have to place the sensors to satisfy (3.13) for isotropic performance. In order to have $P_{xy} = 0$, we need to satisfy the following equations.

$$\begin{aligned} (d_1 + \cdots + d_{M_1}) &= (d_{M_1+2} + \cdots + d_M) \\ (d_1^2 + \cdots + d_{M_1}^2) &= (d_{M_1+2}^2 + \cdots + d_M^2) \end{aligned} \tag{3.20}$$

The details of the derivation of the isotropic angle are presented in Appendix B. The closed form expression which returns the V-angle for isotropic performance, γ_{iso}, for nonuniform V-shaped arrays is given as,

$$\gamma_{iso} = 2 \arctan\left(\sqrt{1 - \frac{2}{M} \frac{\left(\sum_{i=1}^{M_1} d_i \right)^2}{\sum_{i=1}^{M_1} d_i^2}} \right) \tag{3.21}$$

Both (3.20) and (3.21) should be satisfied in order to obtain isotropic performance for a nonuniform V-shaped array.

We can design nonuniform V-shaped arrays for isotropic DOA performance in two steps. In the first step, the sensor locations are selected to satisfy (3.20). Then the isotropic angle for the nonuniform V-shaped array is obtained as in (3.21).

3.4 Directional V-shaped Planar Array Design

In the previous part, we derived analytic expressions for the design of isotropic V-shaped arrays. While it is useful to have isotropic response in many cases, directional arrays perform better when the array is constrained to look more sensitively to a certain angular sector. In this part we present a design procedure for the directional V-shaped arrays.

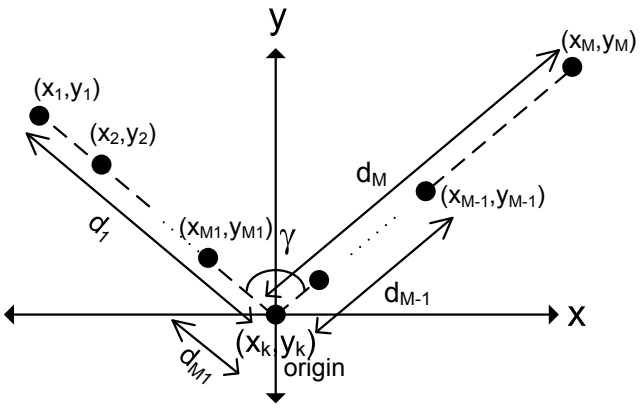

Figure 3.3: Nonuniform V-shaped array geometry.

3.4.1 Design Procedure

The design procedure finds the optimum γ° angle to obtain the best DOA performance. Before going through the design steps we need to understand the characteristics of the V-shaped arrays. CRB for different DOA angles are shown in Figure 3.4 for different V-angles. The characteristic is periodic by 180 degrees. The best performance is seen at 90 and 270 degrees and the worst performance is seen at 0 and 180 degrees. This characteristic is observed when the V-shaped array is configured as shown in Figure 3.1, where the subarrays are placed symmetrically with respect to y axis. Note that such kind of configuration can always be realized by defining x and y axes appropriately. When we change the V-angle, γ, the best and worst performance levels and the width of these regions are changing. We need to find the best V-angle for the desired directional response.

In the design procedure, two regions are specified as shown in Figure 3.5. Focused region is the angular sector where the best possible DOA accuracy is desired. Unfocused region is an angular sector where a DOA accuracy below a certain level, H_1, is acceptable. If a focused region different from the one shown in Figure 3.5, is desired, array and coordinate axis can be rotated appropriately. Note that focused region is centered at 90 degrees where the array shows the best performance. The azimuth angles α_1 and α_2 determine the focused region limits. While α_1 and α_2 can be arbitrary in general, the best performance is obtained if $\alpha_1 + \alpha_2 = 180^\circ$. Note that in this case α_1 and α_2 are symmetrically placed with respect to the 90 degrees. The target is to find γ° given the parameters α_1, α_2 and H_1.

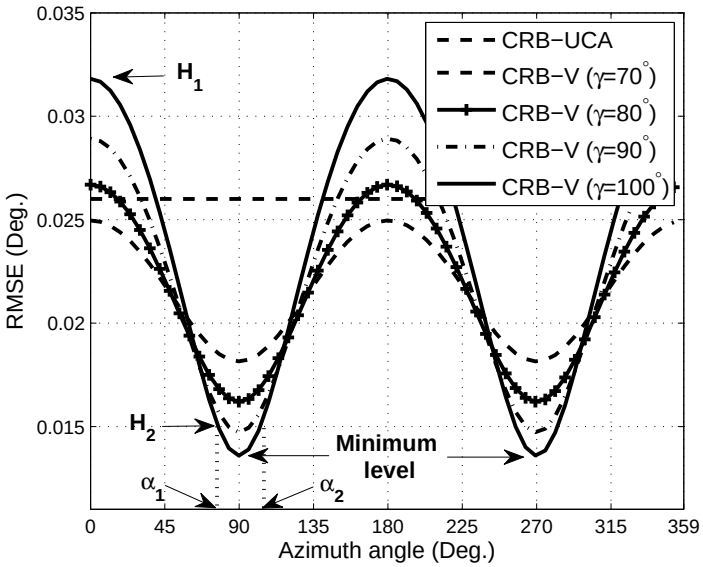

Figure 3.4: DOA performance of 9 elements V-shaped arrays with different γ angles for a single source which is swept between all azimuth angles with 256 snapshots and 20 dB SNR.

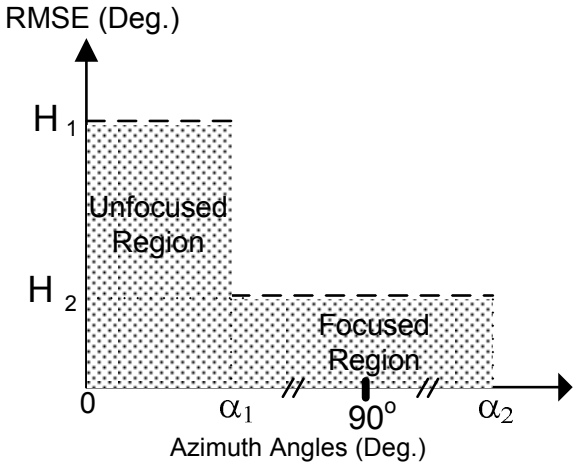

Figure 3.5: The design regions and parameters for V-shaped planar array geometry.

In Figure 3.6 the best and the worst performance levels are plotted with respect to γ angle when the coupling effect of the azimuth and elevation angle estimation is taken into account. Note that if the coupling effect is not taken into account, design of V-array can converge to a degenerate case, such as, a linear array (γ=180 degrees). In this case H_1 level goes to infinity and therefore both azimuth and elevation angles cannot be resolved simultaneously. As it is seen, H_1-γ and H_2-γ curves are monotonic. Once H_1 is specified, the corresponding angle in Figure 3.6 is an upper bound for the best performance. Therefore optimum V-angle, γ°, should be less than this angle. The proposed design method has the following steps:

Step 1: H_1, α_1, and α_2 values are specified (Figure 3.5). We assume that α_2=180 $-$ α_1 for simplicity.

Step 2: From Figure 3.6, γ angle (γ_1) corresponding to H_1 is found.

Step 3: CRB expression in (3.10) is evaluated for the α_1 azimuth angle corresponding to the V-angle, γ_k, namely, CRB(α_1, γ_k). The cost for γ_k is $e(k)$ = CRB(α_1, γ_k).

Step 4: Decrease γ_k angle by Δ, $\gamma_{k+1} = \gamma_k - \Delta$, and repeat step 3 for $k = 2, \ldots, K$. Δ is the step size and $K = (\gamma_1 - \gamma_{iso})/\Delta$

Step 5: Find the minimum $e(k)$ and the corresponding γ_k angle as the optimum V-angle, γ°

$$\gamma^\circ = \arg\min_{\gamma_k}\{e(k)\}. \tag{3.22}$$

3.5 Analysis of Mutual Coupling Effects

Mutual coupling between antenna elements is an important factor which degrades the DOA estimation performance. CRB for unknown mutual coupling matrix (MCM), **C**, is the fundamental tool in order to quantify the DOA performance [23]-[25]. In this study, the CRB formulation in [25] is implemented in order to compare the UCA and isotropic V-shaped arrays. The array output in case of mutual coupling can be expressed as,

$$\mathbf{y}(t) = \mathbf{CA}(\Theta)\mathbf{s}(t) + \mathbf{n}(t). \tag{3.23}$$

The target in this part is to compare the DOA performances for UCA and V-shaped arrays in a fair manner. In order to achieve this target, both arrays are constructed by employing dipole

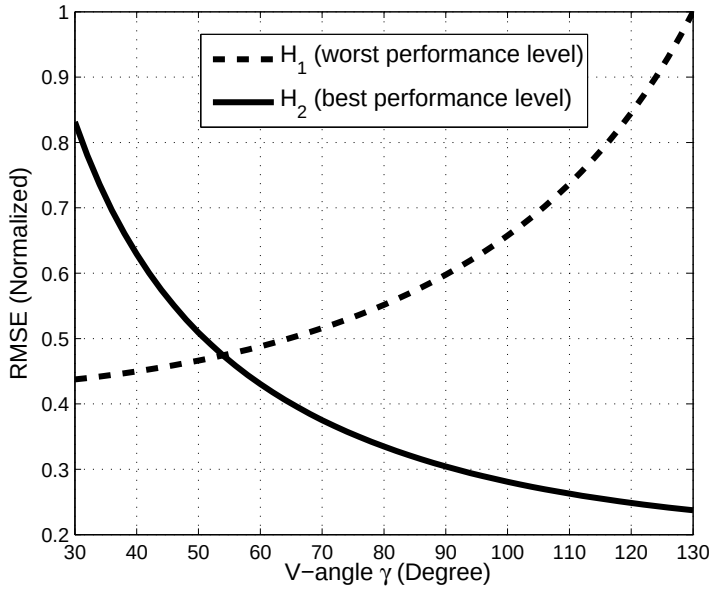

Figure 3.6: The best and worst performance levels of the azimuth CRB versus V-angle, γ, when α_1 and α_2 are 90 degrees.

antennas with $\lambda/2$ size and 50 ohm load in FEKO, [50]. The radius of the dipole is selected as $1.5 \times 10^{-3}\lambda$ and the operating frequency is 30 MHz. There are 9 antennas and the intersensor distance is set to $\lambda/2$ for both arrays. FEKO is an electromagnetic simulation tool which can model the antenna elements with sufficient accuracy and close to the practical situation. Table 3.1 and 3.2 present the distance between array elements for UCA and UI V-shaped array, respectively. The mutual coupling between two antennas depends on the distance between antennas. As the distance increases, the magnitude of the coupling coefficient decreases. In the literature, MCM for UCA is usually represented with only one coefficient [23]. In addition, the coefficients for the antennas with a distance greater than 0.707λ are ignored [25]. In this study, we ignored the coefficients when the distance between antennas is greater than λ in order to have a more accurate evaluation. Table 3.3 and 3.4 show the MCM matrices and the mutual coupling coefficients for the two arrays. It can be seen that UI V-shaped array uses seven coefficients whereas the UCA array uses only two coefficients. In addition, coupling coefficients for the same distance may be different for the V-shaped array due to the different interaction between antennas. The coupling coefficients for two arrays are given in Table 3.5.

The real and imaginary parts of the elements of the MCM contribute to the Fisher Information

Table 3.1: Distance between sensors for 9 elements UCA in terms of λ.

UCA	1	2	3	4	5	6	7	8	9
1	0	0.5	0.939	1.266	1.439	1.439	1.266	0.939	0.5
2	0.5	0	0.5	0.939	1.266	1.439	1.439	1.266	0.939
3	0.939	0.5	0	0.5	0.939	1.266	1.439	1.439	1.266
4	1.266	0.939	0.5	0	0.5	0.939	1.266	1.439	1.439
5	1.439	1.266	0.939	0.5	0	0.5	0.939	1.266	1.439
6	1.439	1.439	1.266	0.939	0.5	0	0.5	0.939	1.266
7	1.266	1.439	1.439	1.266	0.939	0.5	0	0.5	0.939
8	0.939	1.266	1.439	1.439	1.266	0.939	0.5	0	0.5
9	0.5	0.939	1.266	1.439	1.439	1.266	0.939	0.5	0

Table 3.2: Distance between sensors for 9 elements UI V-shaped array in terms of λ.

V	1	2	3	4	5	6	7	8	9
1	0	0.5	1	1.5	2	1.753	1.627	1.649	1.815
2	0.5	0	0.5	1	1.5	1.272	1.219	1.361	1.649
3	1	0.5	0	0.5	1	0.814	0.908	1.219	1.627
4	1.5	1	0.5	0	0.5	0.454	0.814	1.272	1.753
5	2	1.5	1	0.5	0	0.5	1	1.5	2
6	1.753	1.272	0.814	0.454	0.5	0	0.5	1	1.5
7	1.627	1.219	0.908	0.814	1	0.5	0	0.5	1
8	1.649	1.361	1.219	1.272	1.5	1	0.5	0	0.5
9	1.815	1.649	1.627	1.753	2	1.5	1	0.5	0

Table 3.3: Mutual coupling matrix for 9 elements UCA.

UCA	1	2	3	4	5	6	7	8	9
1	1	c_1	c_2					c_2	c_1
2	c_1	1	c_1	c_2					c_2
3	c_2	c_1	1	c_1	c_2				
4		c_2	c_1	1	c_1	c_2			
5			c_2	c_1	1	c_1	c_2		
6				c_2	c_1	1	c_1	c_2	
7					c_2	c_1	1	c_1	c_2
8	c_2					c_2	c_1	1	c_1
9	c_1	c_2					c_2	c_1	1

Table 3.4: Mutual coupling matrix for 9 elements UI V-shaped array.

V	1	2	3	4	5	6	7	8	9
1	1	v_4							
2	v_4	1	v_2						
3		v_2	1	v_3		v_7	v_6		
4			v_3	1	v_5	v_1	v_7		
5				v_5	1	v_5			
6			v_7	v_1	v_5	1	v_3		
7			v_6	v_7		v_3	1	v_2	
8							v_2	1	v_4
9								v_4	1

Table 3.5: Mutual Coupling Coefficients of UCA and UI V-shaped array.

UCA	UI V-array
$c_1 = 0.1534 + 0.1019i$	$v_1 = 0.1334 + 0.2059i$
$c_2 = -0.0347 - 0.0960i$	$v_2 = 0.1386 + 0.1198i$
	$v_3 = 0.1549 + 0.0924i$
	$v_4 = 0.1268 + 0.1210i$
	$v_5 = 0.0876 + 0.1482i$
	$v_6 = 0.0124 - 0.1490i$
	$v_7 = 0.0722 - 0.0915i$

Matrix (FIM). Therefore as the number of coefficients increases, the size of the FIM and its condition number increases. It may be no longer well conditioned [24]. This also disturbs the smoothness of the CRB characteristics. As a result, the increase in the number of coupling coefficients decreases the accuracy of DOA performance.

For a single source, the number of unknowns is large compared to the number of equations for UI V-shaped array in (3.23). When some of the unknowns are ignored and MCM is estimated, the DOA accuracy decreases. As a result, the DOA performance of UI V-shaped array is worse than the UCA for a single source. It is also observed that its performance gets better than the UCA when the number of coupling coefficients is decreased. As the number of sources increases, the number of equations increases and MCM can be estimated accurately. In our simulations, we have found that UI V-shaped arrays perform better than UCA when there are more than one source. The comparisons of the performances of the two arrays are presented in the following section.

3.6 Simulation Results

In this section, we consider the isotropic and directional V-shaped arrays in order to show the characteristics of the V-array for different cases. Examples of the isotropic uniform and nonuniform V-arrays are considered and compared with UCA. Furthermore the effect of sensor position error is investigated for both V-shaped and circular arrays by using the MUSIC algorithm.

In simulations, source angles are considered in degrees where azimuth angles are between 0 and 360 degrees and elevation angles are between 0 and 90 degrees (Figure 3.1). There are 1000 trials for each experiment and the number of snapshots is 256.

3.6.1 Simulations for Uniform Isotropic V-shaped Arrays

UI V-shaped planar arrays can be easily designed from equation (3.18) for a specified number of sensors, M. For example if M=9, γ_{iso} is 53.9681°. The performance of this V-shaped array is compared with the UCA in Figure 3.7. There are three sources at the azimuth angles ϕ_1=60, ϕ_2=100 and ϕ_3=120 degrees and elevation angles are fixed at θ=90 degrees for all sources.

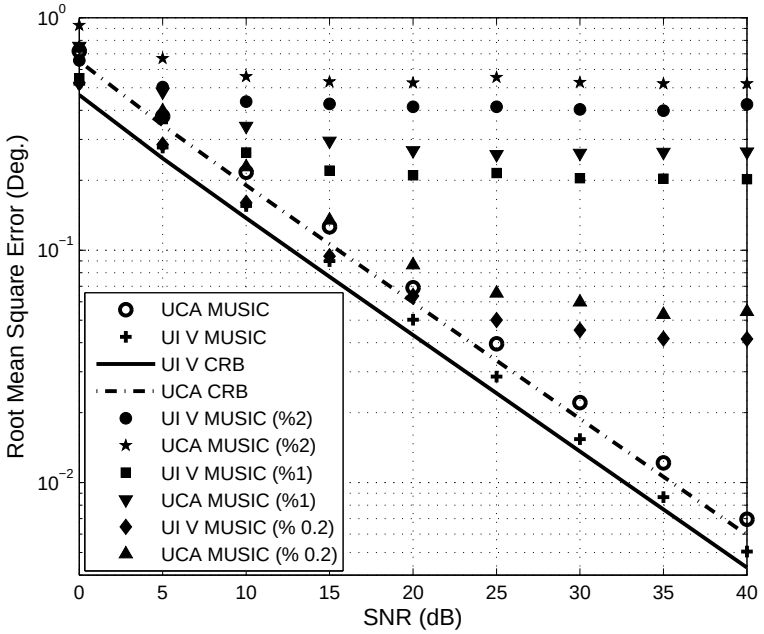

Figure 3.7: Azimuth DOA performance for three sources at 60, 100 and 120 degrees, respectively, when UI V-shaped array and UCA are used without and with sensor position errors (2%, 1%, 0.2%).

Source signals are uncorrelated. As it is seen from Figure 3.7, UI V-shaped array shows better performance than the circular array when both arrays have the same number of sensors and inter-sensor distances. In Figure 3.7, the performances of V-shaped array and UCA are outlined when there is an error in sensor positions denoted by p_e. p_e is an error with respect to the intersensor distance, $d = \lambda/2$ where λ is the wavelength. Therefore 2% position error corresponds to $\frac{|p_e|}{d} = 0.02$. Error displacement is on a circle with radius $|p_e|$ and the circle center is at the true sensor position. Figure 3.7 shows that both the UI V-array and UCA have similar robustness for the various position errors (2%, 1% and 0.2%). Also it is evident that the UI V-array has better performance for each of the position errors.

Figure 3.8 shows the DOA performance of UI V-array and UCA for correlated source signals. There are two sources at the azimuth angles ϕ_1=80 and ϕ_2=85 degrees, respectively, and the elevation angle is fixed at θ=90 degrees for each source. SNR is set to 15 dB for the equi-power sources. The source covariance matrix, $\mathbf{R}_s$ is taken as,

$$\mathbf{R}_s = \begin{bmatrix} 1 & \rho \\ \rho & 1 \end{bmatrix} \tag{3.24}$$

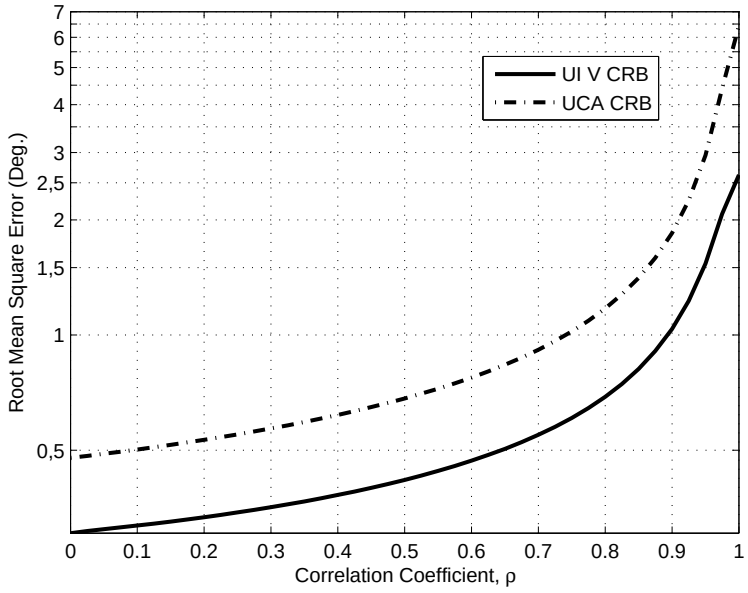

Figure 3.8: Azimuth CRB DOA performance of 9 elements UI V-array and UCA for two sources when the sources are correlated with the correlation coefficient ρ. Sources are at 80 and 85 degrees and elevations are fixed at 90 degrees. SNR = 15 dB.

where ρ is selected as a positive real value in $[0, 1]$ for simplicity. It turns out that the UI V-array has better performance for the correlated sources signals. The difference between V-array and the UCA increases as the value of ρ increases especially for the values close to $\rho = 1$. Note that $\rho = 1$ corresponds to the coherent source case.

Figure 3.9 shows the DOA performance when there are two sources fixed at 161 and 180 degrees and the third source is swept between 0 and 360 degrees. This figure shows the CRB characteristics with and without unknown mutual coupling. The SNR is fixed at 20 dB. It can be easily seen that the coupling decreases the DOA performance. However the DOA performance for UI V-shaped array is better than the UCA for all of the DOA angles.

Figure 3.10 shows the SNR performance of the UCA and UI V-shaped array for three sources at 60, 100 and 120 degrees, respectively, with and without unknown mutual coupling. It can be seen that the DOA performance degrades due to mutual coupling but the performance of UI V-shaped array is better than the UCA.

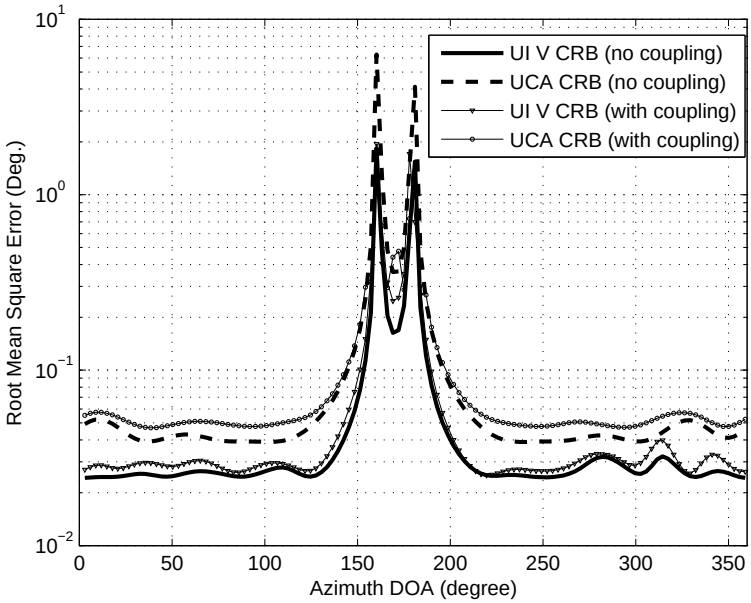

Figure 3.9: CRB DOA performance with and without unknown mutual coupling of UI V-shaped array and UCA for two sources when one source is swept between 0 and 360 degrees while the other two sources are at 161 and 180 degrees. Elevation angles are fixed to 90 degrees.

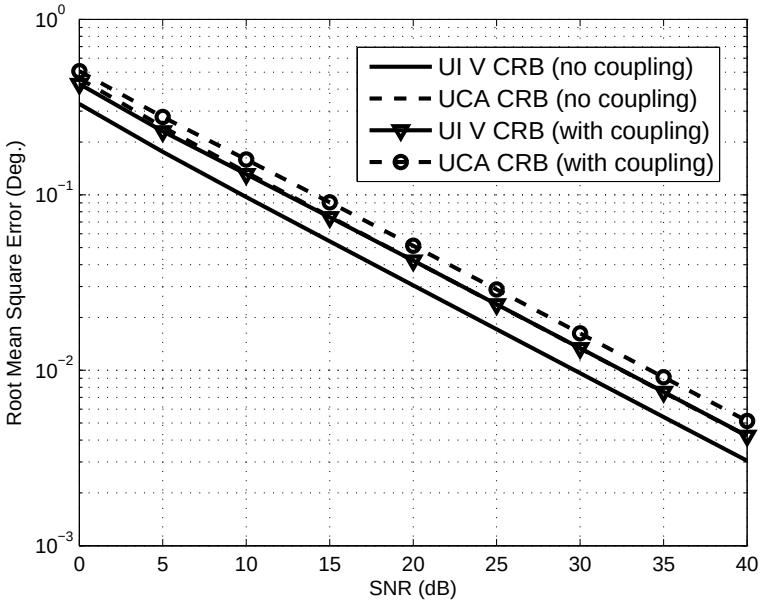

Figure 3.10: CRB DOA performance with and without unknown mutual coupling for three sources at 60, 100 and 120 degrees, respectively, when UI V-array and UCA are used. Elevation angles are fixed to 90 degrees.

Table 3.6: Isotropic nonuniform V-shaped design examples for $M_1 = M_2$ and $M_1 \neq M_2$.

Nonuniform sensor positions	γ_{iso}^{o} (deg.)
$[\underbrace{6,4,1}_{M1=3},0,\underbrace{1,4,6}_{M2=3}]$	61.0530^{o}
$[\underbrace{6,4,1}_{M1=3},0,\underbrace{1.691,2.809,6.5}_{M2=3}]$	61.0530^{o}
$[\underbrace{17,12,10,4,1}_{M1=5},0,\underbrace{5,10,13,16}_{M2=4}]$	57.0976^{o}

3.6.2 Simulations for Nonuniform Isotropic V-shaped Arrays

In case of nonuniform V-shaped array, we select the left arm as a non-redundant nonuniform linear array (NLA) for simplicity. The sensor locations for the NLA with respect to $d = \frac{\lambda}{2}$ are d_{NLA}=[0,1,4,6]. The right arm can be adjusted to have $M_1 = M_2$ or $M_1 \neq M_2$. Sensor positions of the right sub-array are selected in order to satisfy (3.20). Then γ_{iso}° is determined from (3.21). Some of the examples for isotropic nonuniform arrays are presented in Table 3.6. CRB levels of the designed isotropic nonuniform arrays are given in Figure 3.11. This figure shows that DOA accuracy can be significantly improved with nonuniform V-shaped arrays for the same number of sensors. Note that this result is obvious due to the fact that array aperture is increased. However, NLA still returns unambiguous solutions since there is at least two sensors with the intersensor distance less than $\frac{\lambda}{2}$.

3.6.3 Simulations for Directional Uniform V-shaped Arrays

In the directional case, sources are assumed to be localized in an angular sector. We choose design parameters as α_1=80^{o}, α_2=100^{o} and $H_1 = 0.5^{\circ}$. Angular step size is $\Delta = 1^{\circ}$ for M=9 sensors and the number of snapshots N=256. If the design procedure is applied for these parameters, the best DOA performance is obtained for $\gamma^{\circ} = 119^{\circ}$. In Figure 3.12, there are two sources at ϕ_1=81° and ϕ_2=98°. This figure shows that designed directional uniform (DU) V-shaped array has better DOA performance than UCA and L-shaped array (γ=90°). The DOA performance for the elevation angle is shown in Figure 3.13 for ϕ_1. As it is seen from the figure, elevation performance of the directional V-shaped array, changes depending on the azimuth angle. Circular array has uncoupled azimuth and elevation angle response. Figure 3.14 shows the DOA performance when there are two sources fixed at 83 and 99 degrees and

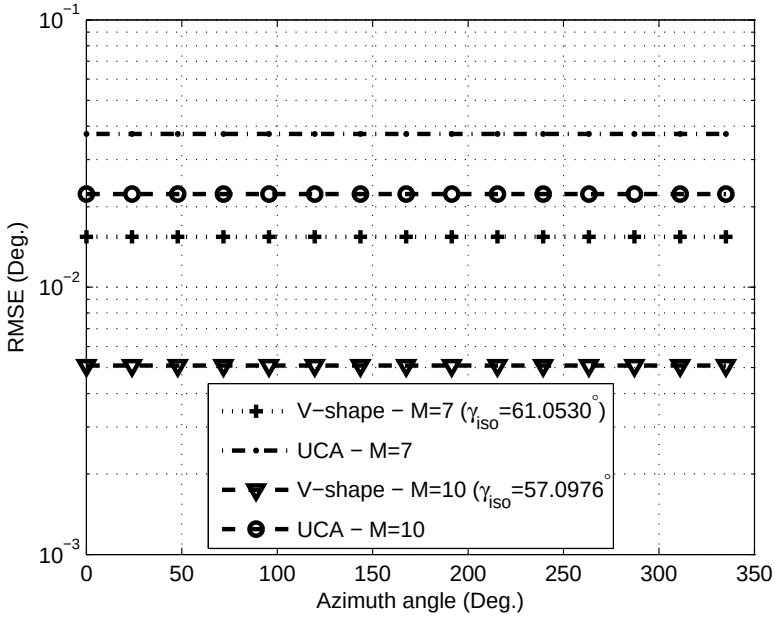

Figure 3.11: CRB DOA performance of nonuniform isotropic (NUI) V-array and UCA for a single source is swept between 0 and 360 degrees when $M = 7$, $M = 10$ and elevation angles are fixed to $\theta = 90^\circ$ and SNR = 20 dB.

third source is swept between 0 and 360 degrees in one degree resolution. SNR is fixed at 20 dB. This figure shows that DU V-shaped array has significantly better resolution and DOA performance than UCA.

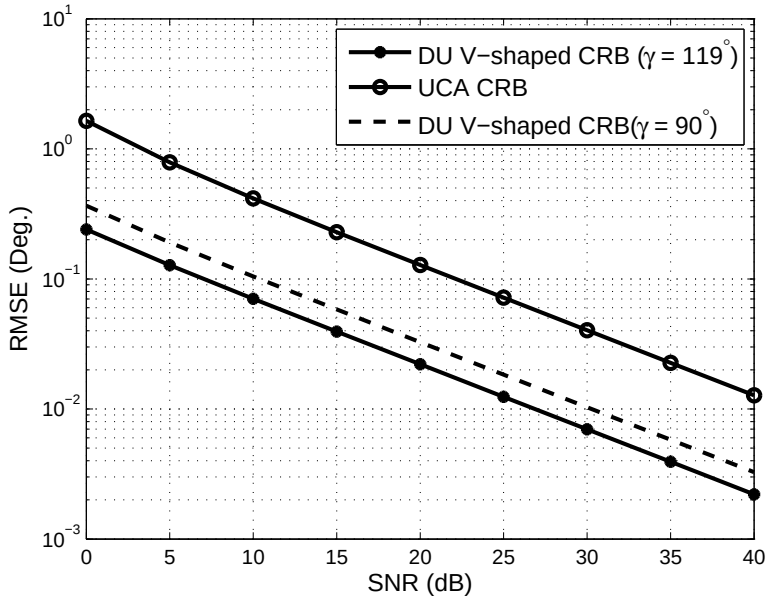

Figure 3.12: CRB DOA performance for two sources at $\phi_1 = 81°$, $\phi_2 = 98°$, respectively, when DU V-array and UCA are used (elevation angles are fixed to $\theta = 90°$).

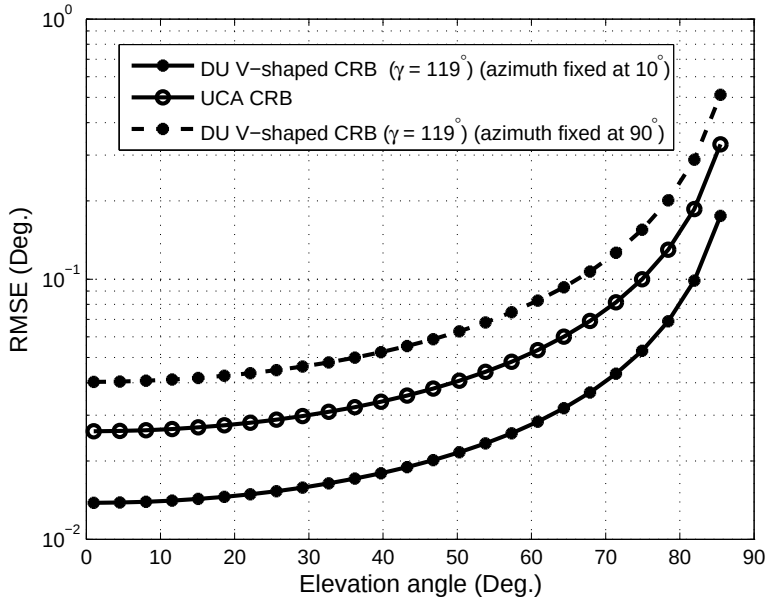

Figure 3.13: The elevation CRB for DU V-array and UCA with different azimuth angles (for ϕ_1).

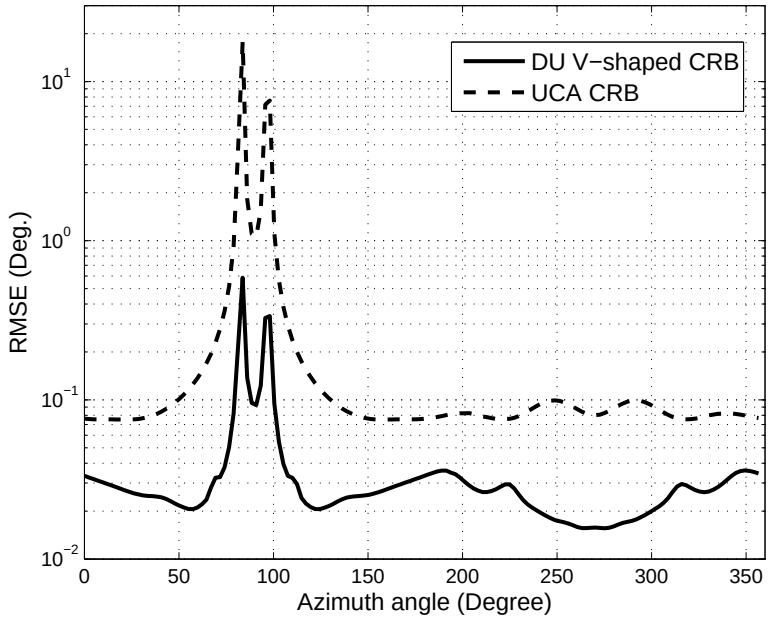

Figure 3.14: CRB DOA performance of DU V-array and UCA for three sources when one source is swept between 0 and 360 degrees while the other sources are at 83 and 99 degrees. Elevation angles are fixed to 90 degrees.

3.7 Conclusion

We have investigated the uniform and nonuniform isotropic and directional V-shaped planar arrays. Closed form expressions for the isotropic performance are presented for both uniform and nonuniform V-arrays. V-shaped isotropic arrays are compared with UCA. The comparison is done for a variety of cases which include correlated sources, sensor position errors and mutual coupling. It turns out that the isotropic V-shaped array has better performance than UCA for the same number of sensors and intersensor distance. The source signal correlation and sensor position error do not change the superiority of the UI V-array. In case of mutual coupling, UI V-shaped array has better performance for multiple sources. It is shown that DOA performance can be improved significantly when isotropic nonuniform V-shaped arrays are used.

A design method for directional uniform V-shaped array is proposed. The proposed method finds the optimum V-angle, γ°, for the specified design parameters. When the sources are in an angular sector, DU V-shaped array performs significantly better compared to UCA. It

turns out that V-shaped arrays have the better performance for the same number of sensors and inter-element distance due to its effective aperture.

CHAPTER 4

FAST AND AUTOMATICALLY PAIRED 2-D DOA ESTIMATION

4.1 Introduction

Classical DOA estimation methods including interferometer are known to perform poorly in case of multiple sources. Super-resolution techniques such as MUSIC and ESPRIT algorithms provide high accuracy for multiple sources [8], [13]. Fast methods are preferred for the implementation of super-resolution techniques in order to reduce the computational complexity. While super-resolution techniques are very effective for DOA estimation, the three important problems for DOA estimation with antenna arrays should be solved. These are the errors in antenna positions [51], antenna mutual coupling [23] and antenna gain/phase mismatches [52], [53]. These error sources are corrected to a certain extend during a calibration process. However, calibration is a long and tedious process which should be repeated periodically. In this chapter, a fast 2D paired DOA estimation method is proposed which does not require the calibration for the antenna mutual coupling. The presented technique uses the antennas in the most effective manner with the help of the array interpolation [41]. In fact, the same problem setting can be solved with more than three times the number of antennas if alternative methods [54] are used.

The target in DOA estimation is to find both azimuth and elevation angles of multiple sources. While the majority of previous works is devoted to only the estimation of azimuth angle by assuming a fixed and known elevation angle, 2-D DOA estimation is required for accurate estimation of DOA angles in practice. In fact, azimuth angle accuracy depends on the elevation and vice versa. 2-D DOA estimation can be done by a 2-D search in azimuth and

elevation simultaneously. The computational complexity of this search operation is high and fast algorithms are usually desired for practical applications. The main drawback of the fast algorithms is the pairing problem. Since the azimuth and elevation angles are found separately, a pairing problem arises where each source azimuth angle should be paired with the corresponding elevation angle. Several pairing techniques are proposed in the literature [20], [27] –[32]. Some of these methods are based on searching all the possible pairs. However the performance of these pairing methods is not satisfactory especially at low SNR. In [34], a closed form automatically paired 2-D DOA estimation algorithm is proposed which is based on phase mode excitation for UCA. The method requires special array geometry and inherits some limitations. Unitary ESPRIT based automatically paired 2-D angle estimation method is presented in [35] which uses a uniform rectangular array (URA). While this method works well, it requires several antennas and mutual coupling between antennas becomes a major problem. ESPRIT based technique in [29] automatically pairs the 2-D angles by using a marker matrix based on the eigenvectors of the signal subspace. It requires $2M + 1$ elements in the array in order to solve for M sources and it can be applied for arrays with matched co-directional triplets. The method in [36] solves the pairing problem by using $3M$ antennas while it can only distinguish $M - 1$ sources. In [37], two parallel uniform linear array (PULA) is used to have 2-D paired DOA estimation.

In this thesis, paired interpolated ESPRIT (PIE) algorithm is proposed to solve the pairing problem for arbitrary arrays. This technique requires three arrays where two of these arrays are positioned specifically with respect to the base array. In this case, the eigenvalues of the rotational transformation matrix for the ESPRIT algorithm [55], [56] contain the azimuth and elevation angle information both in the magnitude and phase terms. Closed form expressions for azimuth and elevation angles can be obtained from the resulting two equations [57]. The proposed technique is integrated with array interpolation in order to use antennas efficiently. Furthermore when $3M$ antennas are used, ESPRIT algorithm cannot be employed due to different mutual coupling terms for the doublets. Proposed method is a fast and effective technique which performs well even at low SNR.

Compensation of mutual coupling between antenna elements is critical in DOA estimation [23]. A search based method for 2-D DOA estimation for URA is proposed in the presence of mutual coupling in [25]. In [58], a fast 2-D DOA estimation method is proposed in case of mutual coupling which has pairing problem especially at low SNR. In this study, we propose

an extension of the PIE algorithm adopted for the case when there is mutual coupling. This technique works for any array which has a Toeplitz coupling matrix like the UCA. The mutual coupling matrix (MCM) for UCA has a banded Toeplitz form. This allows one to reflect the effect of mutual coupling onto the signal vector due to the commutative property of the convolution. This fact is observed in [59] and a blind technique is presented for 1-D search-based DOA estimation. Note that Isotropic Uniform (IU) V-shaped array, which is proposed in the previous chapter, has not a Toeplitz MCM. Therefore, although IU V-shaped array has better 2-D DOA performance than UCA, it is not preferred in this case.

In this chapter, two different approaches are proposed for 2-D paired DOA estimation in UCA. The first approach, blind PIE (BPIE) algorithm, does not need to estimate the mutual coupling coefficients. A modified array interpolation matrix is used to map the physical array outputs to two virtual array outputs. This mapping matrix is independent of the mutual coupling coefficients. ESPRIT algorithm is used for the 2-D paired DOA estimation by considering the virtual array outputs. While the performance of BPIE is good for a variety of cases, it degrades as the number of sources increases due to the array interpolation error. The second approach, PIE with coupling estimation (PIECE) algorithm, estimates the mutual coupling coefficients and iteratively improves both the coefficients and the 2-D DOA estimates. In this technique, an initial 2-D DOA estimate is supplied by the BPIE algorithm for the estimation of the coupling coefficients. Then both the 2-D DOA and coupling coefficient estimates are improved through iterations. It is shown that the second approach is very effective for 2-D paired DOA estimation under unknown mutual coupling.

This chapter is organized as follows: In Section 4.2, the model and the problem formulation is restated. In Section 4.3, PIE algorithm is presented for arbitrary array geometries. In Section 4.4, BPIE approach is presented for 2-D paired DOA estimation when there is mutual coupling. In addition, PIECE method is proposed in order to improve the performance of BPIE for multiple sources. The evaluations of the proposed algorithms are done in Section 4.5.

4.2 Problem Formulation

It is assumed that there are D narrowband plane waves impinging on a planar array composed of M sensors located at the positions (x_i,y_i), i=1,...,M. The DOA's of the sources are Θ_d=(ϕ_d,θ_d), d=1,...,D, where ϕ and θ are the azimuth and elevation angles, respectively. The antennas are assumed to be identical and omni-directional. Far-field assumption is made. The array output, $\mathbf{y}$(t), can be written as,

$$\mathbf{y}(t) = \mathbf{C}\mathbf{A}(\mathbf{\Theta})\mathbf{s}(t) + \mathbf{n}(t), \quad t = 1, \ldots, N \tag{4.1}$$

where N is the number of snapshots and $\mathbf{s}$(t) is a $D \times 1$ signal vector which represents a stationary, zero-mean random process uncorrelated with the noise. It is assumed that the noise, $\mathbf{n}$(t), is both spatially and temporally white with variance σ_n^2. $\mathbf{C}$ denotes the $M \times M$ symmetric mutual coupling matrix (MCM) for the antenna array. In this study, it is assumed that a special array geometry is selected such that $\mathbf{C}$ has the Toeplitz structure. For example, $\mathbf{C}$ is a complex circulant matrix with a banded Toeplitz structure for UCA [23], [46]. This matrix is composed of three bands, namely, a center band, a band at the upper right corner and a band at the lower left corner. It is assumed that the main diagonal of the MCM is normalized to unity and coupling coefficient vector which is used to construct $\mathbf{C}$ is $\mathbf{c} = [1, c_1, \ldots, c_K]^T$ where K is the number of the significant mutual coupling coefficients. Note that there is some deviation from this banded Toeplitz structure for the MCM in practical cases. The simulations done by the numerical electromagnetic field solver show that this deviation is small and its effects for the proposed method for 2-D DOA estimation can be ignored in general.

$\mathbf{A}(\mathbf{\Theta}) = [\mathbf{a}(\Theta_1) \ldots \mathbf{a}(\Theta_D)]$ is the $M \times D$ steering matrix for the planar array and the steering vector $\mathbf{a}(\Theta_d)$ is given as,

$$\mathbf{a}(\Theta_d) = [a_1(\phi_d, \theta_d) \ldots a_M(\phi_d, \theta_d)]^T, \quad d = 1, \ldots, D \tag{4.2}$$

where

$$a_i(\phi_d, \theta_d) = \exp\left\{ j\frac{2\pi}{\lambda}(x_i \cos\alpha_d + y_i \cos\beta_d) \right\}, \quad i = 1, \ldots, M \tag{4.3}$$

λ is the wavelength of the narrow-band source signals and

$$\cos\alpha_d = \cos\phi_d \sin\theta_d \tag{4.4}$$

$$\cos\beta_d = \sin\phi_d \sin\theta_d. \tag{4.5}$$

are defined for simplicity. Note that the array is positioned on a plane with $z = 0$ without loss of generality. The output covariance matrix, $\mathbf{R}$, is

$$E\{\mathbf{y}(t)\mathbf{y}(t)^H\} = \mathbf{R} = \mathbf{C}\mathbf{A}(\mathbf{\Theta})\mathbf{R}_s\mathbf{A}(\mathbf{\Theta})^H\mathbf{C}^H + \sigma^2\mathbf{I} \tag{4.6}$$

where $(.)^H$ denotes the conjugate transpose of a matrix, $\mathbf{R}_s$ is the source correlation matrix and $\mathbf{I}$ is the identity matrix.

The problem is to find the 2-D paired DOA angles, $\mathbf{\Theta}$, given the array output in (4.1). When there is no mutual coupling, $\mathbf{C} = \mathbf{I}$.

4.3 2-D Paired DOA Estimation with Array Interpolation

In this part, we present the 2-D array interpolation and the proposed method of 2-D paired interpolated ESPRIT algorithm when there is no mutual coupling. This part builds the basis for the following parts and algorithms.

4.3.1 2-D Paired DOA Estimation For No-Coupling

In this study, array interpolation is used to generate two shifted virtual arrays as shown in Figure 4.1. These virtual arrays are required to estimate the azimuth and elevation angles without the pairing problem. The virtual measurements from these arrays are combined to generate angle information in magnitude and phase terms of the eigenvalues of the rotational transformation matrix in the ESPRIT algorithm.

4.3.1.1 Automatically Pairing the Azimuth and Elevation Angles

It is assumed that the only available data comes from the real array as shown in Figure 4.1. The array output for the real array is $\mathbf{y}_1(t) = \mathbf{A}_1(\mathbf{\Theta})\mathbf{s}(t) + \mathbf{n}_1(t)$ where the positions of the M sensors are (x_i,y_i), i=1,. . . ,M. Two virtual arrays in Figure 4.1 are obtained by array interpolation and by shifting the real array. The coordinates of the antennas in virtual array-1 and 2 are selected as $(x_i + d_x,y_i + d_y)$ and $(x_i - d_x,y_i + d_y)$, respectively, where d_x and d_y are the constant terms. $\mathbf{B}_{12}$ and $\mathbf{B}_{13}$ are the mapping matrices obtained from (2.21).

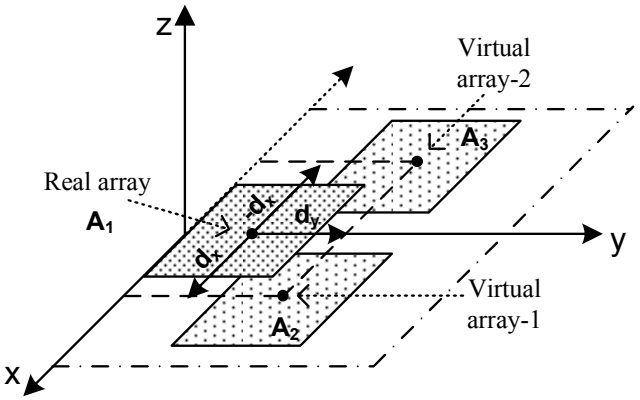

Figure 4.1: Positioning of the virtual arrays for 2-D paired DOA estimation. Virtual array-1 is obtained from the real array with a shift by (d_x, d_y). Virtual array-2 is obtained with a shift by $(-d_x, d_y)$.

The array output for the virtual array-1 is obtained as,

$$\begin{aligned} \mathbf{y}_2(t) &= \mathbf{B}_{12}\mathbf{y}_1(t) \\ \mathbf{y}_2(t) &= \mathbf{B}_{12}\mathbf{A}_1(\mathbf{\Theta})\mathbf{s}(t) + \mathbf{B}_{12}\mathbf{n}_1(t) = \mathbf{A}_2(\mathbf{\Theta})\mathbf{s}(t) + \mathbf{B}_{12}\mathbf{n}_1(t), \quad t = 1, \ldots, N \end{aligned} \tag{4.7}$$

Similarly, the array output for the virtual array-2 becomes,

$$\begin{aligned} \mathbf{y}_3(t) &= \mathbf{B}_{13}\mathbf{y}_1(t) \\ \mathbf{y}_3(t) &= \mathbf{B}_{13}\mathbf{A}_1(\mathbf{\Theta})\mathbf{s}(t) + \mathbf{B}_{13}\mathbf{n}_1(t) = \mathbf{A}_3(\mathbf{\Theta})\mathbf{s}(t) + \mathbf{B}_{13}\mathbf{n}_1(t), \quad t = 1, \ldots, N \end{aligned} \tag{4.8}$$

In (4.7) and (4.8), perfect array interpolation is assumed and $\mathbf{B}_{12}\mathbf{A}_1(\mathbf{\Theta}) = \mathbf{A}_2(\mathbf{\Theta})$, $\mathbf{B}_{13}\mathbf{A}_1(\mathbf{\Theta}) = \mathbf{A}_3(\mathbf{\Theta})$. In practice, these relations hold approximately even though the error is small. The effect of array interpolation error is considered in section 4.5. Virtual array steering matrices $\mathbf{A}_2(\mathbf{\Theta})$ and $\mathbf{A}_3(\mathbf{\Theta})$ are related to the real array as,

$$\mathbf{A}_2(\mathbf{\Theta}) = \mathbf{A}_1(\mathbf{\Theta})\mathbf{\Phi}_1 \tag{4.9}$$

$$\mathbf{A}_3(\mathbf{\Theta}) = \mathbf{A}_1(\mathbf{\Theta})\mathbf{\Phi}_2 \tag{4.10}$$

The displacements should be selected as,

$$d_x = d_y = d \leq \lambda/4 \tag{4.11}$$

in order to have an unambiguous angle solution. $\mathbf{\Phi}_1$ and $\mathbf{\Phi}_2$ can be written as,

$$\mathbf{\Phi}_1 = diag\left\{\exp\left(j\frac{2\pi}{\lambda}d(\cos\alpha_1 + \cos\beta_1)\right), \ldots, \exp\left(j\frac{2\pi}{\lambda}d(\cos\alpha_D + \cos\beta_D)\right)\right\} \tag{4.12}$$

$$\mathbf{\Phi}_2 = diag\left\{\exp\left(j\frac{2\pi}{\lambda}d(-\cos\alpha_1+\cos\beta_1)\right),\ldots,\exp\left(j\frac{2\pi}{\lambda}d(-\cos\alpha_D+\cos\beta_D)\right)\right\} \quad (4.13)$$

The virtual array outputs $\mathbf{y}_2(t)$ and $\mathbf{y}_3(t)$ are combined in order to obtain, $\mathbf{y}_4(t)$ as,

$$\begin{aligned}\mathbf{y}_4(t) &= \mathbf{y}_2(t)+\mathbf{y}_3(t)\\ &= (\mathbf{A}_2(\mathbf{\Theta})+\mathbf{A}_3(\mathbf{\Theta}))\mathbf{s}(t)+(\mathbf{B}_{12}+\mathbf{B}_{13})\mathbf{n}_1(t)\\ \mathbf{y}_4(t) &= \mathbf{A}_1(\mathbf{\Theta})(\underbrace{\mathbf{\Phi}_1+\mathbf{\Phi}_2}_{\mathbf{\Phi}})\mathbf{s}(t)+(\mathbf{B}_{12}+\mathbf{B}_{13})\mathbf{n}_1(t), \quad t=1,\ldots,N \end{aligned} \quad (4.14)$$

where

$$\begin{aligned}\mathbf{\Phi} &= diag\left\{2\cos(\frac{2\pi}{\lambda}d\cos\alpha_1)e^{j\frac{2\pi}{\lambda}d(\cos\beta_1)},\ldots,2\cos(\frac{2\pi}{\lambda}d\cos\alpha_D)e^{j\frac{2\pi}{\lambda}d(\cos\beta_D)}\right\}\\ &= diag\{v_1,v_2,\ldots,v_D\}\end{aligned} \quad (4.15)$$

Note that the magnitude components of v_i in (4.15), $2\cos(\frac{2\pi}{\lambda}d\cos\alpha_i)$, are always positive due to (4.11). The phase component is $\arg(v_i) = \frac{2\pi}{\lambda}d\sin\phi_i\sin\theta_i$. These terms have DOA information for $i = 1,\ldots,D$ sources. The automatically paired azimuth and elevation DOA angles can be easily obtained by using the magnitude and phase terms, i.e.,

$$\frac{\arg(v_i)}{\arccos(\frac{|v_i|}{2})} = \frac{\sin\phi_i}{\cos\phi_i} = \tan\phi_i \quad (4.16)$$

$$\left(\frac{\arg(v_i)}{\frac{2\pi}{\lambda}d}\right)^2+\left(\frac{\arccos\left(\frac{|v_i|}{2}\right)}{\frac{2\pi}{\lambda}d}\right)^2 = \sin^2\theta_i. \quad (4.17)$$

Then the azimuth and elevation angles can be found as,

$$\phi_i = \arctan\left(\frac{\arg(v_i)}{\arccos\left(\frac{|v_i|}{2}\right)}\right) \quad (4.18)$$

$$\theta_i = \arcsin\left(\sqrt{\left(\frac{\arg(v_i)}{\frac{2\pi}{\lambda}d}\right)^2+\left(\frac{\arccos\left(\frac{|v_i|}{2}\right)}{\frac{2\pi}{\lambda}d}\right)^2}\right). \quad (4.19)$$

In the following subsection, the steps of the ESPRIT based automatically paired 2-D DOA estimation algorithm are presented. The proposed technique uses the real array output $\mathbf{y}_1(t)$ and the interpolated virtual measurements, $\mathbf{y}_4(t)$.

4.3.1.2 2-D Paired Interpolated ESPRIT (PIE) Algorithm

The procedure for the proposed algorithm is as follows:

Step A: Initialization

- A-1) Construct $\mathbf{B}_{12}$ and $\mathbf{B}_{13}$ by using (2.21) for the indicated real and virtual arrays as in Figure 4.1. Use an initial angular sector, $\tilde{\Theta}$, which is defined as in Section 2.4.1.

Step B: DOA Estimation

- B-1) Given $\mathbf{B}_{12}$ and $\mathbf{B}_{13}$, compute the virtual sensor outputs $\mathbf{y}_2(t)$ and $\mathbf{y}_3(t)$ using (4.7) and (4.8). Obtain an intermediate output $\mathbf{y}_4(t)$ as,

$$\mathbf{y}_4(t) = \mathbf{B}_{12}\mathbf{y}_1(t) + \mathbf{B}_{13}\mathbf{y}_1(t), \quad t = 1, \ldots, N \tag{4.20}$$

  Combine the measurements as,

$$\mathbf{y}_5(t) = \begin{bmatrix} \mathbf{y}_1(t) \\ \mathbf{y}_4(t) \end{bmatrix}, \quad t = 1, \ldots, N \tag{4.21}$$

- B-2) Apply the ESPRIT algorithm [55], [56] to the combined measurement (4.21) to compute the sample covariance matrix $\hat{\mathbf{R}} = \frac{1}{N}\sum_{t=1}^{N} \mathbf{y}_5(t)\mathbf{y}_5^H(t)$ and to find $\hat{\mathbf{S}}_1$ and $\hat{\mathbf{S}}_4$. $\hat{\mathbf{S}}_1$ and $\hat{\mathbf{S}}_4$ are matrices composed of eigenvectors in the signal spaces [55] corresponding to $\mathbf{y}_1(t)$ and $\mathbf{y}_4(t)$, respectively. The relation between $\hat{\mathbf{S}}_1$ and $\hat{\mathbf{S}}_4$ is

$$\hat{\mathbf{S}}_4 = \hat{\mathbf{S}}_1\hat{\mathbf{\Phi}} \tag{4.22}$$

  Find the least squares (LS) optimum solution for $\hat{\mathbf{\Phi}}$ as $\hat{\mathbf{\Phi}} = \hat{\mathbf{S}}_1^{\dagger}\hat{\mathbf{S}}_4$ where $\hat{\mathbf{S}}_1^{\dagger}=(\hat{\mathbf{S}}_1^H\hat{\mathbf{S}}_1)^{-1}\hat{\mathbf{S}}_1^H$ is the Moore-Penrose pseudoinverse.

- B-3) Compute the eigenvalues of $\hat{\mathbf{\Phi}}$ as

$$\hat{\mathbf{v}} = eig\{\hat{\mathbf{\Phi}}\} \tag{4.23}$$

  where $\hat{\mathbf{v}}$ is a $D \times 1$ vector. Compute the azimuth and elevation angles by using (4.18) and (4.19), respectively, for $i = 1, \ldots, D$.

For the iterative improvement, we can add the following additional step:

Step C: Iteration

- C-1) Use the estimated angles in Step B to construct $\mathbf{B}_{12}$ and $\mathbf{B}_{13}$ using (2.21) by defining the angular sectors in the neighborhood of the available DOAs as in section 2.4.2. Repeat Step B, L times (PIE-L) in order to improve the 2-D paired DOA estimates.

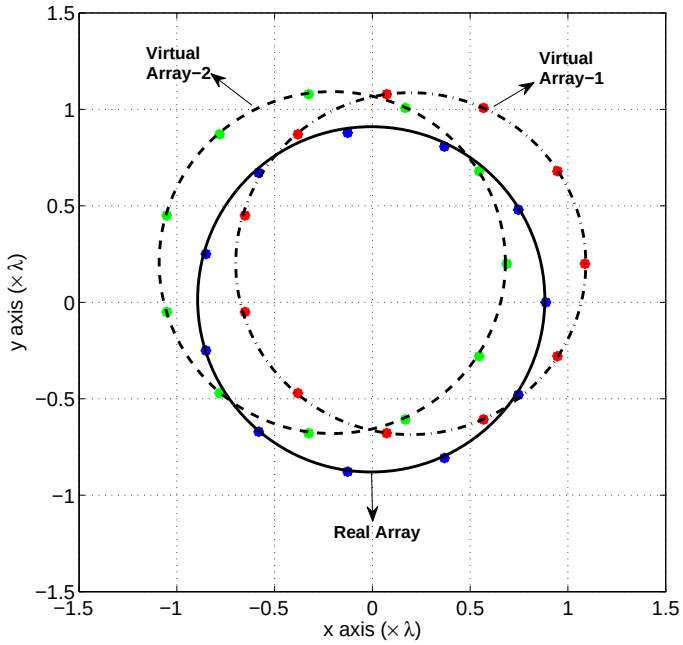

Figure 4.2: Virtual arrays positioned accordingly for UCA when $d_x = d_y = \lambda/5$.

It should be underlined again that the above method, PIE, can be applied to arbitrary array geometries if there is no mutual coupling between array elements. In the following subsection the array structures, which are used in the simulations, are presented in order to see the performance of the PIE algorithm. The selected array structures are the UCA and two Parallel Uniform Linear Array (PULA).

4.3.1.3 Uniform Circular Array (UCA)

UCA is a well known and commonly used planar array geometry in practical applications. We used $M = 11$ element UCA in simulations where the shifted virtual arrays are shown in Figure 4.2. In this case, $\mathbf{A}_1(\boldsymbol{\Theta})$ is the steering matrix of the real array and the only measurement that we have, is the outputs of this array. Then the PIE algorithm in Section 4.3.1.2 can be applied for UCA.

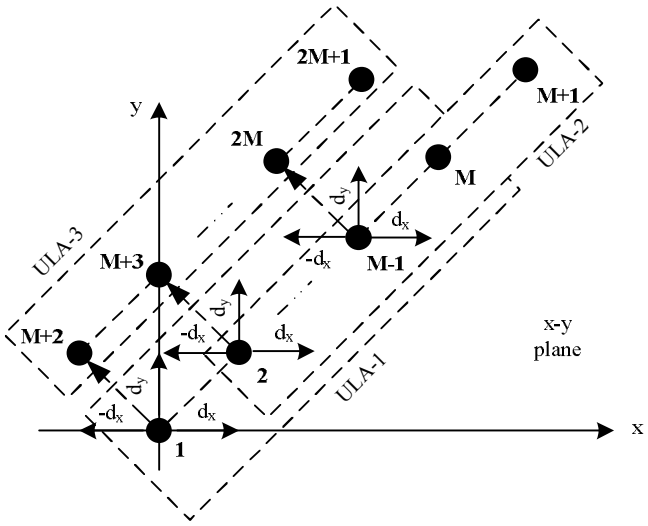

Figure 4.3: Positioning of the real PULA. ULA-2 is obtained from the ULA-1 with a shift by (d_x, d_y). ULA-3 is obtained with a shift by $(-d_x, d_y)$.

4.3.1.4 Two Parallel Uniform Linear Array (PULA)

The PULA can be placed into plane such that the shifted arrays fully overlap if the ULA is selected as the real array. In addition, PULA uses small number of sensors compared to certain planar array structures such as UCA or uniform rectangular arrays (URAs) for the same purpose. In simulations we also compare the PULA with real sensors and with the PULA generated by array interpolation.

The PULA is composed of $2M + 1$ sensors and partitioned in three ULA structures, ULA-1, ULA-2 and ULA-3 as in Figure 4.3. These three ULA structures are considered as a triplet where the proposed algorithm is applied. Each ULA is composed of M sensors. In this part, real and virtual PULAs are defined in order to compare the performances when the proposed technique is used. The real PULA structure in Figure 4.3 has $2M+1$ real sensors. On the other hand, the virtual PULA has only $M + 2$ sensors and the missing sensor data is obtained by array interpolation as shown in Figure 4.4. In both of these two array structures, it is possible to estimate M sources.

Real PULA structure: The PULA is placed at the x-y plane as in Figure 4.3. The positions of the M element ULA-1's are $[x_i, y_i]$, i=1,...,M. The coordinates of the sensors in ULA-2 and 3 are selected as $[x_i + d_x, y_i + d_y]$ and $[x_i - d_x, y_i + d_y]$, respectively, similar to Section

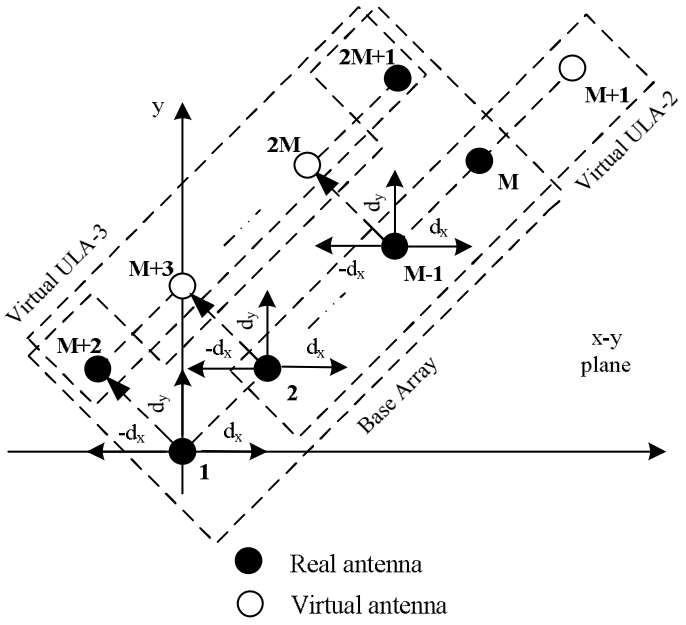

Figure 4.4: Positioning of the virtual PULA. Virtual ULA-2 and ULA-3 are obtained from the base array with array interpolation. ULA-1 is available in the base array.

4.3.1.1. The array output; ULA-1, ULA-2 and ULA-3 are,

$$\mathbf{y}_{(1)}(t) = [y_1(t), \cdots, y_M(t)]^T = \mathbf{A}_1(\mathbf{\Theta})\mathbf{s}(t) + \mathbf{n}_1(t), \quad t = 1, \ldots, N \tag{4.24}$$

$$\mathbf{y}_{(2)}(t) = [y_2(t), \cdots, y_{M+1}(t)]^T = \mathbf{A}_2(\mathbf{\Theta})\mathbf{s}(t) + \mathbf{n}_2(t), \quad t = 1, \ldots, N \tag{4.25}$$

$$\mathbf{y}_{(3)}(t) = [y_{M+2}(t), \cdots, y_{2M+1}(t)]^T = \mathbf{A}_3(\mathbf{\Theta})\mathbf{s}(t) + \mathbf{n}_3(t), \quad t = 1, \ldots, N \tag{4.26}$$

The numbers in parentheses show the ULA number. There are three ULAs which are called triplet. These array outputs of the triplet, (4.24), (4.25) and (4.26), are applied to the proposed algorithm (given in Section 4.3.1.2) in order to estimate the 2-D DOA angles. The only difference in this case is that we have all the measurements data and we do not need to use array interpolation. We can skip Step A in Section 4.3.1.2 and construct $\mathbf{y}_{(4)}(t)$ as,

$$\mathbf{y}_{(4)}(t) = \mathbf{y}_{(2)}(t) + \mathbf{y}_{(3)}(t), \quad t = 1, \ldots, N \tag{4.27}$$

Then combine $\mathbf{y}_{(4)}(t)$ as in (4.21). The rest is the same as in Step B and there is no need to use Step C.

Virtual PULA structure: The triplet outputs in the previous section can also be found using 2-D array interpolation [46]. Array interpolation is used to map a real array to a virtual array.

In this case, we have the measurements of the real sensors (black sensors) in Figure 4.4 as the base array. These sensor outputs can be written as,

$$\hat{\mathbf{y}}_{(1B)}(t) = [y_1(t), \cdots, y_M(t), y_{M+2}(t), y_{2M+1}(t)]^T = \mathbf{A}_{(1B)}(\tilde{\mathbf{\Theta}})\mathbf{s}(t) + \mathbf{n}_{(1B)}(t) \quad (4.28)$$

The size of $\hat{\mathbf{y}}_{(1B)}(t)$ is $(M+2) \times N$ and the sensor output of the base array is given in (4.28). The output of ULA-1 is $\hat{\mathbf{y}}_{(1)}(t) = [y_1(t), \cdots, y_M(t)]^T$ and the other outputs of the triplet can be calculated similar to (4.7) and (4.8) using the array mapping matrices such as,

$$\hat{\mathbf{y}}_{(2)}(t) = \mathbf{B}_{12}\hat{\mathbf{y}}_{(1B)}(t)$$

$$\hat{\mathbf{y}}_{(2)}(t) = \mathbf{B}_{12}\mathbf{A}_{(1B)}(\tilde{\mathbf{\Theta}})\mathbf{s}(t) + \mathbf{B}_{12}\mathbf{n}_{(1B)}(t) = \mathbf{A}_2(\tilde{\mathbf{\Theta}})\mathbf{s}(t) + \mathbf{B}_{12}\mathbf{n}_{(1B)}(t) \quad (4.29)$$

$$\hat{\mathbf{y}}_{(3)}(t) = \mathbf{B}_{13}\hat{\mathbf{y}}_{(1B)}(t)$$

$$\hat{\mathbf{y}}_{(3)}(t) = \mathbf{B}_{13}\mathbf{A}_{(1B)}(\tilde{\mathbf{\Theta}})\mathbf{s}(t) + \mathbf{B}_{13}\mathbf{n}_{(1B)}(t) = \mathbf{A}_3(\tilde{\mathbf{\Theta}})\mathbf{s}(t) + \mathbf{B}_{13}\mathbf{n}_{(1B)}(t) \quad (4.30)$$

where the mapping matrix $\mathbf{B}_{12}$ is used for mapping the base array outputs in (4.28), to the shifted ULA-2. Similarly $\mathbf{B}_{13}$ is used for mapping the base array outputs to the shifted ULA-3. These mapping matrices are calculated by considering two dimensional interpolation sectors for the azimuth and elevation angles. $\mathbf{B}_{12}$ and $\mathbf{B}_{13}$ are $M \times (M+2)$ matrices and computed as in Section 2.4.1. The virtual triplet outputs are obtained as in (4.28) and (4.29) and (4.30). It is now possible to apply PIE algorithm to these array outputs to find 2-D DOA angles. In section 4.5 the PIE algorithm is evaluated for these array structures.

4.4 2-D Paired DOA Estimation with Unknown Mutual Coupling

When there is mutual coupling between antennas, array interpolation cannot be used directly. In this case, array interpolation requires $\mathbf{B}_{12}\mathbf{C}\mathbf{A}_1(\mathbf{\Theta}) = \mathbf{C}\mathbf{A}_2(\mathbf{\Theta})$. Since $\mathbf{C}$ is not known, array interpolation matrix, $\mathbf{B}_{12}$, cannot be found. In order to use array interpolation, equation (4.1) should be modified such that the effect of mutual coupling is reflected onto the source signal. This can be done for circular arrays since they have a banded Toeplitz structure for the mutual coupling. Therefore equation (4.1) can be modified by using the commutative property of the convolution operation.

In this study, two different blind methods are proposed for 2-D paired DOA estimation under the mutual coupling between antennas. The first method does not require the estimation of

the mutual coupling coefficients. In the second method, mutual coupling coefficients are estimated in order to apply array interpolation.

4.4.1 2-D DOA Estimation Without Estimating the Coupling Coefficients

Coupling matrix, $\mathbf{C}$, for UCA has a banded Toeplitz form and it generates a convolution operation in (4.1). Since convolution is commutative, (4.1) can be modified to reflect the effect of coupling to the source signals. This point was considered in [23] and then in [59] where in [59], a blind search-based method is proposed for 1-D DOA estimation by estimating the mutual coupling coefficients. In this study, we use the same idea to find 2-D paired DOA estimates without estimating the mutual coupling coefficients and without employing a search process. The equation in (4.1) can be modified as,

$$\begin{aligned} \mathbf{y}(t) &= \mathbf{C}\mathbf{A}(\mathbf{\Theta})\mathbf{s}(t) + \mathbf{n}(t) \\ &= \mathbf{T}(\mathbf{\Theta})\mathbf{G}_c\mathbf{s}(t) + \mathbf{n}(t), \quad t = 1, \ldots, N \end{aligned} \tag{4.31}$$

where $\mathbf{T}(\mathbf{\Theta}) = [\mathbf{T}(\Theta_1) \ldots \mathbf{T}(\Theta_D)]$. $\mathbf{T}(\Theta_i)$ is a complex $M \times (K+1)$ matrix where K is the number of unique coefficients in the MCM. $\mathbf{T}(\Theta_i)$ is given as,

$$\mathbf{T}(\Theta_i) = \begin{cases} [\mathbf{a}(\Theta_i) \;\; f_1(\mathbf{a}(\Theta_i)) + f_{2K}(\mathbf{a}(\Theta_i)) \;\; f_2(\mathbf{a}(\Theta_i)) + f_{2K-1}(\mathbf{a}(\Theta_i)) \ldots \\ \qquad \ldots f_K(\mathbf{a}(\Theta_i)) + f_{K+1}(\mathbf{a}(\Theta_i))], & \text{if } M \text{ is odd} \\ [\mathbf{a}(\Theta_i) \;\; f_1(\mathbf{a}(\Theta_i)) + f_{2K}(\mathbf{a}(\Theta_i)) \;\; f_2(\mathbf{a}(\Theta_i)) + f_{2K-1}(\mathbf{a}(\Theta_i)) \ldots \\ \qquad \ldots f_{K-1}(\mathbf{a}(\Theta_i)) + f_{K+1}(\mathbf{a}(\Theta_i)) \;\; f_K(\mathbf{a}(\Theta_i))], & \text{if } M \text{ is even} \end{cases} \tag{4.32}$$

where $f_n(\mathbf{z})$ is the circular shift function which shifts the elements of the vector $\mathbf{z}$ by n. $\mathbf{G}_c$ is the $D(K+1) \times D$ matrix given as,

$$\mathbf{G}_c = \begin{bmatrix} \mathbf{c} & \cdots & \mathbf{0} \\ \vdots & \ddots & \vdots \\ \mathbf{0} & \cdots & \mathbf{c} \end{bmatrix}. \tag{4.33}$$

where $\mathbf{c} = [1, c_1, \ldots, c_K]_{1\times K+1}$ and $\mathbf{0} = [0, \ldots, 0]_{1\times K+1}$. Given equation (4.31), array interpolation matrices, $\bar{\mathbf{B}}_{12}$, $\bar{\mathbf{B}}_{13}$ for two virtual arrays in Figure 4.2 can be written as,

$$\begin{aligned} \bar{\mathbf{B}}_{12}\mathbf{T}_1(\tilde{\Theta}) &= \mathbf{T}_2(\tilde{\Theta}) \\ \bar{\mathbf{B}}_{13}\mathbf{T}_1(\tilde{\Theta}) &= \mathbf{T}_3(\tilde{\Theta}) \end{aligned} \tag{4.34}$$

where $\mathbf{T}_1(\tilde{\Theta})$, $\mathbf{T}_2(\tilde{\Theta})$ and $\mathbf{T}_3(\tilde{\Theta})$ are $M \times D(K+1)$ matrices obtained from (4.32) by considering the corresponding array steering vectors. They are the modified or transformed versions of the steering matrices $\mathbf{A}_1(\tilde{\Theta})$, $\mathbf{A}_2(\tilde{\Theta})$ and $\mathbf{A}_3(\tilde{\Theta})$, respectively. $\bar{\mathbf{B}}_{12}$ and $\bar{\mathbf{B}}_{13}$ are $M \times M$ matrices. $\mathbf{A}_1(\tilde{\Theta})$ is the steering matrix for the real array. $\mathbf{A}_2(\tilde{\Theta})$ and $\mathbf{A}_3(\tilde{\Theta})$ are the steering matrices for the virtual arrays as shown in Figure 4.2. $\mathbf{A}_1(\tilde{\Theta})$, $\mathbf{A}_2(\tilde{\Theta})$ and $\mathbf{A}_3(\tilde{\Theta})$ are constructed for an initial angular sector as described in section 2.4.1. The coordinates of the antennas in virtual array-1 and 2 are $(x_i + d_x, y_i + d_y)$ and $(x_i - d_x, y_i + d_y)$, respectively. The real array is positioned at (x_i, y_i), $i = 1, \ldots, M$. The mapping matrices, $\bar{\mathbf{B}}_{12}$ and $\bar{\mathbf{B}}_{13}$ can be found as in (2.21), i.e.,

$$\begin{aligned}
\bar{\mathbf{B}}_{12} &= \sigma_s^2 \mathbf{T}_2(\tilde{\Theta}) \mathbf{T}_1(\tilde{\Theta})^H \left(\sigma_s^2 \mathbf{T}_1(\tilde{\Theta}) \mathbf{T}_1(\tilde{\Theta})^H + \sigma_n^2 \mathbf{I} \right)^{-1} \\
\bar{\mathbf{B}}_{13} &= \sigma_s^2 \mathbf{T}_3(\tilde{\Theta}) \mathbf{T}_1(\tilde{\Theta})^H \left(\sigma_s^2 \mathbf{T}_1(\tilde{\Theta}) \mathbf{T}_1(\tilde{\Theta})^H + \sigma_n^2 \mathbf{I} \right)^{-1}
\end{aligned} \tag{4.35}$$

The sensor outputs of the two virtual arrays can be found similar to (4.7) and (4.8) using $\bar{\mathbf{B}}_{12}$ and $\bar{\mathbf{B}}_{13}$ and by considering the equation in (4.31). $\mathbf{T}_1(\tilde{\Theta})$, $\mathbf{T}_2(\tilde{\Theta})$ and $\mathbf{T}_3(\tilde{\Theta})$ are related as

$$\mathbf{T}_2(\tilde{\Theta}) \mathbf{G}_c = \mathbf{T}_1(\tilde{\Theta}) \mathbf{G}_c \mathbf{\Phi}_1 \tag{4.36}$$

$$\mathbf{T}_3(\tilde{\Theta}) \mathbf{G}_c = \mathbf{T}_1(\tilde{\Theta}) \mathbf{G}_c \mathbf{\Phi}_2 \tag{4.37}$$

similar to (4.9) and (4.10). (4.36) and (4.37) allow us to use the ESPRIT algorithm for fast DOA estimation. In addition, due to the special form of the virtual arrays, azimuth and elevation angles are found in pairs. In this approach, it is sufficient to know the number of coupling coefficients, K. This algorithm is called 2-D Blind Paired Interpolated ESPRIT (2-D BPIE). The algorithmic steps for the BPIE algorithm are given as,

Step 1: Initialization

- Select an initial angular sector $\tilde{\Theta}$ as in section 2.4.1 and construct the array interpolation matrices $\bar{\mathbf{B}}_{12}$ and $\bar{\mathbf{B}}_{13}$ using (4.32) and (4.35).

Step 2: DOA Estimation

- Apply Step B of the PIE algorithm in section 4.3.1.2 for DOA estimation.

Step 3: Iteration

- Iterate Step 2 L times, (BPIE-L), to construct $\bar{\mathbf{B}}_{12}$ and $\bar{\mathbf{B}}_{13}$ by using (4.35) and the angular sectors in the neighborhood of the available DOAs as in section 2.4.2.

4.4.2 2-D DOA Estimation by Estimating the Coupling Coefficients

While the performance of BPIE is good for one source, it is not satisfactory in case of multiple sources. The size and the condition number of the mapping matrices, $\bar{\mathbf{B}}_{12}$ and $\bar{\mathbf{B}}_{13}$ are large for multiple sources and this degrades the array interpolation performance. In this part, we present a blind method which estimates the coupling coefficients before array interpolation. Then, coupling coefficients and DOA angles are estimated in sequence and it is called 2-D Paired Interpolated ESPRIT with Coupling Estimation (2-D PIECE).

PIECE algorithm uses the BPIE algorithm in order to find an initial DOA estimate as a first step. Then the coupling coefficients are found in order to improve the array interpolation performance. The estimation of DOA angles and the coupling coefficients are done iteratively to improve the performance. While the iterations do not guarantee the convergence, they improve the accuracy significantly with high probability as in [41]. The main reason for this is the technique that uses a small angular sector in the neighborhood of the initial DOA estimation. Therefore the accuracy of the array interpolation improves with the first iteration assuming that the initial DOA angle is estimated sufficiently well.

In order to estimate the mutual coupling coefficients, a similar approach is followed as in [59]. The difference in our case is the initial 2-D paired DOA estimates are available through the BPIE algorithm. Furthermore a closed form solution is used for the coefficients instead of a search process as in [23] and [59]. The mutual coupling vector, $\mathbf{c}$, is found by considering the array output of the real array and by solving the following constrained minimization problem,

$$\mathbf{c} = \arg\min_{\mathbf{c}} \|\mathbf{E}^H \mathbf{T}_1(\hat{\boldsymbol{\Theta}})\mathbf{G}_{\mathbf{c}}\|^2 \quad \text{subject to} \quad \mathbf{c}^H\mathbf{w} = 1 \tag{4.38}$$

where $\mathbf{E}$ is the matrix composed of eigenvectors in the noise subspace obtained from the sample covariance matrix of $\mathbf{y}(t)$, $\mathbf{R}_y = \frac{1}{N}\sum_{t=1}^{N} \mathbf{y}(t)\mathbf{y}(t)^H$, and $\mathbf{w} = [1, 0, \ldots, 0]^T$. The constraint $\mathbf{c}^H\mathbf{w} = 1$ is used to obtain a nontrivial solution. Note that $\mathbf{T}_1(\hat{\boldsymbol{\Theta}})$ is constructed from (4.32) for the real array by using the initial estimate $\hat{\boldsymbol{\Theta}}$=[$\hat{\Theta}_1$, ..., $\hat{\Theta}_D$] for the source DOAs. The normed expression in (4.38) can be written as,

$$\|\mathbf{E}^H\mathbf{T}_1(\hat{\Theta})\mathbf{G}_c\|^2 = tr\{\mathbf{G}_c^H \underbrace{\mathbf{T_1}(\hat{\mathbf{\Theta}})^H\mathbf{E}\mathbf{E}^H\mathbf{T_1}(\hat{\mathbf{\Theta}})}_{\mathbf{Q}}\mathbf{G}_c\} = tr\{\mathbf{G}_c^H\mathbf{Q}\mathbf{G}_c\} \tag{4.39}$$

where

$$\mathbf{G}_c^H\mathbf{Q}\mathbf{G}_c = \begin{bmatrix} \mathbf{c}^H & \cdots & \mathbf{0} \\ \vdots & \ddots & \vdots \\ \mathbf{0} & \cdots & \mathbf{c}^H \end{bmatrix}\begin{bmatrix} \mathbf{Q}_{11} & \cdots & \mathbf{Q}_{1D} \\ \vdots & \ddots & \vdots \\ \mathbf{Q}_{D1} & \cdots & \mathbf{Q}_{DD} \end{bmatrix}\begin{bmatrix} \mathbf{c} & \cdots & \mathbf{0} \\ \vdots & \ddots & \vdots \\ \mathbf{0} & \cdots & \mathbf{c} \end{bmatrix}. \tag{4.40}$$

The dimensions of the $\mathbf{Q}_{i,j}$ sub-matrices are $(K+1)\times(K+1)$. It is possible to express $tr\{\mathbf{G}_c^H\mathbf{Q}\mathbf{G}_c\}$ as

$$tr\{\mathbf{G}_c^H\mathbf{Q}\mathbf{G}_c\} = \mathbf{c}^H\left(\sum_{i=1}^{D}\mathbf{Q}_{ii}\right)\mathbf{c}. \tag{4.41}$$

If we apply the Lagrangian approach for the solution of the modified constraint equation of (4.38), we obtain the coupling coefficients as,

$$\hat{\mathbf{c}} = \frac{\left(\sum_{i=1}^{D}\mathbf{Q}_{ii}\right)^{-1}\mathbf{w}}{\mathbf{w}^H\left(\sum_{i=1}^{D}\mathbf{Q}_{ii}\right)^{-1}\mathbf{w}}. \tag{4.42}$$

Once the coupling coefficients are found, banded Toeplitz MCM estimate, $\hat{\mathbf{C}}$, can be constructed easily [23], [46]. The array interpolation matrices $\hat{\mathbf{B}}_{12}$ and $\hat{\mathbf{B}}_{13}$ required for generating the two virtual arrays in Figure 4.2 can be found from,

$$\begin{aligned} \hat{\mathbf{B}}_{12}\hat{\mathbf{C}}\mathbf{A}_1(\tilde{\Theta}) &= \hat{\mathbf{C}}\mathbf{A}_2(\tilde{\Theta}) \\ \hat{\mathbf{B}}_{13}\hat{\mathbf{C}}\mathbf{A}_1(\tilde{\Theta}) &= \hat{\mathbf{C}}\mathbf{A}_3(\tilde{\Theta}) \end{aligned} \tag{4.43}$$

where $\mathbf{A}_1(\tilde{\Theta})$, $\mathbf{A}_2(\tilde{\Theta})$ and $\mathbf{A}_3(\tilde{\Theta})$ are constructed as explained in section 2.4.1 for the given angular sector. In this case, the mapping matrices can be found as,

$$\begin{aligned} \hat{\mathbf{B}}_{12} &= \sigma_s^2\hat{\mathbf{C}}\mathbf{A}_2(\tilde{\Theta})\mathbf{A}_1(\tilde{\Theta})^H\hat{\mathbf{C}}^H\left(\sigma_s^2\hat{\mathbf{C}}\mathbf{A}_1(\tilde{\Theta})\mathbf{A}_1(\tilde{\Theta})^H\hat{\mathbf{C}}^H + \sigma_n^2\mathbf{I}\right)^{-1} \\ \hat{\mathbf{B}}_{13} &= \sigma_s^2\hat{\mathbf{C}}\mathbf{A}_3(\tilde{\Theta})\mathbf{A}_1(\tilde{\Theta})^H\hat{\mathbf{C}}^H\left(\sigma_s^2\hat{\mathbf{C}}\mathbf{A}_1(\tilde{\Theta})\mathbf{A}_1(\tilde{\Theta})^H\hat{\mathbf{C}}^H + \sigma_n^2\mathbf{I}\right)^{-1}. \end{aligned} \tag{4.44}$$

$\hat{\mathbf{B}}_{12}$ and $\hat{\mathbf{B}}_{13}$ are used in the PIECE algorithm for array interpolation in order to decrease

the error for multiple sources. $\hat{\mathbf{C}}$ and DOAs are improved iteratively. The procedure for the PIECE algorithm is as follows:

Step 1: Initialization

- Apply the BPIE algorithm in section 4.4.1, L times (BPIE-L) in order to obtain an estimate for paired 2-D DOA angles. Usually $L = 1$ gives satisfactory results, but $L > 1$ can improve the performance to a certain extend.

Step 2: DOA and C Estimation

- Using the 2-D DOA angles, estimate the coupling coefficients $\hat{\mathbf{c}}$ as in (4.42) and construct MCM, $\hat{\mathbf{C}}$. Find $\hat{\mathbf{B}}_{12}$ and $\hat{\mathbf{B}}_{13}$ by using (4.44) and by defining angular sectors in the neighborhood of the available DOA's as in Section 2.4.2. Apply the Step B of the PIE algorithm in section 4.3.1.2 to find DOA angles.

Step 3: Iteration

- Repeat Step 2, P times (PIECE-P) in order to improve the 2-D paired DOA and coupling coefficients estimates iteratively.

4.5 Simulation Results

In this section, the proposed methods are evaluated in order to show the 2-D paired DOA performance. A UCA with $M = 11$ omni-directional and identical antennas is used as shown in Figure 4.2. The distance between adjacent elements in the UCA is half a wavelength, i.e., $\lambda/2$. There are 250 trials for each experiment and the number of snapshots is 256. The results are the average of all trials and none of the trial results are excluded in order to have an unbiased evaluation of the proposed methods. The array mapping described in previous sections is used to obtain the shifted virtual UCA as shown in Figure 4.2. 2-D array interpolation sectors are chosen as $\phi \in [-10^\circ, 20^\circ]$ and $\theta \in [20^\circ, 50^\circ]$. These sectors are indicated in each figure as vertical dashed lines. The displacements in (4.11) are taken as $d_x = d_y = \lambda/5$ in simulations.

The evaluations are done in two parts, namely, when there is no coupling and when there is mutual coupling. The experimental settings in case of mutual coupling are the same as

in the case when there is no mutual coupling. In addition to this simulation setting, another array structure which is given in Section 4.3.1.4 is used only in no mutual coupling case. Accordingly, for the real and virtual PULA there are 250 trials for each experiment and the number of snapshots is 256. The number of sensors in the real PULA is $2M + 1 = 15$ where M is the number of sensors of ULA-1 in Figure 4.3. For the virtual PULA in Figure 4.4, the total number of the real sensors is $M + 2 = 9$ and 2-D array interpolation sectors are chosen as $\phi \in [130°, 160°]$, $\theta \in [30°, 60°]$. In the simulations, $d_x = d_y = \lambda/4$ is selected and the distance between each antenna in the PULA is $\sqrt{2}\lambda/4$.

4.5.1 No mutual coupling

In this part, it is assumed that there is no mutual coupling, $\mathbf{C} = \mathbf{I}$, and the proposed PIE algorithm is evaluated.

4.5.1.1 UCA

In this section the UCA is used as the array structure. Figure 4.5(a) shows the azimuth DOA performance when there is a single source. SNR is set to 15 dB. The source elevation angle is fixed at 28 degrees. The azimuth angle of the source is swept between -65 and 70 degrees in one degree resolution. This figure shows that iterations improve the DOA performance significantly. Furthermore the performance is good even for the out-of-sector sources. The elevation performance is given in Figure 4.5(b). In this case, azimuth angle is fixed at 6 degrees and the elevation angle is swept between 0 and 89 degrees. The elevation angle performance of PIE is good after eight iterations. Overall, DOA performance approaches to the CRB.

Figure 4.6(a) shows the azimuth DOA performance when there are two sources and SNR=15 dB. One source is inside the interpolation sector fixed at (ϕ_1=11°, θ_1=40°). The elevation angle for the second source is fixed at θ_2=26°. The azimuth angle is swept between $-65°$ and 70° in one degree resolution. This figure shows that PIE algorithm performs well even for the out-of-sector sources. In addition, no outlier is observed for 250 trials and PIE accurately solves the pairing problem. In fact, the 2-D paired DOA estimation is achieved for a larger sector than the initial one. Figure 4.6(b) shows the elevation performance. In this case, there

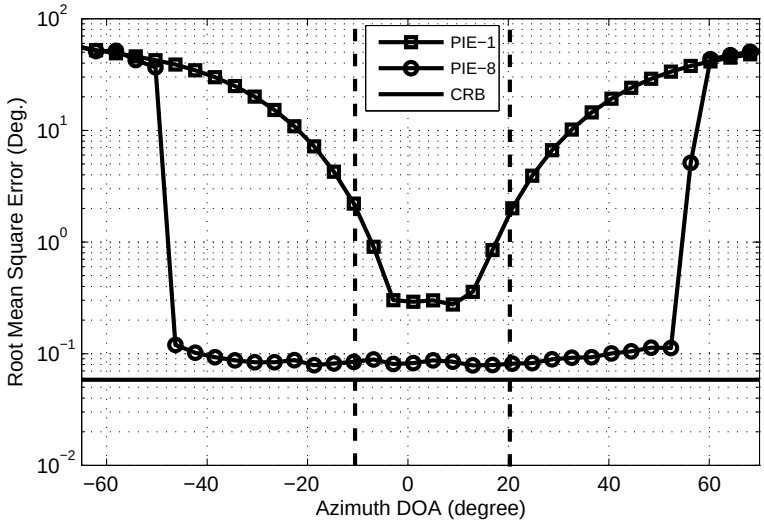

(a)

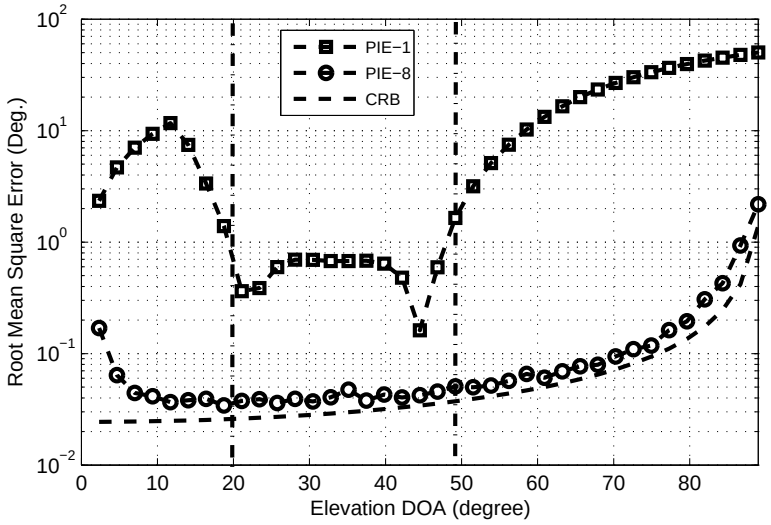

(b)

Figure 4.5: 2-D paired DOA performance for a single source. SNR is 15 dB. There is no mutual coupling between antennas. (a) Azimuth performance (b) Elevation performance.

is one source inside the sector and it is fixed at (ϕ_1=11°, θ_1=40°). The azimuth angle of the second source is kept fixed at ϕ_2=−2°. The elevation angle is swept between 0° and 89°. The elevation angle performance is also good for a large sector.

In Figure 4.7(a) and Figure 4.7(b), the performance of the proposed method is shown for closely spaced sources. While it is known that the performance of superresolution algorithms are limited by the CRB, array beamwidth is used as an auxiliary factor for performance evaluation. It is also known that the superresolution algorithms such as the one proposed in this paper, have a resolution which is approximately one tenth of the array half power beamwidth [60]. The azimuth and elevation beamwidths for the circular array are 53 and 32 degrees, respectively for the given simulation settings. In Figure 4.7(a), there is a fixed source inside the sector at (11°, 26°) and the second source has a fixed elevation angle at 26°. Its azimuth angle is swept between -70 and 80 degrees in 0.5 degree resolution. Figure 4.7(a) shows the azimuth angle performance and it is seen that the proposed method performs well. In Figure 4.7(b), there is a fixed source inside the sector at (-2°, 40°) and the second source azimuth angle is fixed at -2 degrees while its elevation angle is swept between 0 and 89 degrees. The performance of the proposed method is also good for the elevation angle in case of closely spaced sources. Array interpolation can be performed more accurately for the closely spaced sources since the interpolation sector is narrow for such sources after the initial DOA estimation. This in turn improves the DOA performance as it is observed in Figure 4.7. However as the SNR is improved, the array interpolation error becomes dominant and this leads to a flooring effect in case of closely spaced sources.

In Figures 4.5, 4.6 and 4.7, it is observed that 2-D paired DOA estimation can be done accurately for some out-of-sector sources as well. Even though the initial array interpolation matrices are constructed to map only the inside-the-sector sources accurately, iterations and narrow sectors in the neighborhood of DOA estimates generate a convergence towards the true DOA angles. While there is no guarantee for a monotonic DOA improvement at each iteration, the convergence towards the true DOA angle is with high probability. In Figure 4.8, this phenomenon is shown for both single and two source cases. SNR=15 dB and the results of four iterations are shown. In Figure 4.8(a), the elevation angle of the single source is inside the sector and at 30 degrees while the azimuth angle is outside the sector and at -36 degrees. The initial azimuth estimate after array interpolation is found inside the sector as shown in the figure. Arrows indicate the move in the estimations as the iterations increase. As it is seen

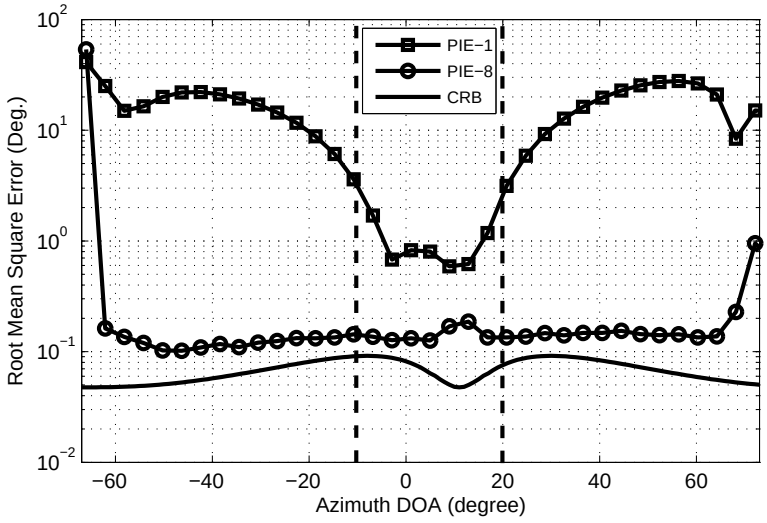

(a)

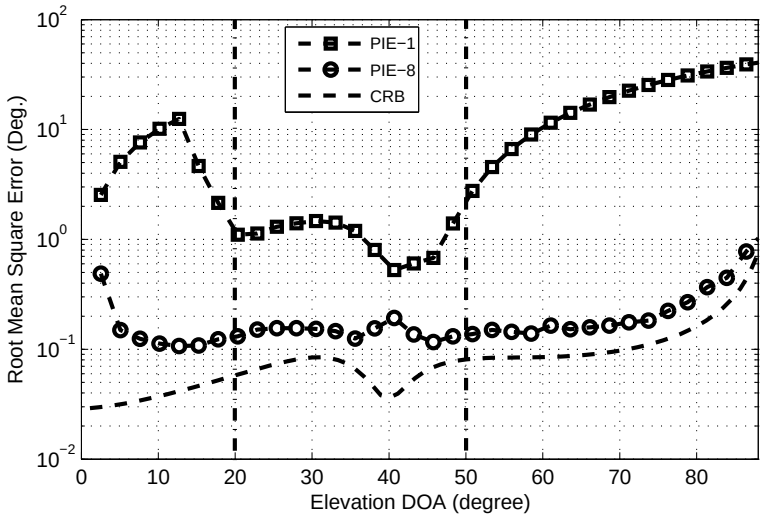

(b)

Figure 4.6: 2-D paired DOA performance for two sources for PIE algorithm. SNR is 15 dB. There is no mutual coupling between antennas. (a) Azimuth performance (b) Elevation performance.

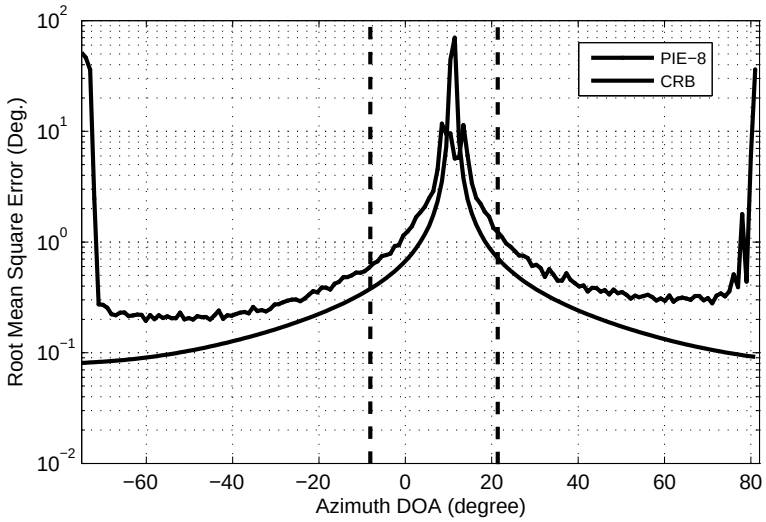

(a)

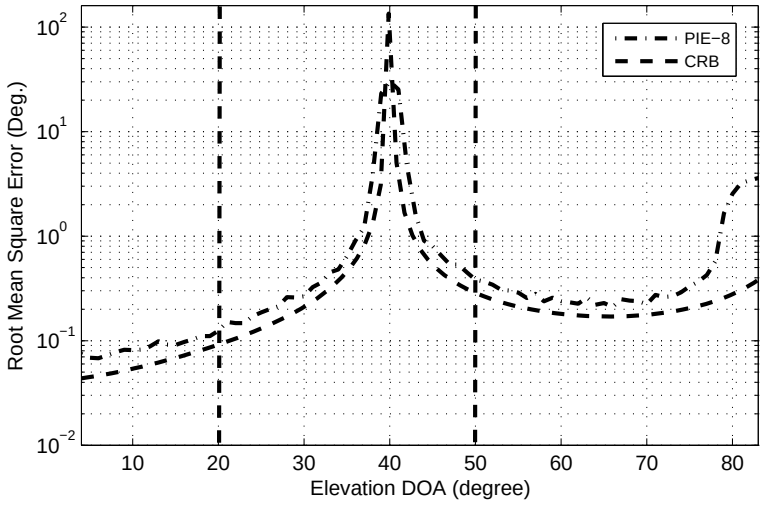

(b)

Figure 4.7: 2-D paired DOA performance for closely spaced sources for the PIE algorithm. SNR is 15 dB. (a) Azimuth performance (b) Elevation performance.

from this figure, iterations generate a convergence towards the true DOA angle. In Figure 4.8(b), a similar experiment is performed with two sources. One source is inside the sector at (ϕ_1=11°, θ_1=40°). The second source is outside the sector at (ϕ_2=−36°, θ_2=25°). It seems that the existence of one source inside the sector is useful for the convergence of the second out-of-sector source. The first estimate is found outside the sector. Convergence is achieved after four iterations.

Figure 4.9 shows the 2-D DOA performance for different SNR levels when there are two sources. The first source is at (ϕ_1=−6°, θ_1=26°) and the second source is at (ϕ_2=11°, θ_2=40°). Figure 4.9(a) and Figure 4.9(b) show the azimuth and elevation paired DOA performances, respectively. It is seen that the performance of the PIE algorithm is approximately 5 dB far from the CRB for the azimuth angle. It is about 7 dB away from the CRB for the elevation angle. Overall it is an effective algorithm when there is no mutual coupling between antennas.

4.5.1.2 PULA

In this section the real PULA and virtual PULA are used as the array structures in order to analyze the array interpolation effect.

Figure 4.10 shows the 2-D DOA performance for different SNR levels when there are two sources. The first source is at (ϕ_1=140°, θ_1=38°) and the second source is at (ϕ_2=155°, θ_2=52°). In this figure, both the azimuth and elevation DOA performances are presented. It is seen that the proposed algorithm is able to find the paired azimuth and elevation angles. Virtual PULA performance is approaching to the real PULA performance.

Figure 4.11 shows the 2-D DOA performance in the same scenario in terms of the number of snapshots. SNR is fixed at 15 dB. As the number of snapshots is increased the performance of the real and virtual PULA improve.

In Figure 4.12, the 2-D DOA estimates of the proposed method for real and virtual PULA are marked for each trial to see the angular distributions for SNR=15dB. There are 256 trials for each experiment. All the trials are marked and none of the trial results are excluded. It is seen that the real and virtual PULA have similar performances even though the real PULA has slightly better performance as expected. It is shown that virtual PULA obtained through array interpolation performs well approaching the performance of the real PULA.

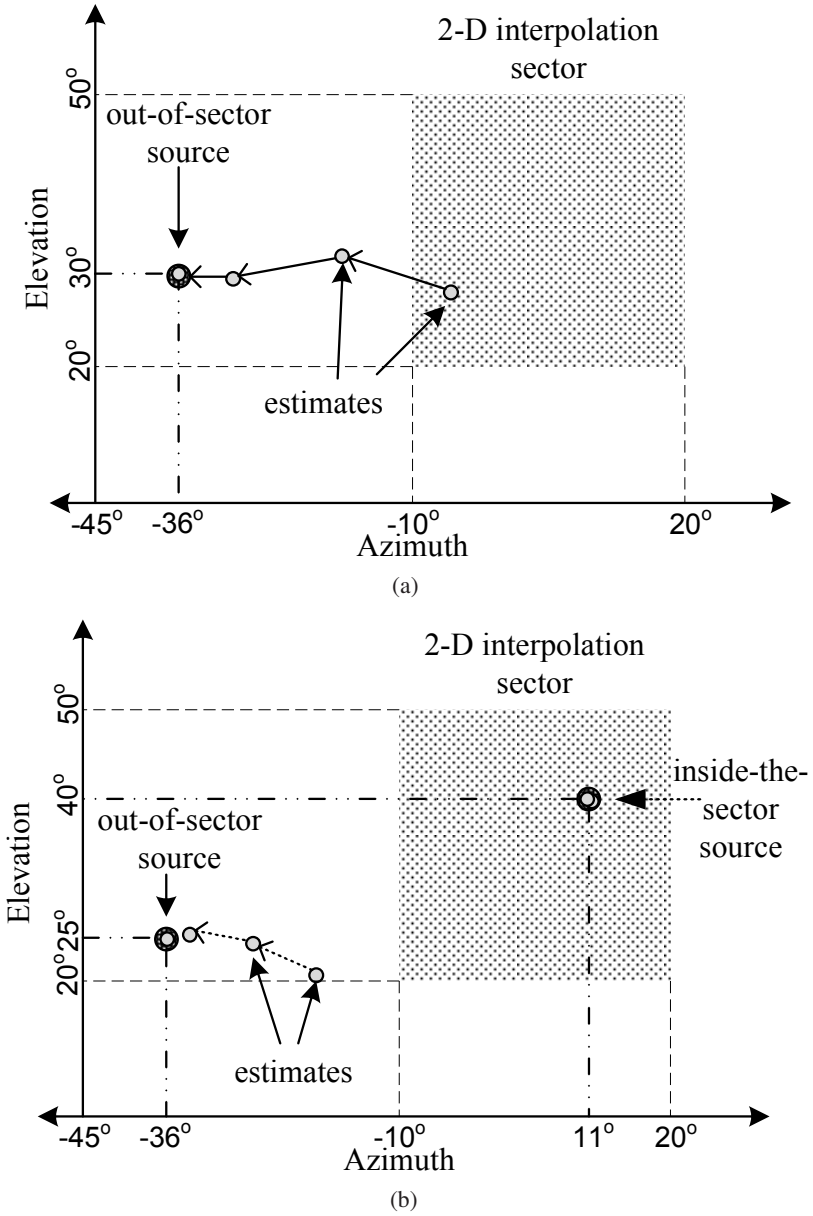

Figure 4.8: The progress in DOA estimation during iterations for the resolution of out-of-sector sources. SNR is 15 dB and there are four iterations. (a) Single source, (b) Two sources.

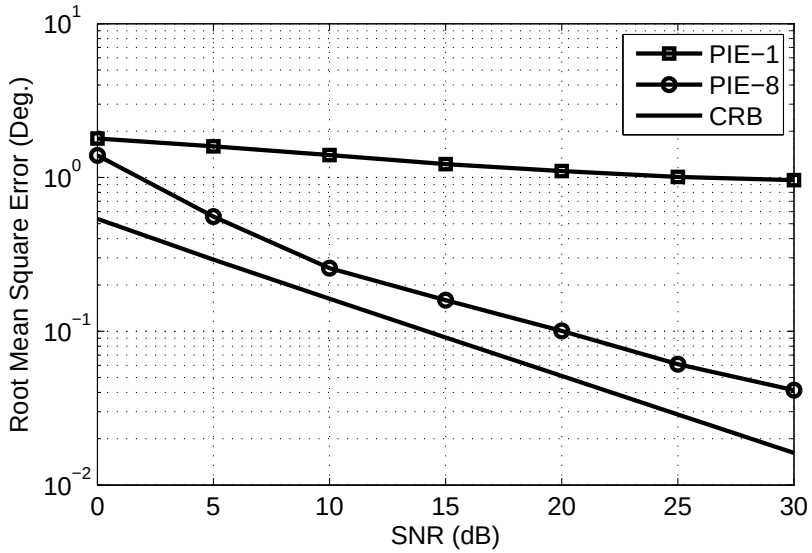

(a)

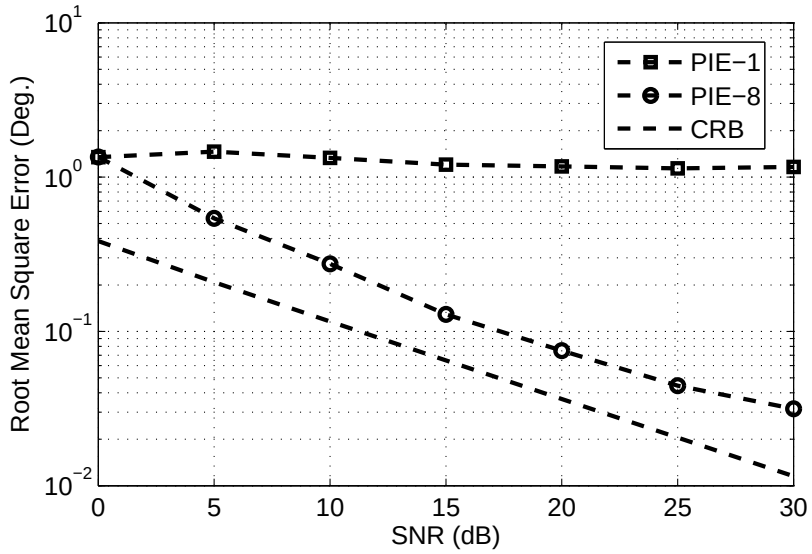

(b)

Figure 4.9: 2-D paired DOA performance for PIE when there is no-coupling between antennas and there are two sources. (a) Azimuth performance (b) Elevation performance.

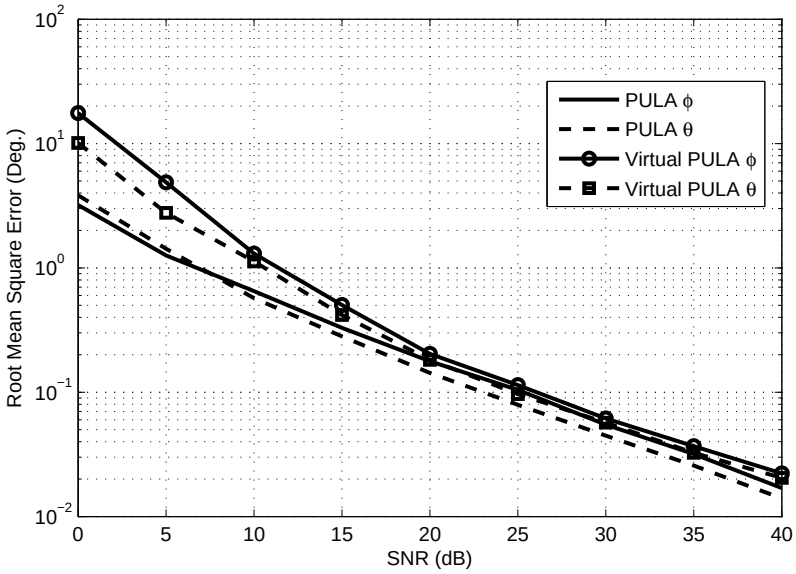

Figure 4.10: 2-D paired azimuth and elevation DOA performance for different SNR levels when there are two sources.

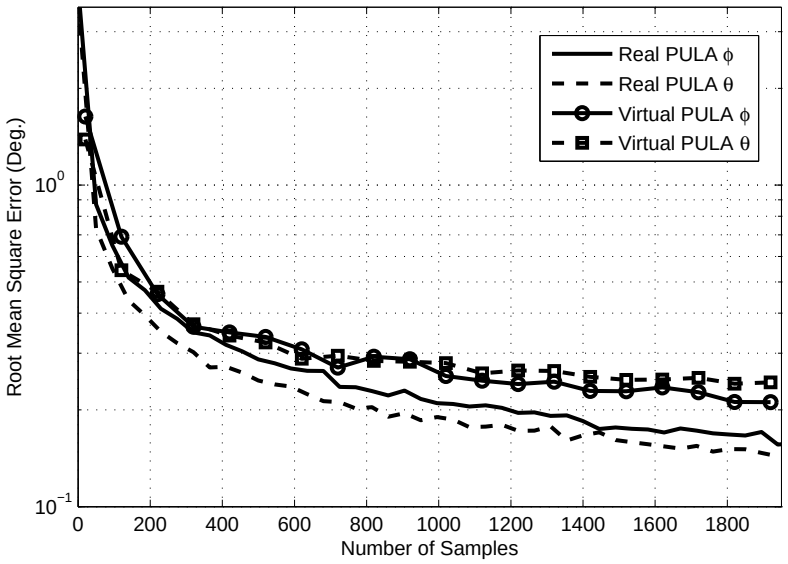

Figure 4.11: 2-D paired azimuth and elevation DOA estimates when there are two sources and SNR=15dB.

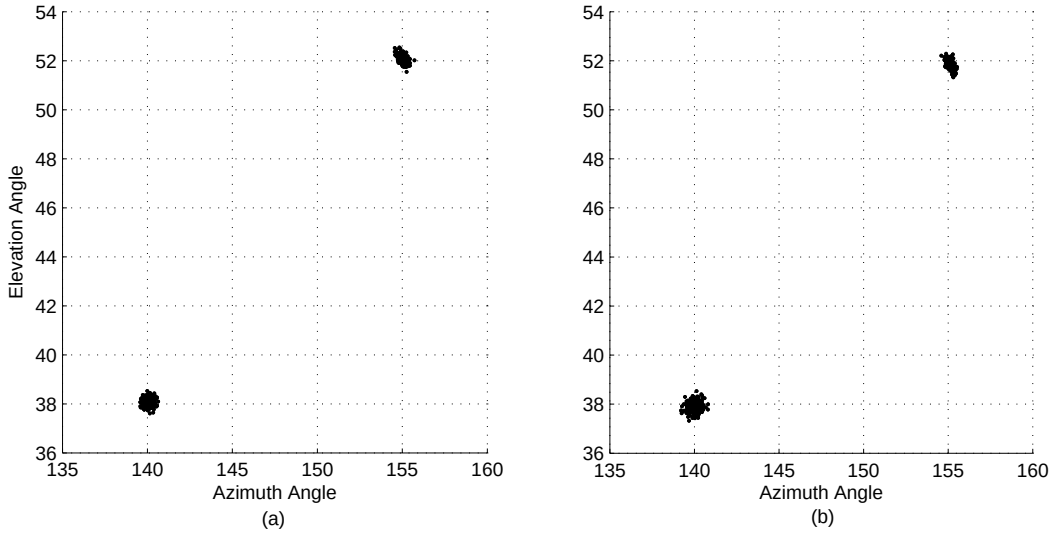

Figure 4.12: 2-D DOA distribution when there are two closely located sources and SNR=15dB. (a) Real PULA (b) Virtual PULA.

In Figure 4.13, there are four distributed sources where (ϕ_1=100°, θ_1=55°), (ϕ_2=150°, θ_2=40°), (ϕ_3=180°, θ_3=30°) and the last source is at (ϕ_4=190°, θ_4=50°). In this case, only the result of the real PULA is shown. It is seen that the proposed method can automatically solve the azimuth and elevation angles in a paired manner.

4.5.2 Mutual coupling

In this part, it is assumed that there is mutual coupling between antennas and the BPIE and PIECE algorithms are evaluated. The settings of the experiments in this part are exactly the same as described in the previous UCA part in order to have a comparison for the mutual coupling case. The same UCA structure is used. Usually it is assumed that each antenna is coupled to its nearest neighbors and coupling with other antennas are ignored as in [23], [25]. Therefore $\mathbf{c} = [1\ c_1]$ and MCM is a 11×11 banded Toeplitz matrix with five nonzero diagonals. The coupling coefficient is selected as, $c_1 = 0.35 + 0.10j$ as in [46].

First the performance of the BPIE algorithm is investigated. In Figure 4.14, BPIE performance is shown for a single source. BPIE does not estimate the mutual coupling coefficient but it performs well for a single source. Its performance follows the CRB [23] for both azimuth

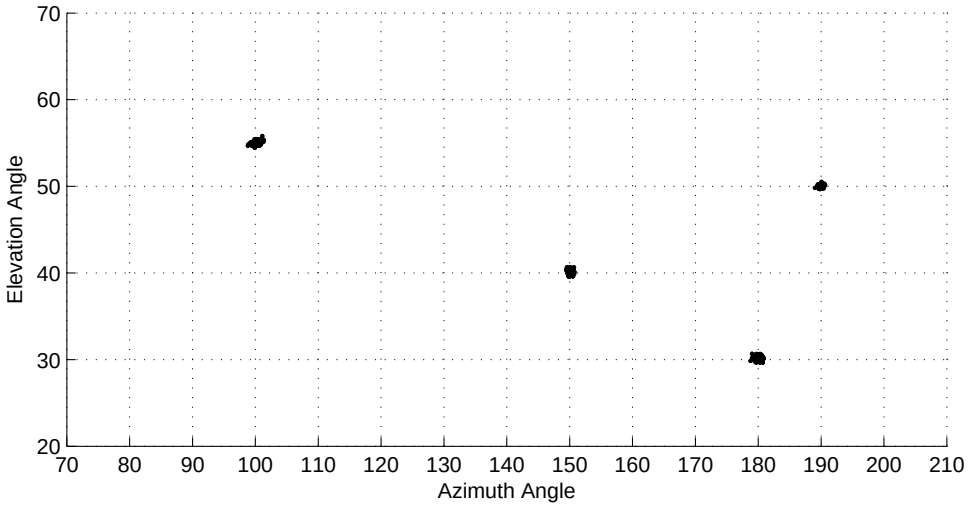

Figure 4.13: 2-D DOA distribution when there are four sources and SNR=15dB.

and elevation angles. In addition, some out-of-sector sources are also found accurately like the PIE algorithm. In fact, BPIE performs well for a larger sector than the initial one for both azimuth and elevation angles.

While the performance of BPIE is very good for a single source, it is not satisfactory for multiple sources. Figure 4.15 shows the azimuth and elevation DOA performances when there are two sources as in Figure 4.6 while there is unknown mutual coupling. Both azimuth and elevation DOA performances degrade compared to the single source case. While the azimuth performance of BPIE is acceptable for a large sector, elevation performance is satisfactory only within a limited part inside the initial sector. The performance of BPIE depends on the number of sources and it usually degrades as the number of sources increases.

The 2-D DOA performance for different SNR levels is shown in Figure 4.16 when there are two inside-the-sector sources. While azimuth SNR performance is satisfactory, elevation performance degrades significantly compared to the single source case.

In order to improve the performance of the BPIE algorithm for multiple sources, PIECE algorithm is proposed where mutual coupling coefficient is estimated. PIECE uses BPIE in order to obtain an initial DOA estimate. It is possible to iterate BPIE L times in order to obtain the initial 2-D paired DOA estimate. In the following part, the figure caption “BPIE-1, PIECE-8”is used to indicate that BPIE is iterated by $L = 1$ and PIECE algorithm is iterated

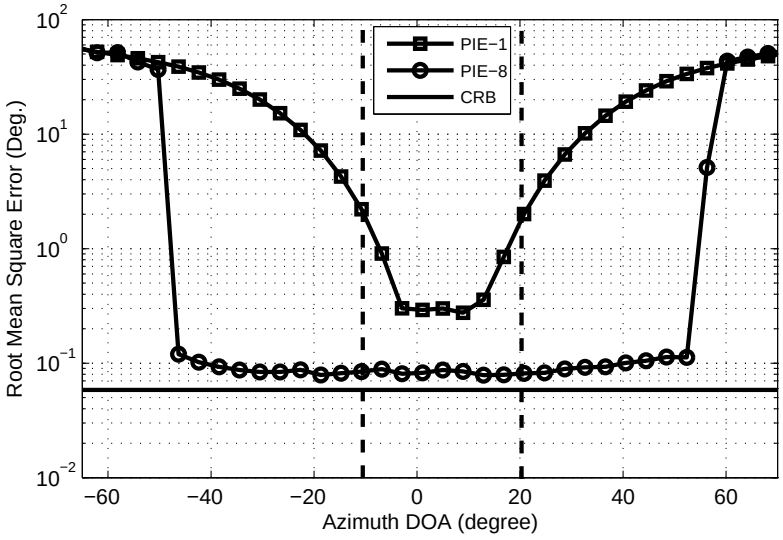

(a)

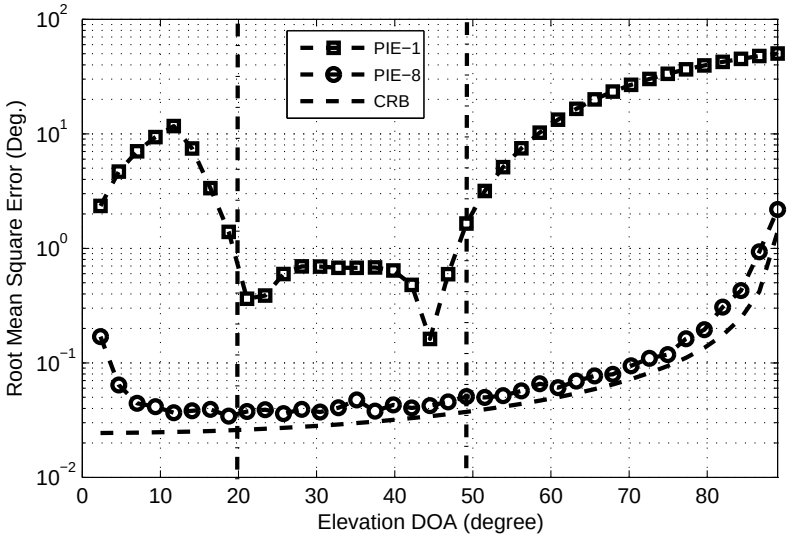

(b)

Figure 4.14: 2-D paired DOA performance for BPIE for a single source. SNR is 15 dB. There is unknown mutual coupling between antennas. (a) Azimuth performance (b) Elevation performance.

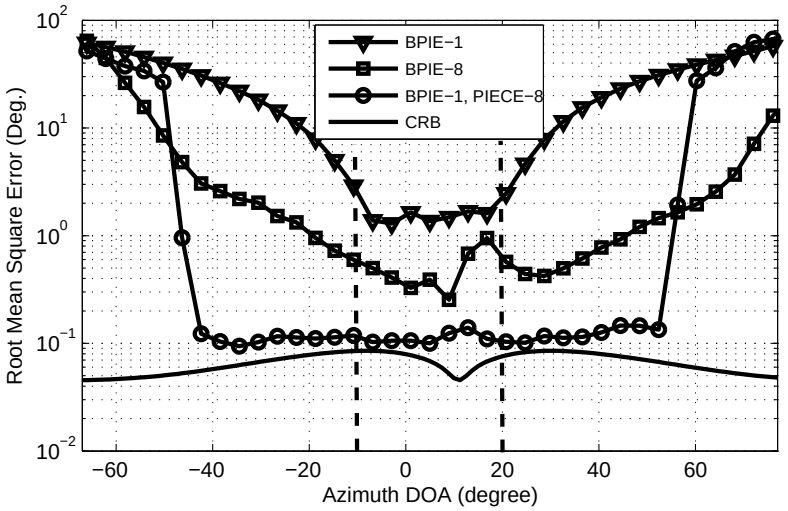

(a)

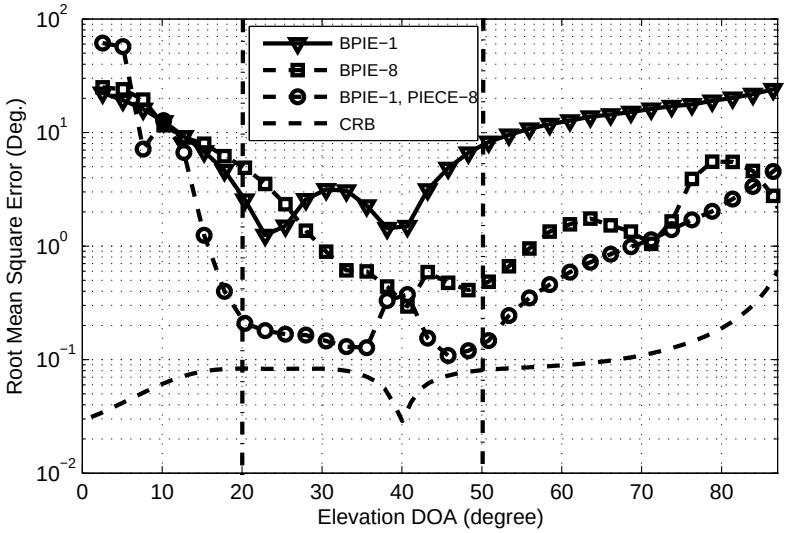

(b)

Figure 4.15: 2-D paired DOA performance for two sources for BPIE and PIECE algorithms. SNR is 15 dB. There is unknown mutual coupling between antennas. (a) Azimuth performance (b) Elevation performance.

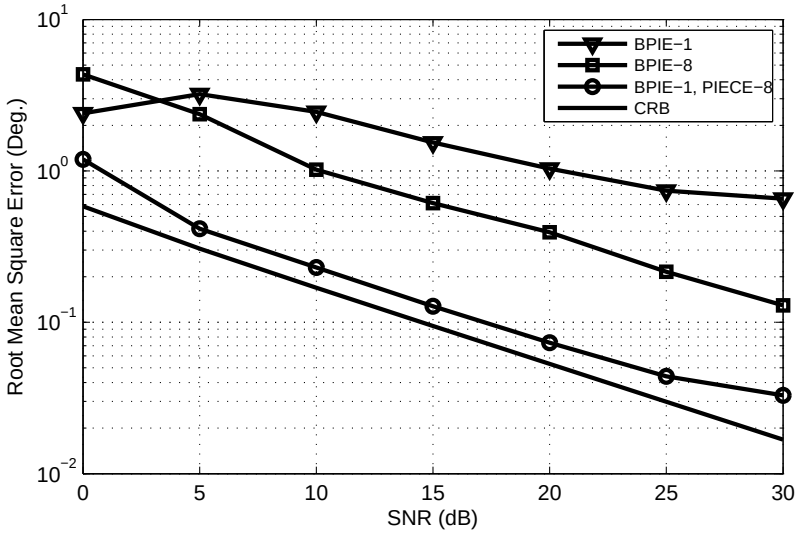

(a)

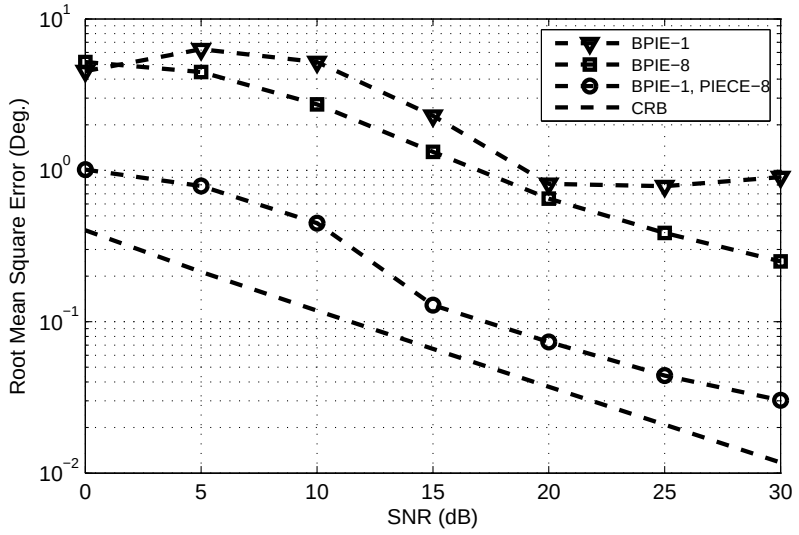

(b)

Figure 4.16: 2-D paired DOA performance for BPIE and PIECE algorithms when there is unknown mutual coupling between antennas and there are two sources. (a) Azimuth performance (b) Elevation performance.

by $P = 8$.

Figure 4.15(a) shows the azimuth performance. The application of PIECE algorithm for $L = 1$, ("BPIE-1, PIECE-8") gives significantly better result than the BPIE-8. The increase of L further improves the performance and increases the azimuth sector for a good performance. Figure 4.15(b) shows the elevation performance. The application of PIECE algorithm for $L = 1$, ("BPIE-1, PIECE-8") significantly improves the elevation performance as well. However the increase of L does not generate the same impact as in the case of azimuth angle.

Figure 4.16 shows the SNR performance for the PIECE algorithm in case of two sources. The performance of PIECE algorithm is good and it follows the CRB sufficiently well for both azimuth and elevation.

Figure 4.17 shows the normalized RMSE [25] for the coupling coefficient estimation and for the simulation setting as in Figure 4.16.

4.6 Discussions

In this chapter, three methods are presented for 2-D paired DOA estimation. Each of these methods has some advantages and application scenarios. PIE can be used for arbitrary arrays if the mutual coupling can be ignored. BPIE performs well for single source when there is mutual coupling and it can be used to get an initial estimate in case of multiple sources. It performs independent of the value of coupling coefficients and requires only the number of coupling coefficients for generating the mapping matrices. PIECE estimates the coupling coefficients and iteratively improves the estimates of coupling coefficients and DOA's. While these algorithms solve an important problem effectively, they have also certain limitations. They do not perform well when there are multipath or coherent sources. In addition, the sensor array should have sufficient number of sensors in order to decrease the array interpolation error. It turns out that when the number of sensors is less than nine, interpolation error degrades the accuracy for multiple sources while single source case can be still handled sufficiently well.

In practical implementations, the errors generated by the resolution and finite quantization of A/D converters affect the performance of the proposed methods in a similar manner as the

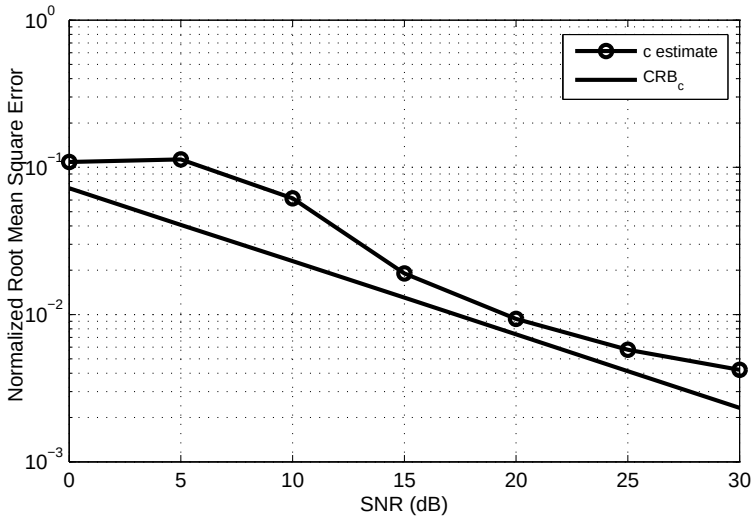

Figure 4.17: Mutual coupling coefficient estimation performance.

additive noise. In this case, SNR is lower than the one presented in our simulations and by the figures such as Figure 4.9, 4.16 and 4.17. The proposed methods work well for small number of snapshots, such as $N = 10$. This may be an advantage especially when the direction finding scenario varies with time.

4.7 Conclusion

2-D DOA estimation by fast algorithms generates a pairing problem where the azimuth and elevation angles for multiple sources are required to be matched. In this chapter, a new technique for 2-D paired DOA estimation is proposed for arbitrary arrays. This technique is based on the array interpolation to generate two shifted virtual arrays positioned accordingly in order to have the azimuth and elevation angles in the magnitude and phase parts of the eigenvalues of a matrix. Therefore 2-D angles can be obtained from the equations due to magnitude and phase at once and in a paired manner. This technique uses the ESPRIT algorithm and can be seen as a fast 2-D paired DOA estimation method. This new method is called PIE and it works well when there is no mutual coupling. In case of mutual coupling, two methods are proposed for the 2-D paired DOA estimation, namely, the BPIE and PIECE algorithms. These algorithms are also based on the same technique used in the PIE algorithm. However, they can be applied for only special arrays such as UCA where the mutual coupling matrix

has the Toeplitz form. The array output is modified in order to apply the array interpolation under mutual coupling. BPIE algorithm is a blind technique and estimates the 2-D paired DOA without finding the mutual coefficients. While this algorithm performs well for a single source, its performance degrades for multiple sources. PIECE algorithm is proposed to improve the DOA performance for multiple sources. It uses an initial paired 2-D DOA estimate obtained from the BPIE algorithm and then estimates the coupling coefficients in order to improve the array interpolation accuracy. The estimation of 2-D paired DOA angles and mutual coupling coefficients is done iteratively. The resulting performance for the algorithms is good and approaches to the CRB. The proposed methods use the sensors effectively since the same technique cannot be applied for the real sensor arrays due to coupling and the fact that identical doublets are required for the ESPRIT algorithm.

CHAPTER 5

2-D DOA ESTIMATION IN CASE OF UNKNOWN MUTUAL COUPLING FOR MULTIPATH SIGNALS

5.1 Introduction

The main difference between the technique presented in this chapter and that presented in chapter 4 is that a real array with a special geometry, namely, parallel ULA (PULA) is used and spatial smoothing is applied in order to handle multipath signals. 2-D paired DOA estimation is done similar to the techniques in chapter 4. However in this chapter, an additional step which improves the DOA estimation is used. In this additional step, ESPRIT algorithm is applied with an increased baseline.

As stated in the previous chapter, in 2-D DOA estimation, search-free and fast algorithms are usually desired. The main disadvantage of the fast 2-D DOA estimation is the pairing problem [31] where the multiple source azimuth and elevation angles should be paired accordingly. In chapter 4, the proposed methods PIE, BPIE and PIECE methods use array interpolation, which allows efficient antenna usage and possibility to compensate the mutual coupling. In case of multipath sources the proposed methods performances are not sufficient. In practical scenarios, it is required to find 2-D DOA angles when mutual coupling and multipath signals jointly exist.

In this chapter, a fast and automatically paired 2-D DOA estimation method is presented for two parallel ULA (PULA). PULA structure is previously used for the fast 2-D DOA estimation [63], [64]. A polynomial root-finding based method is presented in [63]. In [64], a propagator based method is presented with additional computational complexity for the solution of pairing problem. To our knowledge, there is no previous work where the closed

form paired 2-D DOA estimates are given when there is mutual coupling between antennas and in case of multipath signals.

In [57], a closed form solution is given for arbitrary arrays for the fast 2-D DOA estimation. While the method in [57] is general, the handling of the mutual coupling and multipath signals simultaneously requires some special array geometry. In this study, PULA is used to solve the problem in an effective manner.

5.2 Problem Formulation

It is assumed that there are D narrowband plane waves impinging on a planar array composed of $2(M+K+5)$ sensors located at the positions (x_i,y_i), i=1,...,$\bar{M}$ as shown in Figure 5.1 where $\bar{M} = 2(M + K + 5)$. There are eight auxiliary sensors in order to generate approximately the same Toeplitz coupling matrix structure for each ULA. These auxiliary sensors are shown in Figure 5.1 as white circles. Note that all the sensors in Figure 5.1 are the real sensors. The array is partitioned into triple ULA structures, as ULA-1, ULA-2 and ULA-3, respectively. These three ULA structures are considered as a triplet where the proposed algorithm is applied. K is the total number of triplets in the array. The overall array is composed of the shifted triplets in order to deal with the multipath signals by employing spatial smoothing [16]. Each ULA is composed of M sensors and spatial smoothing is applied for the shifted arrays. The largest shift is by $K-1$ sensors. The DOA angles of the sources are Θ_d=(ϕ_d,θ_d), d=1,...,D, where ϕ and θ are the azimuth and elevation angles, respectively. The antennas are assumed to be identical and omni-directional. Far-field assumption is made. The array output of the $\bar{M}$ sensors which are located as in Figure 5.1, can be written as follows:

$$\mathbf{y}(t) = \mathbf{A}(\mathbf{\Theta})\mathbf{s}(t) + \mathbf{n}(t), \quad t = 1, \ldots, N \tag{5.1}$$

where $\mathbf{y}(t) = [y_1(t) \ldots y_{\bar{M}}(t)]^T$, N is the number of snapshots and $\mathbf{s}(t)$=$[s_1(t), \ldots, s_D(t)]^T$ is the signal vector which represents a stationary, zero-mean random process uncorrelated with the noise. It is assumed that the noise, $\mathbf{n}(t)$, is both spatially and temporally white with variance σ_n^2. $\mathbf{A}(\mathbf{\Theta}) = [\mathbf{a}(\Theta_1) \ldots \mathbf{a}(\Theta_D)]$ is the $\bar{M} \times D$ ideal steering matrix including the auxiliary sensors. The steering vector $\mathbf{a}(\Theta_d)$ is given as,

$$\mathbf{a}(\Theta_d) = [a_1(\phi_d, \theta_d) \ldots a_{\bar{M}}(\phi_d, \theta_d)]^T, d = 1, \ldots, D \tag{5.2}$$

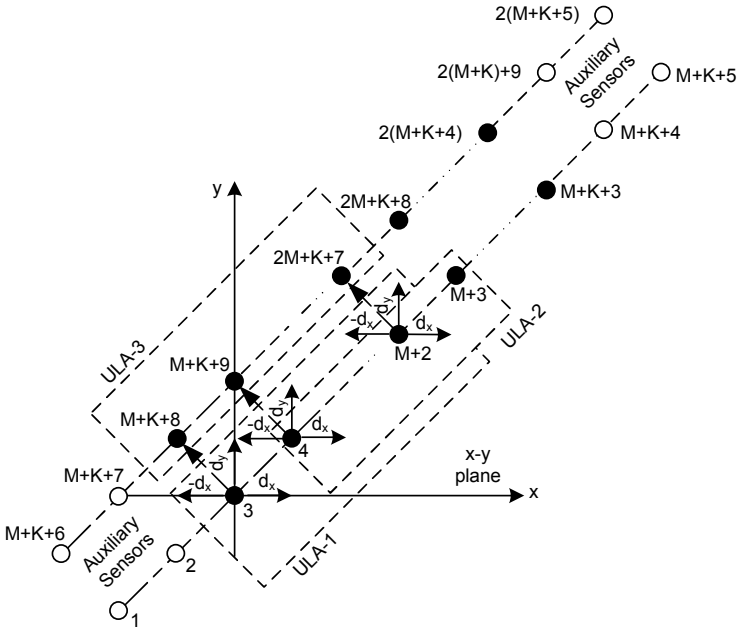

Figure 5.1: ULA structures in a triplet.

where

$$a_i(\phi_d, \theta_d) = \exp\left\{ j\frac{2\pi}{\lambda}(x_i\alpha_d + y_i\beta_d) \right\} \quad i = 1, \ldots, \bar{M} \tag{5.3}$$

(x_i, y_i) is the position of the i^{th} sensor, λ is the wavelength of the narrow-band source signals and

$$\alpha_d = \cos\phi_d \sin\theta_d \tag{5.4}$$

$$\beta_d = \sin\phi_d \sin\theta_d. \tag{5.5}$$

are defined for simplicity.

In practical arrays, array elements are located close to each other as in Figure 5.1 and this results mutual coupling between array elements. Mutual coupling distorts the theoretical steering vector in (5.2) and this situation can be modeled as $\mathbf{C}(\mathbf{\Theta})\mathbf{A}(\mathbf{\Theta})$ where $\mathbf{C}(\mathbf{\Theta})$ is called the mutual coupling matrix (MCM). The MCM is a $\bar{M} \times \bar{M}$ matrix with complex coupling coefficients and generally considered to be independent of DOA angles $\mathbf{\Theta}$. It is also assumed that the coupling coefficients are constant in the range of observation interval which is reasonable. In this case, the array output in (5.1) can be rewritten as,

$$\mathbf{y}(t) = \mathbf{C}\mathbf{A}(\mathbf{\Theta})\mathbf{s}(t) + \mathbf{n}(t), \quad t = 1, \ldots, N. \tag{5.6}$$

The coupling effect beyond $3\lambda/4$ is usually ignored for simplicity while the proposed method works equally well when the full MCM is considered. The function of the auxiliary sensors is to generate a symmetric banded Toeplitz structure for two parallel ULA as in [54]. It is assumed that the main diagonal of the MCM is normalized. The $\mathbf{C}$ matrix for the PULA structure can be written as,

$$\mathbf{C} = \begin{bmatrix} \mathbf{C}_1 & \mathbf{C}_2 \\ \mathbf{C}_2 & \mathbf{C}_1 \end{bmatrix}_{\bar{M}\times\bar{M}} \tag{5.7}$$

where $\mathbf{C}_1$ and $\mathbf{C}_2$ are $(\bar{M}/2) \times (\bar{M}/2)$ sub-matrices. The structures of the $\mathbf{C}_1$ and $\mathbf{C}_2$ matrices are expressed in Appendix C in (C.1) and (C.2), respectively. The output covariance matrix, $\mathbf{R}$, is

$$E\{\mathbf{y}(t)\mathbf{y}(t)^H\} = \mathbf{R} = \mathbf{C}\mathbf{A}(\mathbf{\Theta})\mathbf{R}_s\mathbf{A}(\mathbf{\Theta})^H\mathbf{C}^H + \sigma^2\mathbf{I} \tag{5.8}$$

where $(.)^H$ denotes the conjugate transpose of a matrix, $\mathbf{R}_s$ is the source correlation matrix and $\mathbf{I}$ is the identity matrix. If the signal vector is composed of coherent sources, then the signal vector can be rewritten as, $\mathbf{s}(t)=[b_1 s(t), \ldots, b_D s(t)]^T$ where $\forall b_i \in \mathbb{C}$, are complex coefficients. $\mathbf{s}(t)$ can be represented as $\mathbf{s}(t) = \mathbf{b}s(t)$ where $\mathbf{b} = [b_1, \ldots, b_D]^T$. In this case, the source correlation matrix becomes $\mathbf{R}_s = \mathbf{b}\mathbf{b}^H$, which is a singular matrix. It is known that the subspace based techniques can only work when the covariance matrix of the sources, $\mathbf{R}_s$, is nonsingular [16].

The problem is to find the 2-D paired DOA angles, $\mathbf{\Theta}$, given the array output in (5.6) when $\mathbf{R}_s$ is a singular matrix and there is unknown mutual coupling between array elements. In this case, it is essential to find a search-free fast technique which is invariant from the unknown mutual coupling.

5.3 Closed form 2-D Paired DOA Estimation

In order to solve the problem defined in the previous section, the proposed method uses the triplets. The base triplet is composed of the ULA-1, ULA-2 and ULA-3 as shown in Figure 5.1. The sensor positions for ULA-1 are given in $(\mathrm{x}_i,\mathrm{y}_i)$, i=3,...,$(M + 2)$ coordinates. The sensor positions for ULA-2 and ULA-3 are obtained as $(x_i + d_x, y_i + d_y)$ and $(x_i - d_x, y_i + d_y)$, respectively, where $d_x = d_y = d$ and $\sqrt{2}d$ is the inter-element distance for each ULA. So the positions for ULA-2 are given in $(\mathrm{x}_i,\mathrm{y}_i)$, i=4,...,$(M+3)$ and the positions of ULA-3 are given in $(\mathrm{x}_i,\mathrm{y}_i)$, i=$(M + K + 8)$,...,$(2M + K + 8)$ coordinates. The array outputs of ULA-1, ULA-2

and ULA-3 for the base triplet can be represented as,

$$\mathbf{y}_{(1),1}(t) = \mathbf{J}_{(1),1}\mathbf{y}(t) = [y_3(t), \cdots, y_{M+2}(t)]^T \tag{5.9}$$

$$\mathbf{y}_{(1),2}(t) = \mathbf{J}_{(1),2}\mathbf{y}(t) = [y_4(t), \cdots, y_{M+3}(t)]^T \tag{5.10}$$

$$\mathbf{y}_{(1),3}(t) = \mathbf{J}_{(1),3}\mathbf{y}(t) = [y_{M+K+7}(t), \cdots, y_{2M+K+8}(t)]^T \tag{5.11}$$

The index in parenthesis corresponds to the triplet number. There are K triplets in the array. The other index corresponds to the ULA number. $\mathbf{J}_{(k),m}$ is the selection matrix for the specified triplet and ULA where $k = 1, \ldots, K$ is the triplet number and $m = 1, 2, 3$ is the ULA number. $\mathbf{J}_{(k),m}$ matrices are defined as,

$$\mathbf{J}_{(k),1} = [\mathbf{0}_{M\times(k+1)} \ \mathbf{I}_{M\times M} \ \mathbf{0}_{M\times(\bar{M}-M-k-1)}]_{M\times\bar{M}} \tag{5.12}$$

$$\mathbf{J}_{(k),2} = [\mathbf{0}_{M\times(k+2)} \ \mathbf{I}_{M\times M} \ \mathbf{0}_{M\times(\bar{M}-M-k-2)}]_{M\times\bar{M}} \tag{5.13}$$

$$\mathbf{J}_{(k),3} = [\mathbf{0}_{M\times(M+K+k+6)} \ \mathbf{I}_{M\times M} \ \mathbf{0}_{M\times(K-k+4)}]_{M\times\bar{M}} \tag{5.14}$$

where $\mathbf{0}$ is the rectangular zero matrix with all elements are zero and $\mathbf{I}$ is the square identity matrix. In this case, the array output for the k^{th} triplet and m^{th} ULA can be defined as,

$$\mathbf{y}_{(k),m}(t) = \mathbf{J}_{(k),m}\mathbf{y}(t) = \mathbf{J}_{(k),m}(\mathbf{C}\mathbf{A}(\mathbf{\Theta})\mathbf{s}(t) + \mathbf{n}(t)) \tag{5.15}$$

We can define $\mathbf{C}_{(k),m} = \mathbf{J}_{(k),m}\mathbf{C}$ and $\mathbf{n}_{(k),m}(t) = \mathbf{J}_{(k),m}\mathbf{n}(t)$. The array output in (5.15) can be rewritten as,

$$\mathbf{y}_{(k),m}(t) = \mathbf{C}_{(k),m}\mathbf{A}(\mathbf{\Theta})\mathbf{s}(t) + \mathbf{n}_{(k),m}(t) \tag{5.16}$$

The coupling matrices of the ULA-1, 2 and 3 for the k^{th} triplet, namely, $\mathbf{C}_{(k),1}$, $\mathbf{C}_{(k),2}$ and $\mathbf{C}_{(k),3}$, are given in Appendix C in (C.3)-(C.5), respectively. The relation between these matrices can easily be written as,

$$\mathbf{C}_{(k),2} = \mathbf{C}_{(k),1}\mathbf{U} \tag{5.17}$$

$$\mathbf{C}_{(k),3} = \mathbf{C}_{(k),1}\mathbf{L} \tag{5.18}$$

where $\mathbf{U}$ is the $\bar{M}\times\bar{M}$ shifting matrix and its components are defined as, $U_{i,j} = \delta_{i+1,j}$. $\mathbf{L}$ matrix is the $\bar{M} \times \bar{M}$ anti-diagonal identity matrix and its components are defined as, $L_{i,j} = \delta_{i,\bar{M}+1-j}$. These two matrices, $\mathbf{U}$ and $\mathbf{L}$, are given in (C.8). It is also possible to find the relation between the coupling matrices of the base triplet, $\mathbf{C}_{(1),1}$, and k^{th} triplet, $\mathbf{C}_{(k),1}$ as

$$\mathbf{C}_{(k),1} = \mathbf{C}_{(1),1}\mathbf{U}^k \tag{5.19}$$

where $\mathbf{U}^k$ is the k^{th} power of the shifting matrix $\mathbf{U}$ which is defined in (C.9). Using the relations in (5.17), (5.18) and (5.19), the coupling matrices of the k^{th} triplet can be rewritten as,

$$\mathbf{C}_{(k),2} = \bar{\mathbf{C}}\mathbf{U}^k\mathbf{U} \tag{5.20}$$

$$\mathbf{C}_{(k),3} = \bar{\mathbf{C}}\mathbf{U}^k\mathbf{L} \tag{5.21}$$

where $\bar{\mathbf{C}} = \mathbf{C}_{(1),1}$. In this case, the array outputs for the k^{th} triplet can be defined as,

$$\mathbf{y}_{(k),1}(t) = \bar{\mathbf{C}}\mathbf{U}^k\mathbf{A}(\mathbf{\Theta})\mathbf{s}(t) + \mathbf{n}_{(k),1}(t) \tag{5.22}$$

$$\mathbf{y}_{(k),2}(t) = \bar{\mathbf{C}}\mathbf{U}^k\mathbf{U}\mathbf{A}(\mathbf{\Theta})\mathbf{s}(t) + \mathbf{n}_{(k),2}(t) \tag{5.23}$$

$$\mathbf{y}_{(k),3}(t) = \bar{\mathbf{C}}\mathbf{U}^k\mathbf{L}\mathbf{A}(\mathbf{\Theta})\mathbf{s}(t) + \mathbf{n}_{(k),3}(t) \tag{5.24}$$

In order to clarify the relation between these array outputs, it should be considered that

$$\mathbf{U}\mathbf{A}(\mathbf{\Theta}) = \mathbf{A}(\mathbf{\Theta})\mathbf{\Phi}_1(\mathbf{\Theta}) \tag{5.25}$$

$$\mathbf{L}\mathbf{A}(\mathbf{\Theta}) = \mathbf{A}(\mathbf{\Theta})\mathbf{\Phi}_2(\mathbf{\Theta}) \tag{5.26}$$

where $\mathbf{\Phi}_1(\mathbf{\Theta})$ and $\mathbf{\Phi}_2(\mathbf{\Theta})$ are the diagonal matrices as,

$$\mathbf{\Phi}_1(\mathbf{\Theta}) = diag\left\{\exp\left(j\frac{2\pi}{\lambda}d(\alpha_1+\beta_1)\right),\ldots,\exp\left(j\frac{2\pi}{\lambda}d(\alpha_D+\beta_D)\right)\right\} \tag{5.27}$$

$$\mathbf{\Phi}_2(\mathbf{\Theta}) = diag\left\{\exp\left(j\frac{2\pi}{\lambda}d(-\alpha_1+\beta_1)\right),\ldots,\exp\left(j\frac{2\pi}{\lambda}d(-\alpha_D+\beta_D)\right)\right\}, \tag{5.28}$$

α_d and β_d for $d = 1,\ldots,D$ are defined in (5.4) and (5.5), respectively. Finally using (5.25) and (5.26) the subarray outputs in (5.22)-(5.24) for the k^{th} triplet can be rewritten as,

$$\mathbf{y}_{(k),1}(t) = \bar{\mathbf{C}}\mathbf{U}^k\mathbf{A}(\mathbf{\Theta})\mathbf{s}(t) + \mathbf{n}_{(k),1}(t) \tag{5.29}$$

$$\mathbf{y}_{(k),2}(t) = \bar{\mathbf{C}}\mathbf{U}^k\mathbf{A}(\mathbf{\Theta})\mathbf{\Phi}_1(\mathbf{\Theta})\mathbf{s}(t) + \mathbf{n}_{(k),2}(t) \tag{5.30}$$

$$\mathbf{y}_{(k),3}(t) = \bar{\mathbf{C}}\mathbf{U}^k\mathbf{A}(\mathbf{\Theta})\mathbf{\Phi}_2(\mathbf{\Theta})\mathbf{s}(t) + \mathbf{n}_{(k),3}(t) \tag{5.31}$$

In order to find these expressions with unambiguous solution the displacement, d, should be selected as,

$$d_x = d_y = d \leq \lambda/4 \tag{5.32}$$

Using the subarray outputs in (5.29), (5.30) and (5.31), it is possible to find $\mathbf{\Phi}_1(\mathbf{\Theta})$ and $\mathbf{\Phi}_2(\mathbf{\Theta})$ matrices by applying the ESPRIT algorithm twice. But in this case, since the terms of these

diagonal matrices are ordered arbitrary, these terms must be paired for each source. There are some pairing techniques in the literature which require extra efforts. In addition, these methods do not perform well especially at low SNR.

In this study, the ULA outputs of the k^{th} triplet, $\mathbf{y}_{(k),2}(t)$ and $\mathbf{y}_{(k),3}(t)$, are combined in order to obtain virtual subarray output, $\mathbf{y}_{(k),4}(t)$ as,

$$\begin{aligned}
\mathbf{y}_{(k),4}(t) &= \mathbf{y}_{(k),2}(t) + \mathbf{y}_{(k),3}(t) \\
&= \bar{\mathbf{C}}\mathbf{U}^k\mathbf{A}(\mathbf{\Theta})(\underbrace{\mathbf{\Phi}_1(\mathbf{\Theta}) + \mathbf{\Phi}_2(\mathbf{\Theta})}_{\mathbf{\Phi}(\mathbf{\Theta})})\mathbf{s}(t) + \underbrace{\mathbf{n}_{(k),2}(t) + \mathbf{n}_{(k),3}(t)}_{\mathbf{n}_{(k),4}(t)} \\
\mathbf{y}_{(k),4}(t) &= \bar{\mathbf{C}}\mathbf{U}^k\mathbf{A}(\mathbf{\Theta})\mathbf{\Phi}(\mathbf{\Theta})\mathbf{s}(t) + \mathbf{n}_{(k),4}(t) \qquad (5.33)
\end{aligned}$$

The above expression is the output of the virtual (combined) subarray, $\mathbf{y}_{(k),4}(t)$, where $\mathbf{\Phi}(\mathbf{\Theta})$ is the diagonal matrix with complex terms which have both magnitude and phase terms as,

$$\mathbf{\Phi}(\mathbf{\Theta}) = diag\left\{2\cos(\frac{2\pi}{\lambda}d\alpha_1)e^{j\frac{2\pi}{\lambda}d\beta_1}, \ldots, 2\cos(\frac{2\pi}{\lambda}d\alpha_D)e^{j\frac{2\pi}{\lambda}d\beta_D}\right\} = diag\left\{v_1, v_2, \ldots, v_D\right\} \qquad (5.34)$$

Note that the magnitude components of v_i in equation (5.34), $2\cos(\frac{2\pi}{\lambda}d\cos\phi_i\sin\theta_i)$, are always positive due to (5.32). The phase component is $\arg(v_i) = \frac{2\pi}{\lambda}d\sin\phi_i\sin\theta_i$. These terms have DOA information for $i = 1, \ldots, D$ sources. Using these magnitude and phase terms simultaneously the automatically paired azimuth and elevation DOA angles can be easily obtained similar to (4.18) and (4.19) as,

$$\phi_i = \arctan\left(\frac{\arg(v_i)}{\arccos\left(\frac{|v_i|}{2}\right)}\right) \qquad (5.35)$$

$$\theta_i = \arcsin\left(\sqrt{\left(\frac{\arg(v_i)}{\frac{2\pi}{\lambda}d}\right)^2 + \left(\frac{\arccos\left(\frac{|v_i|}{2}\right)}{\frac{2\pi}{\lambda}d}\right)^2}\right). \qquad (5.36)$$

In order to find $\mathbf{\Phi}(\mathbf{\Theta})$, which is defined in (5.34), for each triplet, we apply the ESPRIT algorithm for the covariance matrix of $\mathbf{R}_{(k)} = E\{\mathbf{y}_{(k),5}(t)\mathbf{y}_{(k),5}(t)^H\}$ where $\mathbf{y}_{(k),5}(t)$ is the combined measurement which is defined as,

$$\mathbf{y}_{(k),5}(t) = \begin{bmatrix} \mathbf{y}_{(k),1}(t) \\ \mathbf{y}_{(k),4}(t) \end{bmatrix}. \qquad (5.37)$$

In case of multipath signals, the source correlation matrix will be singular and it is not possible to find $\mathbf{\Phi}(\mathbf{\Theta})$ matrix using the eigenstructure methods. Spatial smoothing should be employed in order to mitigate the multipath signals.

5.3.1 Spatial Smoothing of the Combined Measurements

In this part, spatial smoothing [16] is used for the PULA in the presence of unknown mutual coupling.

Note that it is possible to express the steering matrices of the k^{th} triplets in (5.29) and (5.33) as,

$$\mathbf{U}^k\mathbf{A}(\mathbf{\Theta}) = \mathbf{A}(\mathbf{\Theta})\mathbf{\Phi}_1^k(\mathbf{\Theta}) \tag{5.38}$$

where $\mathbf{\Phi}_1(\mathbf{\Theta})$ is the diagonal matrix which is previously defined in (5.27) and $\mathbf{\Phi}_1^k(\mathbf{\Theta})$ is the k^{th} power of the $\mathbf{\Phi}_1(\mathbf{\Theta})$. $\mathbf{\Phi}_1(\mathbf{\Theta})$ can be written as the multiplication of two matrices for simplicity as $\mathbf{\Phi}_1(\mathbf{\Theta}) = \mathbf{F} = \mathbf{F}_x\mathbf{F}_y$ where

$$\begin{aligned}
\mathbf{F}_x &= diag\left\{\exp\left(j\frac{2\pi}{\lambda}d\alpha_1\right),\ldots,\exp\left(j\frac{2\pi}{\lambda}d(\alpha_D)\right)\right\} \\
\mathbf{F}_y &= diag\left\{\exp\left(j\frac{2\pi}{\lambda}d\beta_1\right),\ldots,\exp\left(j\frac{2\pi}{\lambda}d\beta_D\right)\right\}
\end{aligned}$$

In this case, the combined measurement in (5.37) can be rewritten as,

$$\mathbf{y}_{(k),5}(t) = \begin{bmatrix} \bar{\mathbf{C}}\mathbf{A}(\mathbf{\Theta})\mathbf{F}^k\mathbf{s}(t) \\ \bar{\mathbf{C}}\mathbf{A}(\mathbf{\Theta})\mathbf{F}^k\mathbf{\Phi}(\mathbf{\Theta})\mathbf{s}(t) \end{bmatrix} + \begin{bmatrix} \mathbf{n}_{(k),1}(t) \\ \mathbf{n}_{(k),4}(t) \end{bmatrix} \tag{5.39}$$

Then the output correlation matrix for the k^{th} triplet, $\mathbf{R}_{(k)} = E\{\mathbf{y}_{(k),5}(t)\mathbf{y}_{(k),5}(t)^H\}$, can be written as,

$$\mathbf{R}_{(k)} = \mathbf{Q}\mathbf{E}_x^k\mathbf{E}_y^k\mathbf{P}(\mathbf{E}_y^k)^H(\mathbf{E}_x^k)^H\mathbf{Q}^H + \sigma^2\mathbf{I}_{2\bar{M}\times 2\bar{M}} \tag{5.40}$$

where

$$\mathbf{Q} = \begin{bmatrix} \bar{\mathbf{C}}\mathbf{A}(\mathbf{\Theta}) & \mathbf{0}_{\bar{M}\times D} \\ \mathbf{0}_{\bar{M}\times D} & \bar{\mathbf{C}}\mathbf{A}(\mathbf{\Theta}) \end{bmatrix}_{2\bar{M}\times 2\bar{M}} \quad \mathbf{P} = \begin{bmatrix} \mathbf{R}_s & \mathbf{R}_s\mathbf{\Phi}(\mathbf{\Theta})^H \\ \mathbf{\Phi}(\mathbf{\Theta})\mathbf{R}_s & \mathbf{\Phi}(\mathbf{\Theta})\mathbf{R}_s\mathbf{\Phi}(\mathbf{\Theta})^H \end{bmatrix}_{2\bar{M}\times 2\bar{M}} \tag{5.41}$$

and

$$\mathbf{E}_x^k = \begin{bmatrix} \mathbf{F}_x^k & \mathbf{0}_{\bar{M}\times D} \\ \mathbf{0}_{\bar{M}\times D} & \mathbf{F}_x^k \end{bmatrix}_{2\bar{M}\times 2\bar{M}} \quad \mathbf{E}_y^k = \begin{bmatrix} \mathbf{F}_y^k & \mathbf{0}_{\bar{M}\times D} \\ \mathbf{0}_{\bar{M}\times D} & \mathbf{F}_y^k \end{bmatrix}_{2\bar{M}\times 2\bar{M}} \tag{5.42}$$

The spatially smoothed covariance matrix, $\bar{\mathbf{R}}$, can be found as,

$$\bar{\mathbf{R}} = \frac{1}{K}\sum_{k=1}^{K}\mathbf{R}_{(k)} = \mathbf{Q}\underbrace{\left(\frac{1}{K}\sum_{k=1}^{K}\mathbf{E}_x^k\mathbf{E}_y^k\mathbf{P}(\mathbf{E}_y^k)^H(\mathbf{E}_x^k)^H\right)}_{\bar{\mathbf{P}}}\mathbf{Q}^H + \sigma^2\mathbf{I} \tag{5.43}$$

where $\bar{\mathbf{P}}$ is the smoothed signal covariance, as it is shown in [16].

In the following subsection, the steps of the ESPRIT-based automatically paired 2-D DOA estimation algorithm are presented. This algorithm is named as PULA-1. PULA-1 solves the pairing problem effectively. However, its DOA performance can be improved if a different subarray selection is done. PULA-2 algorithm is employed for this purpose.

5.3.2 Algorithm for PULA-1

The procedure for the proposed algorithm is as follows:

- Step 1) Obtain the triplet data as in (5.37) for three triplets, $\mathbf{y}_{(k),5}(t)$, $k = 1, \ldots, K$ using (5.9)-(5.11).
- Step 2) Apply spatial smoothing by using the shifted triplets as in (5.43). Apply the ESPRIT algorithm to the final covariance matrix $\bar{\mathbf{R}}$ and find $\hat{\mathbf{S}}_1$ and $\hat{\mathbf{S}}_4$. $\hat{\mathbf{S}}_1$ and $\hat{\mathbf{S}}_4$ are the matrices composed of the eigenvectors in the signal spaces corresponding to $\mathbf{y}_{(1),1}(t)$, and $\mathbf{y}_{(1),4}(t)$ as in (5.37) respectively. The relation between $\hat{\mathbf{S}}_1$ and $\hat{\mathbf{S}}_4$ is

  $$\hat{\mathbf{S}}_4 = \hat{\mathbf{S}}_1 \hat{\mathbf{\Phi}} \tag{5.44}$$

  Find the least squares (LS) optimum solution for $\hat{\mathbf{\Phi}}$ as $\hat{\mathbf{\Phi}} = \hat{\mathbf{S}}_1^{\dagger}\hat{\mathbf{S}}_4$ where $\hat{\mathbf{S}}_1^{\dagger}=(\hat{\mathbf{S}}_1^H\hat{\mathbf{S}}_1)^{-1}\hat{\mathbf{S}}_1^H$ is the Moore-Penrose pseudoinverse.
- Step 3) Compute the eigenvalues of $\hat{\mathbf{\Phi}}$ as

  $$\hat{\mathbf{v}} = eig\{\hat{\mathbf{\Phi}}\} \tag{5.45}$$

  where $\hat{\mathbf{v}}$ is a $D \times 1$ vector. Compute the azimuth and elevation angles by using (5.35) and (5.36), respectively, for $i = 1, \ldots, D$.

If we apply the above algorithm, the automatically paired multiple 2-D DOA angles can be easily found by solving the closed form expressions in a fast manner. It is observed in the simulations that the DOA performance of the method is good but not so close to the CRB of the PULA array. Therefore this array structure in Figure 5.1 and the 2-D angle results of the above algorithm are further used to improve the DOA performance. In this case, different subarrays can be selected within the PULA with a larger baseline and 2-D DOA performance can be improved considerably.

5.3.3 Selecting Different Subarrays within PULA and the PULA-2 Algorithm

It can be seen from Figure 5.2 and Figure 5.3 that it is possible to select subarrays with a larger baseline in x and y axes, respectively. In PULA-1 approach, $d_x = d_y = d = \frac{\lambda}{4}$ is chosen and $\sqrt{2}\frac{\lambda}{4}$ is the distance between each ULA as shown in Figure 5.1. In PULA-2 case, the same array as in Figure 5.1 is used. However different ULAs are selected in this case and d_{tx}, d_{ty} are the distances between each ULA as shown in Figure 5.2 and 5.3, respectively. These distances are $\frac{\lambda}{2}$. PULA-2 solves the pairing problem with the help of PULA-1 while DOA accuracy is improved by increasing the subarray distance.

Two arrays are selected as in Figure 5.2 for the x-axis shift and the corresponding selection matrices are defined as,

$$\bar{\mathbf{J}}_{(k),1} = [\mathbf{0}_{M\times(M+K+k+6)} \ \mathbf{I}_{M\times M} \ \mathbf{0}_{M\times(K-k+4)}]_{M\times\bar{M}} \tag{5.46}$$

$$\bar{\mathbf{J}}_{(k),2} = [\mathbf{0}_{M\times(k+2)} \ \mathbf{I}_{M\times M} \ \mathbf{0}_{M\times(M+2K+8-k)}]_{M\times\bar{M}} \tag{5.47}$$

Similarly the other two arrays are selected as in Figure 5.3 for the y-axis shift and the corresponding selection matrices are defined as,

$$\bar{\mathbf{J}}_{(k),3} = [\mathbf{0}_{M\times(k+1)} \ \mathbf{I}_{M\times M} \ \mathbf{0}_{M\times(M+2K-k+9)}]_{M\times\bar{M}} \tag{5.48}$$

$$\bar{\mathbf{J}}_{(k),4} = [\mathbf{0}_{M\times(M+K+k+7)} \ \mathbf{I}_{M\times M} \ \mathbf{0}_{M\times(K-k+3)}]_{M\times\bar{M}} \tag{5.49}$$

Note that the bar, ($\bar{}$), represents the new arrays in Figure 5.2 and 5.3. In this case, the array output can be defined similar to (5.15) as,

$$\bar{\mathbf{y}}_{(k),m}(t) = \bar{\mathbf{J}}_{(k),m}\mathbf{y}(t) = \bar{\mathbf{J}}_{(k),m}(\mathbf{C}\mathbf{A}(\mathbf{\Theta})\mathbf{s}(t) + \mathbf{n}(t)). \tag{5.50}$$

In this case, we can define the $\bar{\mathbf{C}}_{(k),m} = \bar{\mathbf{J}}_{(k),m}\mathbf{C}$ and $\bar{\mathbf{n}}_{(k),m}(t) = \bar{\mathbf{J}}_{(k),m}\mathbf{n}(t)$. The coupling matrices of the arrays in Figure 5.2 and 5.3 are given as,

$$\bar{\mathbf{C}}_{(k),1} = \left[\begin{array}{cccc} \mathbf{0}_{M\times(k-1)} & \mathbf{C}^R_{M\times M} & \mathbf{C}^L_{M\times M} & \mathbf{0}_{M\times(\bar{M}-2M-k+1)} \end{array}\right]_{M\times\bar{M}} \tag{5.51}$$

$$\bar{\mathbf{C}}_{(k),2} = \left[\begin{array}{cccc} \mathbf{0}_{M\times k} & \mathbf{C}^L_{M\times M} & \mathbf{C}^R_{M\times M} & \mathbf{0}_{M\times(\bar{M}-2M-k)} \end{array}\right]_{M\times\bar{M}} \tag{5.52}$$

$$\bar{\mathbf{C}}_{(k),3} = \left[\begin{array}{cccc} \mathbf{0}_{M\times(k-1)} & \mathbf{C}^L_{M\times M} & \mathbf{C}^R_{M\times M} & \mathbf{0}_{M\times(\bar{M}-2M-k+1)} \end{array}\right]_{M\times\bar{M}} \tag{5.53}$$

$$\bar{\mathbf{C}}_{(k),4} = \left[\begin{array}{cccc} \mathbf{0}_{M\times k} & \mathbf{C}^R_{M\times M} & \mathbf{C}^L_{M\times M} & \mathbf{0}_{M\times(\bar{M}-2M-k)} \end{array}\right]_{M\times\bar{M}} \tag{5.54}$$

It is easy to write the relations between coupling matrices, i.e.,

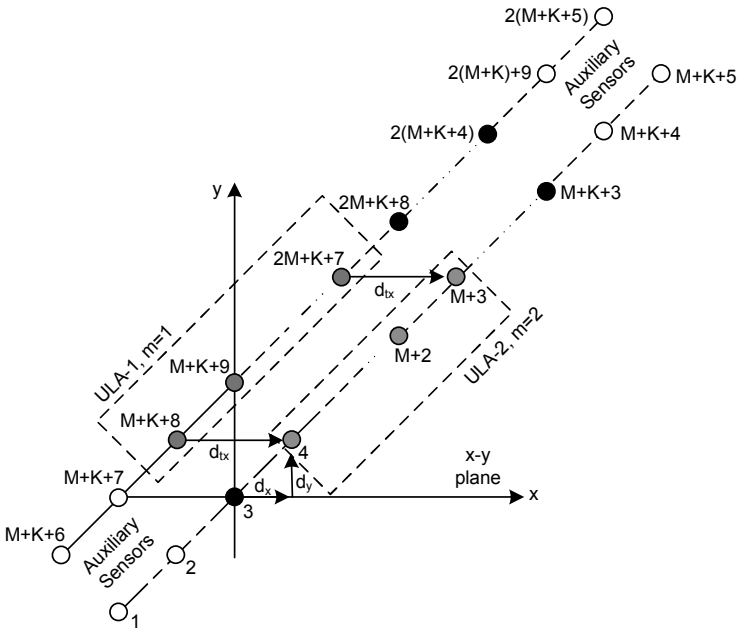

Figure 5.2: Two subarrays within PULA for x-axis shift.

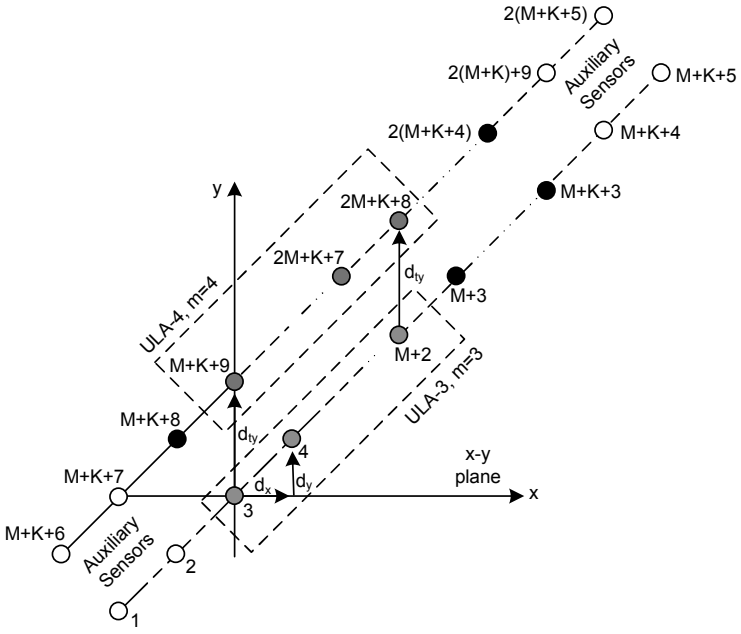

Figure 5.3: Two subarrays within PULA for y-axis shift.

$$\bar{\mathbf{C}}_{(k),1} = \mathbf{C}_{(k),1}\mathbf{L} \tag{5.55}$$

$$\bar{\mathbf{C}}_{(k),2} = \mathbf{C}_{(k),2} = \mathbf{C}_{(k),1}\mathbf{U} \tag{5.56}$$

$$\bar{\mathbf{C}}_{(k),3} = \mathbf{C}_{(k),1} \tag{5.57}$$

$$\bar{\mathbf{C}}_{(k),4} = \mathbf{C}_{(k),2}\mathbf{L} = \mathbf{C}_{(k),1}\mathbf{U}\mathbf{L} \tag{5.58}$$

We can now express the coupling matrices similar to (5.20) and (5.21) by using the equations (5.55)-(5.58) as,

$$\bar{\mathbf{C}}_{(k),1} = \bar{\mathbf{C}}\mathbf{U}^k\mathbf{L} \tag{5.59}$$

$$\bar{\mathbf{C}}_{(k),2} = \bar{\mathbf{C}}\mathbf{U}^k\mathbf{U} \tag{5.60}$$

$$\bar{\mathbf{C}}_{(k),3} = \bar{\mathbf{C}}\mathbf{U}^k \tag{5.61}$$

$$\bar{\mathbf{C}}_{(k),4} = \bar{\mathbf{C}}\mathbf{U}^k\mathbf{U}\mathbf{L} \tag{5.62}$$

The array outputs for the k^{th} triplet of Figure 5.2 can be defined as,

$$\bar{\mathbf{y}}_{(k),1}(t) = \bar{\mathbf{C}}\mathbf{U}^k\mathbf{L}\mathbf{A}(\mathbf{\Theta})\mathbf{s}(t) + \bar{\mathbf{n}}_{(k),1}(t) \tag{5.63}$$

$$\bar{\mathbf{y}}_{(k),2}(t) = \bar{\mathbf{C}}\mathbf{U}^k\mathbf{U}\mathbf{A}(\mathbf{\Theta})\mathbf{s}(t) + \bar{\mathbf{n}}_{(k),2}(t). \tag{5.64}$$

By using (5.25) and (5.26) the subarray outputs of $\bar{\mathbf{y}}_{(k),1}(t)$ and $\bar{\mathbf{y}}_{(k),2}(t)$ can be rewritten as,

$$\bar{\mathbf{y}}_{(k),1}(t) = \bar{\mathbf{C}}\mathbf{U}^k\mathbf{A}(\mathbf{\Theta})\mathbf{\Phi}_2(\mathbf{\Theta})\mathbf{s}(t) + \bar{\mathbf{n}}_{(k),1}(t) \tag{5.65}$$

$$\bar{\mathbf{y}}_{(k),2}(t) = \bar{\mathbf{C}}\mathbf{U}^k\mathbf{A}(\mathbf{\Theta})\mathbf{\Phi}_1(\mathbf{\Theta})\mathbf{s}(t) + \bar{\mathbf{n}}_{(k),2}(t). \tag{5.66}$$

We can write $\mathbf{\Phi}_1(\mathbf{\Theta}) = \mathbf{\Phi}_2(\mathbf{\Theta})\mathbf{\Phi}_x(\mathbf{\Theta})$ where

$$\mathbf{\Phi}_x(\mathbf{\Theta}) = diag\left\{\exp\left(j\frac{2\pi}{\lambda}2d\alpha_1\right), \ldots, \exp\left(j\frac{2\pi}{\lambda}2d\alpha_D\right)\right\}. \tag{5.67}$$

Finally (5.65) and (5.66) can be written as,

$$\bar{\mathbf{y}}_{(k),1}(t) = \bar{\mathbf{C}}\mathbf{A}_{(k)}(\mathbf{\Theta})\mathbf{\Phi}_2(\mathbf{\Theta})\mathbf{s}(t) + \bar{\mathbf{n}}_{(k),1}(t) \tag{5.68}$$

$$\bar{\mathbf{y}}_{(k),2}(t) = \bar{\mathbf{C}}\mathbf{A}_{(k)}(\mathbf{\Theta})\mathbf{\Phi}_2(\mathbf{\Theta})\mathbf{\Phi}_x(\mathbf{\Theta})\mathbf{s}(t) + \bar{\mathbf{n}}_{(k),2}(t) \tag{5.69}$$

where $\mathbf{A}_{(k)}(\mathbf{\Theta}) = \mathbf{U}^k\mathbf{A}(\mathbf{\Theta})$. In this case, if we apply the ESPRIT algorithm to the above array outputs, it is possible to find $\mathbf{\Phi}_x(\mathbf{\Theta})$ matrix.

Similarly the array outputs for the k^{th} triplet of Figure 5.3 can be written using (5.61) and (5.62) as,

$$\bar{\mathbf{y}}_{(k),3}(t) = \bar{\mathbf{C}}\mathbf{U}^k\mathbf{A}(\mathbf{\Theta})\mathbf{s}(t) + \bar{\mathbf{n}}_{(k),3}(t) \tag{5.70}$$

$$\bar{\mathbf{y}}_{(k),4}(t) = \bar{\mathbf{C}}\mathbf{U}^k\mathbf{U}\mathbf{L}\mathbf{A}(\mathbf{\Theta})\mathbf{s}(t) + \bar{\mathbf{n}}_{(k),4}(t). \tag{5.71}$$

By using (5.25) and (5.26) the subarray outputs can be rewritten as,

$$\bar{\mathbf{y}}_{(k),3}(t) = \bar{\mathbf{C}}\mathbf{U}^k\mathbf{A}(\mathbf{\Theta})\mathbf{s}(t) + \bar{\mathbf{n}}_{(k),3}(t) \tag{5.72}$$

$$\bar{\mathbf{y}}_{(k),4}(t) = \bar{\mathbf{C}}\mathbf{U}^k\mathbf{A}(\mathbf{\Theta})\mathbf{\Phi}_1(\mathbf{\Theta})\mathbf{\Phi}_2(\mathbf{\Theta})\mathbf{s}(t) + \bar{\mathbf{n}}_{(k),4}(t). \tag{5.73}$$

We can write $\mathbf{\Phi}_1(\mathbf{\Theta})\mathbf{\Phi}_2(\mathbf{\Theta}) = \mathbf{\Phi}_y(\mathbf{\Theta})$ where

$$\mathbf{\Phi}_y(\mathbf{\Theta}) = diag\left\{\exp\left(j\frac{2\pi}{\lambda}2d\beta_1\right), \ldots, \exp\left(j\frac{2\pi}{\lambda}2d\beta_D\right)\right\}. \tag{5.74}$$

Finally (5.72) and (5.73) can be written as,

$$\bar{\mathbf{y}}_{(k),3}(t) = \bar{\mathbf{C}}\mathbf{A}_{(k)}(\mathbf{\Theta})\mathbf{s}(t) + \bar{\mathbf{n}}_{(k),3}(t) \tag{5.75}$$

$$\bar{\mathbf{y}}_{(k),4}(t) = \bar{\mathbf{C}}\mathbf{A}_{(k)}(\mathbf{\Theta})\mathbf{\Phi}_y(\mathbf{\Theta})\mathbf{s}(t) + \bar{\mathbf{n}}_{(k),4}(t). \tag{5.76}$$

In this case if we apply the ESPRIT algorithm to the above array outputs, it is possible to find $\mathbf{\Phi}_y(\mathbf{\Theta})$ matrix.

As we can see, $\mathbf{\Phi}_x(\mathbf{\Theta})$ and $\mathbf{\Phi}_y(\mathbf{\Theta})$ are the diagonal matrices and include angle information as in (5.67) and (5.74), respectively. These matrices are not ordered and (ϕ, θ) pairs for each source should be identified. We can easily pair these using the 2-D DOA angle estimates of the PULA-1 algorithm. The eigenvalues of the $\mathbf{\Phi}_x(\mathbf{\Theta})$ and $\mathbf{\Phi}_y(\mathbf{\Theta})$ can be defined as $\mathbf{p} = [p_1, \ldots, p_D]$ and $\mathbf{r} = [r_1, \ldots, r_D]$, respectively, where $p_i = \exp(j\frac{2\pi}{\lambda}d_{tx}\alpha_i)$ and $r_i = \exp(j\frac{2\pi}{\lambda}d_{ty}\beta_i)$ for $i = 1, \ldots, D$. In order to pair these vectors according to each other, we can use PULA-1 angle pairs as in 5.3.3. Using these paired terms we can find azimuth and elevation DOA angles as,

$$\phi_i = \arctan\left(\frac{\arg(r_i)}{\arg(p_i)}\right) \tag{5.77}$$

$$\theta_i = \arcsin\left(\sqrt{\left(\frac{\arg(p_i)}{\frac{2\pi}{\lambda}2d}\right)^2 + \left(\frac{\arg(r_i)}{\frac{2\pi}{\lambda}2d}\right)^2}\right). \tag{5.78}$$

PULA-2 Algorithm:

1. Apply PULA-1 algorithm and find the paired 2-D DOA angles $(\hat{\phi}c_d, \hat{\theta}c_d)$ for $d = 1, \ldots, D$.

2. Obtain the subarray data using (5.50) for x-axis and y-axis shifts as,
   x-axis: $\bar{\mathbf{y}}_{(k),1}(t)$ and $\bar{\mathbf{y}}_{(k),2}(t)$ for $k = 1, \ldots, K$.

y-axis: $\bar{\mathbf{y}}_{(k),3}(t)$ and $\bar{\mathbf{y}}_{(k),4}(t)$ for $k = 1, \ldots, K$.

Combine these data for x-axis and y-axis as:

$$\bar{\mathbf{y}}_{(k),x}(t) = \begin{bmatrix} \bar{\mathbf{y}}_{(k),1}(t) \\ \bar{\mathbf{y}}_{(k),2}(t) \end{bmatrix} \tag{5.79}$$

$$\bar{\mathbf{y}}_{(k),y}(t) = \begin{bmatrix} \bar{\mathbf{y}}_{(k),3}(t) \\ \bar{\mathbf{y}}_{(k),4}(t) \end{bmatrix} \tag{5.80}$$

3. Apply spatial smoothing to these shifted subarrays. In this case, find the correlation matrix of x-axis, $\mathbf{R}_{(k),x} = E\{\bar{\mathbf{y}}_{(k),x}(t)\bar{\mathbf{y}}_{(k),x}(t)^H\}$ and the correlation matrix of y-axis, $\mathbf{R}_{(k),y} = E\{\bar{\mathbf{y}}_{(k),y}(t)\bar{\mathbf{y}}_{(k),y}(t)^H\}$ for $k = 1, \ldots, K$ using (5.79) and (5.80). Then find the smoothed correlation matrices as in (5.43) for x and y-axes. Apply the ESPRIT algorithm to these two smoothed covariance matrices separately to estimate the $\mathbf{\Phi}_x(\mathbf{\Theta})$ and $\mathbf{\Phi}_y(\mathbf{\Theta})$ in (5.67) and (5.74).

4. Compute the eigenvalues of estimated $\hat{\mathbf{\Phi}}_x(\mathbf{\Theta})$ and $\hat{\mathbf{\Phi}}_y(\mathbf{\Theta})$ as

$$\hat{\mathbf{p}} = eig\{\hat{\mathbf{\Phi}}_x(\mathbf{\Theta})\}, \quad \hat{\mathbf{r}} = eig\{\hat{\mathbf{\Phi}}_y(\mathbf{\Theta})\} \tag{5.81}$$

where $\hat{\mathbf{p}}$ and $\hat{\mathbf{r}}$ are $D \times 1$ vectors. But in this case we have to pair one of these matrices according to other. In the following algorithm we pair $\hat{\mathbf{r}}$ according to $\hat{\mathbf{p}}$ using the following pairing algorithm.

Pairing Algorithm

0: permutation-number = $D!$

0: all-permutations = $perms(\hat{\mathbf{r}})$

for $i = 1$ to permutation-number **do**

$\hat{\mathbf{r}} \leftarrow$ all-permutations(i) {select a permutation from list}

$(\hat{\phi}t_d, \hat{\theta}t_d) \leftarrow$ {Solve DOA angles using (5.77), (5.78) and $\hat{\mathbf{r}}$, $\hat{\mathbf{p}}$ for this permutation}

$e(i) = \sqrt{\sum_{d=1}^{D}((\hat{\phi}t_d - \hat{\phi}c_d)^2 + (\hat{\theta}t_d - \hat{\theta}c_d)^2)}$ {where $(\hat{\phi}c_d, \hat{\theta}c_d)$ is the angle pairs of PULA-1}

$i \leftarrow i + 1$

end for

{choose the pair which corresponds to the minimum $e(i)$, $i = 1, \ldots,$ permutation-number}.

5.4 Simulations

In this section, the proposed methods, PULA-1 and PULA-2 are evaluated in order to show the 2-D paired DOA performance in case of unknown mutual coupling and for the coherent signals.

In the simulations, $d_x = d_y = \lambda/4$ is selected and the distance between each antenna in ULA is $\sqrt{2}\lambda/4$. The distance between parallel ULA is also $\sqrt{2}\lambda/4$. There are 500 trials for each experiment and the number of snapshots is 500. The number of sensors in each ULA is $M = 7$ and the number of triplets is $K = 3$. There are 8 auxiliary sensors which are not used to collect data. This parallel ULA is constructed by employing dipole antennas and the mutual coupling matrix is found by using a numerical electromagnetic code. The coupling coefficients in (5.7) are $c_1 = 0.2040 + j0.1373$, $c_2 = -0.0736 - j0.0634$, $c_3 = 0.1056 - j0.0399$ and $c_4 = 0.2483 + j0.2432$. c_3 is the diagonal, c_4 is the across term with respect to the first sensor as in Appendix C, (C.1) and (C.2). In the simulations PULA-1 represents the performances of the triple subarrays in Figure 5.1 and PULA-2 represents the performances of the subarrays in Figures 5.2 and 5.3. In this case PULA-2 is the improved version of the PULA-1 with additional computation.

Figure 5.4 shows the 2-D DOA performance for the proposed methods when there are three sources and all the sources are coherent with DOA angles ($\phi_1 = 105°$, $\theta_1 = 60°$), ($\phi_2 = 190°$, $\theta_2 = 20°$) and ($\phi_3 = 210°$, $\theta_3 = 40°$). In this figure, the azimuth DOA performances are given for the PULA-1 and PULA-2. PULA-2 performance is better than PULA-1 and it is close to the CRB.

Figure 5.5 shows the elevation performance in the same scenario. In this case, a similar characteristic as in Figure 5.4 is seen.

Figure 5.6 shows the 2-D DOA performance in the same scenario in terms of the number of snapshots. SNR is set as 15dB. The PULA-2 performance is close to the CRB and PULA-1 follows the CRB.

In Figure 5.7 and Figure 5.8, the 2-D DOA estimates of the proposed method are marked in the figure for each trial to see the angular distribution for PULA-1 and PULA-2, respectively. SNR is set to SNR=15dB. As it is seen from these figures, both algorithms localize the

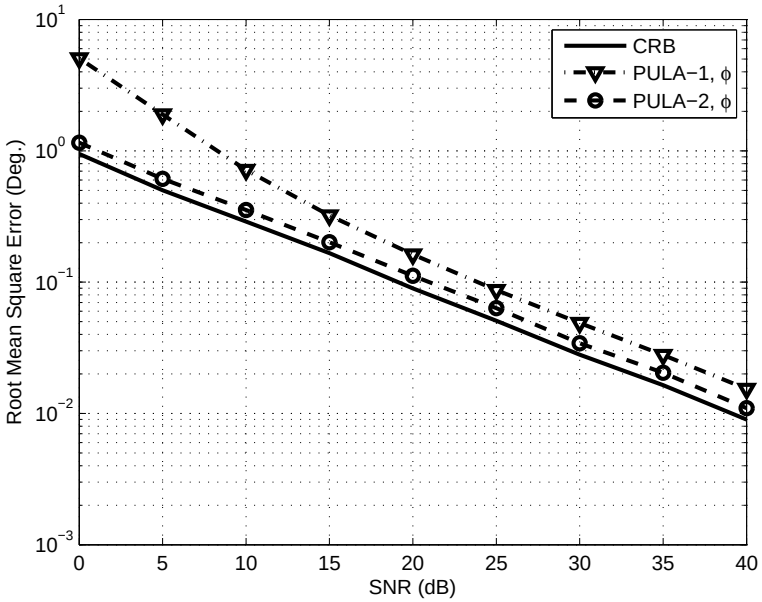

Figure 5.4: 2-D paired azimuth DOA performance for different SNR levels when there are three sources.

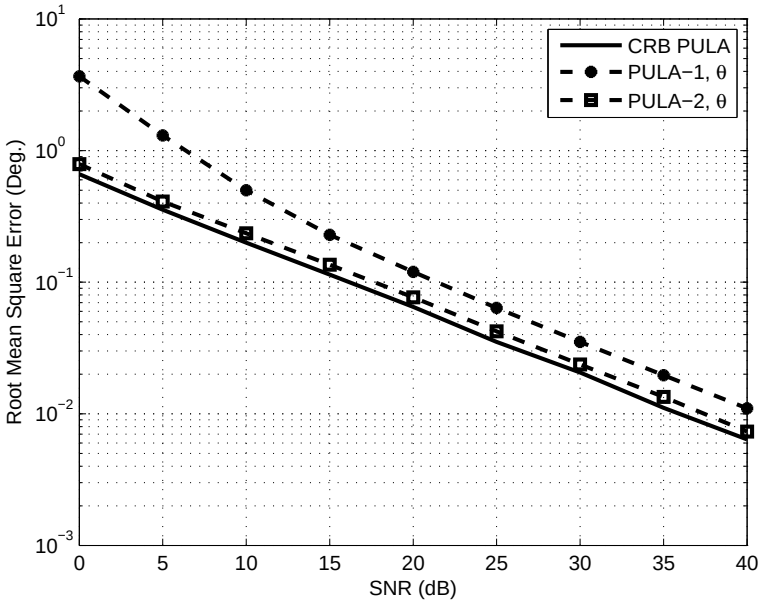

Figure 5.5: 2-D paired elevation DOA performance for different SNR levels when there are three sources.

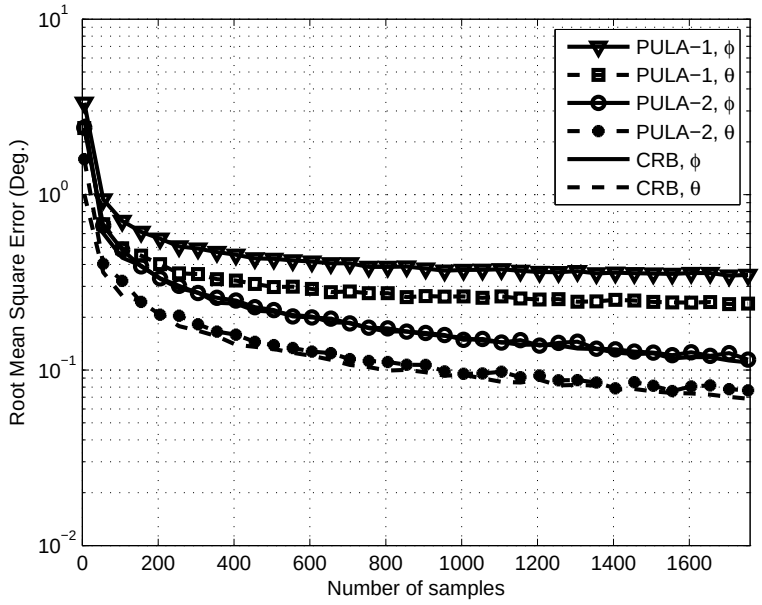

Figure 5.6: 2-D paired azimuth and elevation DOA estimates for different number of snapshots when there are three sources and SNR=15dB.

multiple sources effectively.

Figure 5.9 shows the azimuth DOA performance when there are two coherent sources and SNR=15 dB. One source is at (ϕ_1=100°, θ_1=40°). The elevation angle for the second source is fixed at θ_2=60°. The azimuth angle is swept between 130° and 260° in half degree resolution. This figure shows the algorithm performance of PULA-1 and PULA-2 for the closely spaced sources. In addition, no outlier is observed for 500 trials and the algorithm accurately solves the pairing problem.

Figure 5.10 shows the elevation DOA performance when there are two coherent sources and SNR=15 dB. One source is at (ϕ_1=100°, θ_1=40°). The azimuth angle for the second source is fixed at ϕ_2=180°. The elevation angle is swept between 0° and 89° in half degree resolution. It is seen that PULA-1 and PULA-2 algorithms can resolve elevation angles of multiple coherent sources accurately.

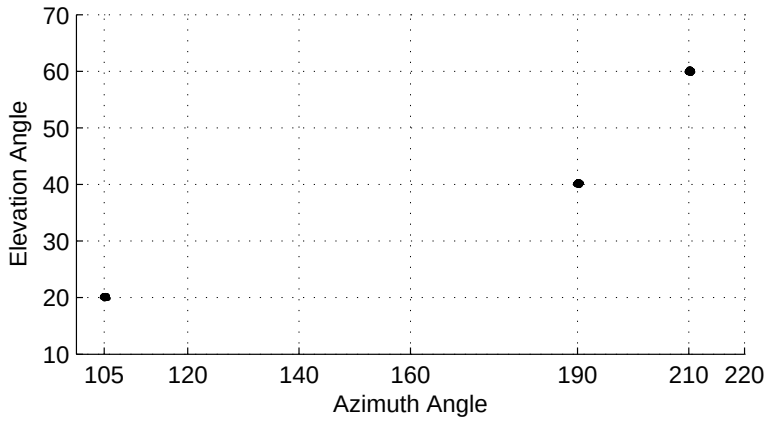

Figure 5.7: 2-D DOA distribution of PULA-1 when there are three coherent sources and SNR=15dB.

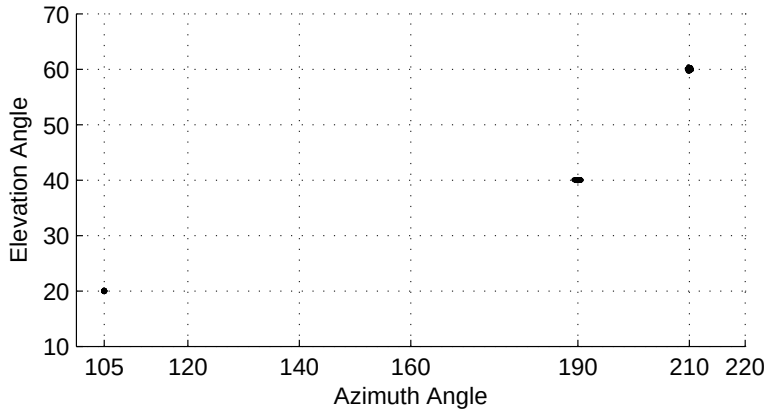

Figure 5.8: 2-D DOA distribution of PULA-2 when there are three coherent sources and SNR=15dB.

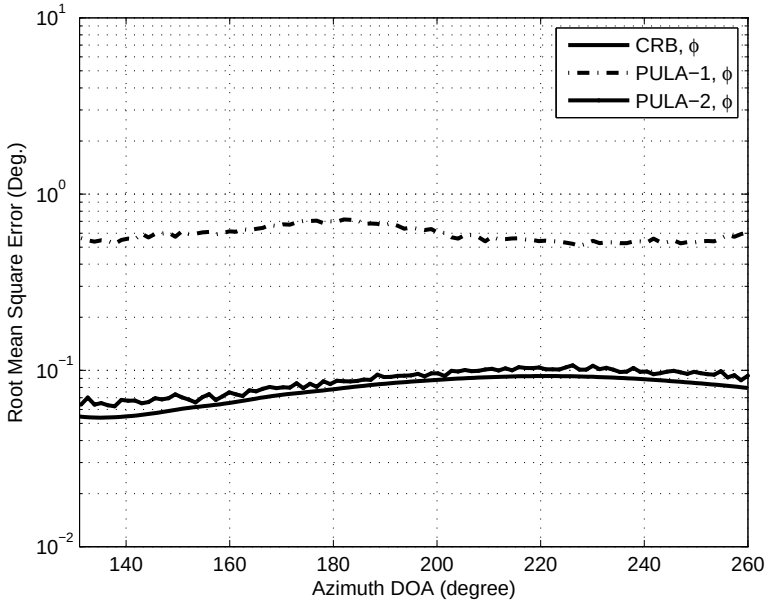

Figure 5.9: 2-D paired azimuth DOA performance for two coherent sources for PULA-1 and PULA-2. SNR is 15 dB. There is unknown mutual coupling between antennas.

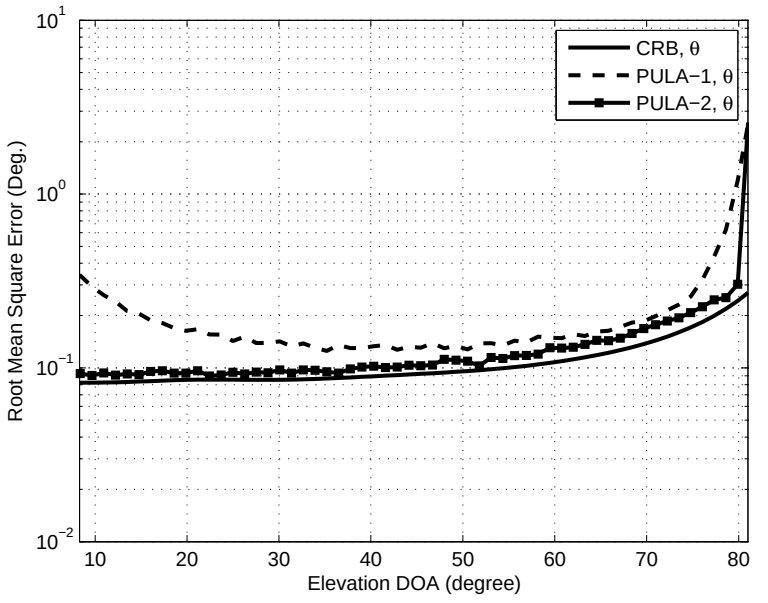

Figure 5.10: 2-D paired elevation DOA performance for two coherent sources for PULA-1 and PULA-2. SNR is 15 dB. There is unknown mutual coupling between antennas.

5.5 Conclusion

A new method of fast 2-D paired DOA estimation in case of mutual coupling between antennas and multipath signals is presented. The method uses a special array geometry which is consisted of two parallel ULA. The array is partitioned into ULA structures such that the ULA structures have the same MCM. The triplet structure and the ESPRIT algorithm are used to obtain closed form expressions for the 2-D DOA angles. It is shown that the proposed approach is effective and can handle multipath signals. It is also shown that selecting different subarrays within PULA which have larger baselines, can significantly improve the performance.

CHAPTER 6

CONCLUSION

In this thesis, 2-D DOA estimation is considered from different perspectives. In the first part, we have investigated the V-shaped planar arrays for the 2-D DOA estimation. These array structures have certain advantages which are not well known in the literature. The sensors on V-shaped array can be placed both uniformly and nonuniformly. It is also possible to design isotropic uniform and nonuniform V-shaped arrays which have the same DOA performance for all directions. The isotropic response is a desired property of planar arrays for some applications. This property is also necessary for uncoupled azimuth and elevation angle estimation.

In this thesis, the closed form expressions are derived which give the angle between the arms of uniform V-array. It is shown that this angle depends on the number of sensors in V-shaped array and converges to $2 \times \arctan(1/2)$ for infinite number of sensors. Two conditions on sensor displacement and an expression for V-angle are also derived for isotropic nonuniform V-shaped array. Nonuniform V-shaped arrays provide good DOA performance with a limited number of sensors. While it is useful to have isotropic response in many cases, directional arrays are preferred in some applications where the source signals are in a certain angular sector. V-shaped arrays can also be configured for good directional DOA performance. We propose a design procedure which allows one to find the required parameters for the desired criteria. In this respect, two regions are defined as focused and unfocused. The proposed design method gives an optimum V-angle which has the best possible DOA accuracy for the focused region while satisfying an acceptable level for unfocused region.

The circular arrays, which are well known in the literature, are compared with the V-shaped arrays for different aspects. This comparison is done by considering the azimuth and elevation

CRB. The most basic advantage of the uniform V-shaped array is the aperture size. When the distance between sensors is fixed to half of the wavelength, V-shaped array has a larger aperture than circular arrays. Therefore, the DOA accuracy of the V-shaped array is better than the circular arrays for the same number of sensors. V-shaped array and circular array have similar robustness for the sensor position errors. It is observed that for the closely spaced and correlated sources, V-shaped array has a better performance. The mutual coupling effect is also investigated and a fair comparison is done by finding the mutual coupling coefficients of both arrays with an electromagnetic simulation tool. It is shown that the number of mutual coupling coefficients for the V-shaped array is larger than the circular array. In ideal case, this situation is not a problem for multiple sources. But in practical situations, V-shaped arrays are affected more than the circular arrays for the mutual coupling.

In this thesis, a new fast and effective 2-D DOA estimation method is presented which performs better than the known methods especially at low SNR. The method is based on the relation of three sub-arrays where two of the arrays are positioned accordingly with respect to the base array. These two arrays are combined to construct a virtual array. ESPRIT algorithm is used by employing both the base and virtual array. The eigenvalues of the rotational transformation matrix have the angle information at both magnitude and phase which allows the estimation of azimuth and elevation angles by using closed form expressions. In order to estimate M multiple 2-D sources, $3M$ sensors are required in general. However in this work, proposed method uses array interpolation technique and virtual arrays. Therefore $M + 1$ sensors are sufficient for 2-D DOA estimation. This method is called paired interpolated ESPRIT (PIE) algorithm which can be applied for arbitrary arrays when there is no mutual coupling between antenna elements or when the mutual coupling can be ignored.

When there is mutual coupling, two approaches are proposed in order to obtain 2-D paired DOA estimates. In the first approach, special array structures which have banded Toeplitz MCM are preferred in order to use array interpolation. In this case, the effect of unknown mutual coupling can be reflected onto the source signal and 2-D paired DOA angles can be estimated without estimating the mutual coupling coefficients. Therefore this technique is called Blind Paired Interpolated ESPRIT (BPIE). BPIE technique is very effective and approaches to the CRB for a single source. But when the number of sources is increased, the size and the condition number of the interpolation mapping matrices are large and this degrades the DOA accuracy. The second approach estimates the coupling coefficients and

DOA angles in sequence and it is called PIE with Coupling Estimation (PIECE). PIECE algorithm uses the BPIE algorithm in order to find initial DOA angle estimates. Then it is possible to estimate the mutual coupling coefficients by using these initial DOA angles. This improves the accuracy of the array interpolation and a better DOA estimate is obtained. The process of mutual coupling coefficient and DOA estimation can be repeated through iterations. In this respect, it is shown that the iterations improve the performance significantly. The proposed technique solves the pairing problem and effectively estimates the multiple 2-D DOA angles in case of unknown mutual coupling. While this new approach performs better, it cannot be used satisfactorily in case of multipath signals. In practical applications such as wireless communications, multipath propagation is a common problem and needs to be addressed.

In this thesis, a search-free, fast and effective technique is proposed in order to solve the 2-D DOA estimation problem in case of both multipath signals and mutual coupling. In this case, parallel uniform linear arrays (PULA) are used. This planar array structure is placed in a plane appropriately such that the 2-D paired DOA estimation technique can be applied to the selected sub-arrays in PULA. PULA is an efficient array structure where overlapping sub-arrays can be used for both spatial smoothing and 2-D DOA estimation. Auxiliary antennas are placed to the beginning and end of PULA, in order to obtain a symmetric banded Toeplitz mutual coupling matrix (MCM). The 2-D paired DOA estimation is done similar to the BPIE approach. But real array outputs are used instead of the virtual array outputs. This improves the performance since array interpolation error does not exist in this case. The price paid for this is the increase of the number of sensors and the following receiver structures. The performance of the proposed approach is further improved by an additional step where a sub-array selection with a larger baseline is done. In this case, 2-D DOA estimates are obtained with better accuracy while the DOA pairing is done by using the previous DOA estimates. Detailed analysis of mutual coupling structure of PULA and its selected sub-arrays are done. It is shown that spatial smoothing can be effectively used by the proposed technique to mitigate the multipath problem.

6.1 Future Works

There are several topics that can be investigated in future works. It is possible to develop new planar array geometries different from the ones proposed in this thesis for 2-D paired DOA estimation in case of unknown mutual coupling and multipath signals. In this case, the problem can be posed to find the optimum array geometry.

The proposed approaches in this thesis can be extended to the case where there is also unknown gain/phase mismatch for the sensors and receivers. In this case, the identifiability problem can be investigated. In addition, the problem setting where a unique solution is found can be constructed.

It is also possible to consider the case where the emitter DOA angle changes with time. This case corresponds to the situations where emitters move. The speed of the emitters dictates the amount of the data collected for determining the DOA angles. The position change of the emitters generates an error for the DOA estimates. This problem is more challenging than the one considered in this thesis and requires a thorough investigation.

It is possible to develop multisource 3-D tracking methods by using the proposed fast 2-D DOA estimation techniques for practical applications.

REFERENCES

[1] Travers, D. N. and S. M. Hixon, Abstracts of the available literature on radio direction finding 1899-1965, Southwest Research Inst., SAN ANTONIO TX, Tech. Rep., Jul 1966.

[2] Watson Watt, R. A. and J. F. Herd, An instantaneous direct reading radio goniometer, J. Inst. Elect. Eng, vol. 64, pp. 611–622, 1926.

[3] Earp, C. W. and R. Godfrey, Radio direction finding by the cyclical differential measurement of phases, Journal of the IEE, vol. Part IIIA, 1947.

[4] Schmidt, R. O., A signal subspace approach to multiple emitter location and spectral estimation, Ph.D. dissertation, Standford Univ., Standford, CA, Nov 1981.

[5] Haykin, S., Radar Array Processing for Angle of Arrival Estimation, In S.Haykin, editor, Array Signal Processing. Prentice-Hall, Englewood Cliffs, New Jersey, 1985

[6] Bohme, J. F., Statistical Array Signal Processing of Measured Sonar and Seismic Data, *In Proc. SPIE 2563 Advanced Signal Processing Algorithms*, San Diego, CA., 1995

[7] Haykin, S., J.P. Reilly, V. Kezys, E. Vertatschitsch, Some Aspects of Array Signal Processing, IEE Proceedings, vol. 139, pp. 1–26, 1992

[8] Krim, H. and M. Viberg, Two decades of array signal processing research: the parametric approach, IEEE Signal Processing Magazine, vol. 13, pp. 67–94, 1996.

[9] Swindlehurst, A. Lee, Highlights of Statistical Signal and Array Processing, IEEE Signal Processing Magazine, vol. 15, pp. 21–64, 1998

[10] Black, Q. R., J. F. Wood Jr., A. G. Sonsteby, and W. M. Sherrill (1993), A direction finding ionosonde for ionospheric propagation research, *Radio Sci.*, vol. 28(5), pp. 795-809, 1993

[11] Van Trees, Harry L., Optimum Array Processing, Wiley, 1472 pages, USA, 2002.

[12] Abramovich, Y.I. and Spencer, N.K., Simultaneous DOA estimation of fully correlated and uncorrelated Gaussian sources in nonuniform linear antenna arrays, Proceedings of the 8th Annual Workshop on Adaptive Sensor Array Processing (ASAP 2000), MIT Laboratory, Lexington, Massachusetts, USA, March 2000

[13] Tuncer, T. E. and B. Friedlander, Classical and Modern Direction-of-Arrival Estimation, Academic Press, 456 pages, 2009.

[14] Gershman, A. B., and J. F. Bohme, A note on most favorable array geometries for DOA estimation and array interpolation, *IEEE Signal Processing Letters*, vol. 4(8), pp. 232–235, 1997.

[15] Barabell, A.J., Improving the resolution performance of eigenstructure based direction finding algorithms, *Proc. IEEE ICASP'83*, pp. 336–339, May 1983.

[16] Shan, Tie-Jun, Wax, M. and Kailath, T., On spatial smoothing for direction-of-arrival estimation of coherent signals, *Acoustics, Speech, and Signal Processing, IEEE Transactions*, vol. 33(4), pp. 806–811, August 1985.

[17] Baysal,U., and R. L. Moses, On the Geometry of Isotropic Arrays, *IEEE Transactions on Signal Processing*, vol. 51(6), pp. 1469–1478, 2003.

[18] Oktel, U., and L. M. Randolph, A Bayesian Approach to Array Geometry Design, *IEEE Transactions on Signal Processing*, vol. 53(5), pp. 1919–1923, 2005.

[19] Manikas, A., Alexiou, A., Karimi, H. R., Comparison of the ultimate direction-finding capabilities of a number of planar array geometries, *IEE Proc.-Radar, Sonar Navig.*, vol. 144(6), pp.312–329, December 1997.

[20] Hua, Y., T. K. Sarkar, and D. D. Weiner, An L-shaped array for Estimating 2-D Directions of Arrival, *IEEE Transactions on Antennas and Propagation*, vol. 39(2), pp. 143–146, 1991.

[21] Hua, Y., and T. K. Sarkar, A Note on the Cramer-Rao Bound for 2-D Direction Finding Based on 2-D Array, *IEEE Transactions on Signal Processing*, vol. 39(5), pp. 1215–1218, 1991.

[22] Gazzah, H., and S. Marcos, Cramer-Rao Bounds for Antenna Array Design, *IEEE Transactions on Signal Processing*, vol. 54(1), pp. 336–345, 2006.

[23] Friedlanderr, B., J. Weiss, Direction Finding in the Presence of Mutual Coupling, *IEEE Transaction on Antennas and Propagation*, vol. 39(3), pp. 273–284, 1991.

[24] Svantesson, T. (1999), Direction Finding in the Presence of Mutual Coupling, *Thesis for the degree of Licentiate of Engineering*, Chalmers University of Technology, Goteborg, Sweden.

[25] Ye, Z., C. Liu, 2-D DOA Estimation in the Presence of Mutual Coupling, *IEEE Transaction on Antennas and Propagation*, vol. 56(10), pp. 3150–3158, 2008.

[26] Chan, A. Y. J. and J. Litva, MUSIC and maximum likelihood techniques on two dimensional DOA estimation with uniform circular array, *Proc. Inst. Elect. Eng. Radar, Sonar and Navigation*, vol. 142(3), pp. 105–114, Jun. 1995.

[27] Veen, A., P. B. Ober, E. F. Deprettere, Azimuth and Elevation Computation in High Resolution DOA Estimation, *IEEE Transactions on Signal Processing*, vol. 40(7), pp. 1828–1832, 1992.

[28] Fernandez, J.E., M.F. Catedra-Perez, The Matrix Pencil Method for Two-Dimensional Direction of Arrival Estimation Employing an L-Shaped Array, *IEEE Transactions on Antenn. Propogat.*, vol. 45(11), pp. 1693–1694, 1997.

[29] Kedia, V. S., B. Chandna, A new algorithm for 2-D DOA estimation, *Signal Processing*, vol. 60, pp. 325–332, 1997.

[30] Liu, T., J. M. Mendel, Azimuth and Elevation Direction Finding Using Arbitrary Array Geometries, *IEEE Transactions on Signal Processing*, vol. 46(7), pp. 2061–2065, 1998.

[31] Kikuchi, S., H. Tsuji, A. Sano, Pair-Matching Method for Estimating 2-D Angle of Arrival With a Cross-Correlation Matrix, *IEEE Antennas and Wireless Propagation Letters*, vol. 5, pp. 35–40, 2006.

[32] Tayem, N., H. M. Kwon, L-Shape 2-Dimensional Arrival Angle Estimation With Propagator Method, *IEEE Transactions on Antenn. Propogat.*, vol. 53(5), pp. 1622–1630, 2005.

[33] Gu, J., P. Wei, H. Tai, 2-D direction-of-arrival estimation of coherent signals using cross-correlation matrix, *Signal Proessing*, vol. 88, pp. 75–85, 2008.

[34] Mathews, C. P., and M. D. Zoltowski, Eigenstructure Techniques for 2-D Angle Estimation with Uniform Circular Arrays, *IEEE Transactions on Signal Processing*, vol. 42(9), pp. 2395–2407, 1994.

[35] Zoltowski, M. D., M. Haardt, C. P. Mathews, Closed-Form 2-D Angle Estimation with Rectangular Arrays in Element Space or Beamspace via Unitary ESPRIT, *IEEE Transactions on Signal Processing*, vol. 44(3), pp. 316–328, 1996.

[36] Liu, Q., Two-dimensional virtual ESPRIT algorithm, *IEEE Electronics Letters*, vol. 37(16), pp. 1052–1053, 2001.

[37] Xia, T., Y. Zheng, Q. Wan, X. Wang, Decoupled Estimation of 2-D Angles of Arrival Using Two Parallel Uniform Linear Arrays, *IEEE Transactions on Antenn. Propogat.*, vol. 55(9), pp. 2627–2632, 2007.

[38] Bronez, T. P., Sector interpolation of non-uniform arrays for efficient high resolution bearing estimation, in *Acoustics, Speech, and Signal Processing, ICASSP-88., 1988 International Conference on*, New York, pp. 2885–2888, 1988.

[39] Friedlander, B., The root-music algorithm for direction finding with interpolated arrays, *Signal Processing, IEEE Transactions on*, vol. 53(12), pp. 4464–4471, 1993.

[40] P. Hyberg, M. Jansson, and B. Ottersten, Array interpolation and DOA MSE reduction, *Signal Processing, IEEE Transactions on*, vol. 53(12), pp. 4464–4471, 2005.

[41] Tuncer, T. E., T. K. Yasar, and B. Friedlander, Direction of arrival estimation for nonuniform linear arrays by using array interpolation, *Radio Sci.*, vol. 42, 2007.

[42] Yasar, T. K., T. E. Tuncer, Wideband DOA estimation for nonuniform linear arrays with Wiener array interpolation, The fifth IEEE Sensor Array and Multichannel Signal Processing Workshop, SAM-2008, Darmstadt, Germany, July 21 2008.

[43] Pillai, S. U., and B. H. Kwon, Forward/backward spatial smoothing techniques for coherent signal identification, *Acoustics, Speech, and Signal Processing, IEEE Transactions on*, vol. 37(1), pp. 8–15, 1989.

[44] Filik, Tansu, and T. Engin Tuncer, Uniform and Nonuniform V-shaped Isotropic Planar Arrays, *The fifth IEEE Sensor Array and Multichannel Signal Processing Workshop*, SAM-2008, Darmstadt, Germany, pp. 99–103, 2008.

[45] Filik, Tansu, and T. Engin Tuncer, Design and evaluation of V-shaped arrays for 2-D DOA estimation, *Int. Conf. on Acoustics Speech and Signal Proc.*, ICASSP-2008, Las Vegas, Nevada, USA, March 30, 2008.

[46] Filik, Tansu, and T. E. Tuncer, Uniform and Nonuniform V-Shaped Planar Arrays for 2-D Direction-of-Arrival Estimation, *Radio Science*, vol.44, pp. 1-12, Sept.22, 2009.

[47] Weiss, A. J., and B. Friedlander, On The Cramer-Rao Bound For Direction Finding Of Correlated Signals, *IEEE Transactions on Signal Processing*, vol. 41(1), pp. 495–499, 1993.

[48] Mirkin, A. N., and L. H. Sibul, Cramer-Rao Bounds on Angle Estimaiton with a Two-Dimensional Array, *IEEE Transactions on Signal Processing*, vol. 39(2), pp. 515–517, 1991.

[49] Nielsen, R. O. (1994), Azimuth and Elevation Angle Estimation with a Three-Dimensional Array, *IEEE Journal of Oceanic Engineering*, vol. 19(1), pp. 84–86, 1994

[50] FEKO User's Manuel, EM Software and Systems, S.A. (Pty) Ltd., July 2008, [Online]. Available: `http://www.feko.info`

[51] See, C. S., and B. Poh, Parametric Sensor Array Calibration Using Measured Steering Vectors of Uncertain Localitions, *IEEE Transactions on Signal Processing*, vol. 47(4), pp. 1133–1137, April 1999.

[52] Boon P.N., J.P. Lie, M.H. Er and A. Fen, A Practical Simple Geometry and Gain/Phase Calibration Technique for Antenna Array Processing, *IEEE Transactions on Antenn. Propogat.*, vol. 57(7), pp. 1963–1972, 2009.

[53] Weiss, A.J., B. Friedlander, DOA and steering vector estimation using a partially calibrated array, *IEEE Transactions on Aerospace and Electronic Systems*, vol. 32(3), pp. 1047–1057, 1996.

[54] Z. Ye, C. Liu, On the resiliency of MUSIC direction finding against antenna sensor coupling, *IEEE Trans. on Antenna Prop.*, vol. 56, pp. 371-380, Feb. 2008.

[55] Roy, R., and T. Kailath, ESPRIT-Estimation of signal parameters via rotational invariance techniques, *Acoustic, Speech and Signal Processing, IEEE Transactions on*, vol. 37(7), pp. 984–995, 1989.

[56] Stoica, P., and A. Nehorai, Performance study of conditional and unconditional direction-of-arrival estimation, *Signal Processing, IEEE Transactions on*, vol. 39(2), pp. 446–453, 1991.

[57] Filik, T. and T. E. Tuncer, Closed-Form Automatically Paired 2-D Direction-of-Arrival Estimation with Arbitrary Arrays, European Signal Processing Conference (EUSIPCO-2009), Glasgow, Scotland, Aug. 24, 2009.

[58] Goossens, R., and H. Rogier, A Hybrid UCA-RARE/Root-MUSIC Approach for 2-D Direction of Arrival Estimation in Uniform Circular Arrays in the Presence of Mutual Coupling, *IEEE Transactions on Antenn. Propogat.*, vol. 55(3), pp. 841–849, 2007.

[59] Lin, M., L. Yang, Blind Calibration and DOA Estimation With Uniform Circular Arrays in the Presence of Mutual Coupling, *IEEE Antennas and Wireless Propagation Letters*, vol. 5, pp. 315–318, 2006.

[60] Swingler, D. N., Narrowband Line-Array Beamforming: Practically Achievable Resolution Limit of Unbiased Estimators, *IEEE Journal of Oceanic Engineering*, vol. 19(2), pp. 225-226, 1994.

[61] Filik, Tansu and T. Engin Tuncer, Fast and Automatically Paired 2-D Direction-of-Arrival Estimation With and Without Estimating the Mutual Coupling Coefficients, *to be published in Radio Science*, 2009.

[62] Filik, Tansu and T. Engin Tuncer, Fast And Paired 2-D DOA Estimation In Case Of Unknown Mutual Coupling For Multipath Signals, *to be submitted to IEEE Transaction on Signal Processing*.

[63] Xia, T., Y. Zheng, Q. Wan, X. Wang, Decoupled Estimation of 2-D Angles of Arrival Using Two parallel Uniform Linear Arrays, *IEEE Trans. on Antenna Prop.*, vol. 55, pp. 2627–2632, 2007.

[64] Wu, Y., G. Liao, H.C. So, A fast algorithm for 2-D direction-of-arrival estimation, *Signal Processing*, vol. 83, pp. 1827–1831, 2003.

APPENDIX A

Isotropic V-angle for Uniform V-shaped Arrays

In this appendix, we derive the closed form equation (3.18) which returns isotropic V-angle for uniform V-shaped arrays. The array center of gravity (x_c, y_c) for uniform and symmetric V-shaped arrays, is given as

$$x_c = \frac{1}{M} d \sin(\gamma/2) \sum_{l=1}^{M} (l-k) = 0 \tag{A.1}$$

$$\begin{aligned} y_c &= \frac{1}{M} d \cos(\frac{\gamma}{2}) \sum_{l=1}^{M} |l-k| \\ &= \frac{1}{M} d \cos(\frac{\gamma}{2}) \frac{(M^2-1)}{4}. \end{aligned} \tag{A.2}$$

For isotropic V-shaped arrays P_{xy}, must be zero. Since $x_c = 0$,

$$P_{xy} = \sum_{l=1}^{M} x_l y_l - \sum_{l=1}^{M} x_l y_c. \tag{A.3}$$

If we open this equation,

$$P_{xy} = d^2 \sin(\frac{\gamma}{2}) \cos(\frac{\gamma}{2}) \left(\sum_{l=1}^{M} (l-k)|l-k| - \frac{(M^2-1)}{4M} \sum_{l=1}^{M} (l-k) \right) \tag{A.4}$$

where $\sum_{l=1}^{M} (l-k)|l-k| = 0$ and $\sum_{l=1}^{M} (l-k) = 0$, so $P_{xy} = 0$. P_{xx} must be equal to P_{yy} for isotropic response. We can find P_{xx} as,

$$P_{xx} = \sum_{l=1}^{M} (x_l)^2 = d^2 \sin^2(\frac{\gamma}{2}) \sum_{l=1}^{M} (l-k)^2$$

which gives

$$P_{xx} = 2d^2 \sin^2(\frac{\gamma}{2}) \frac{(M^2-1)M}{24}. \tag{A.5}$$

Then we need to find P_{yy}

$$\begin{aligned} P_{yy} &= \sum_{l=1}^{M}(y_l - y_c)^2 = \sum_{l=1}^{M}\{y_l^2 + y_c^2 - 2y_l y_c\} \\ &= \sum_{l=1}^{M} y_l^2 + My_c^2 - 2y_c \sum_{l=1}^{M} y_l \end{aligned} \tag{A.6}$$

where

$$\begin{aligned} \sum_{l=1}^{M} y_l^2 &= 2d^2 \cos^2(\frac{\gamma}{2}) \sum_{l=1}^{\frac{M-1}{2}}(l-k)^2 \\ &= 2d^2 \cos^2(\frac{\gamma}{2})\frac{(M^2-1)M}{24} \end{aligned} \tag{A.7}$$

and

$$My_c^2 = d^2 \cos^2(\frac{\gamma}{2})\frac{(M-1)^2(M+1)^2}{16M} \tag{A.8}$$

$$\begin{aligned} 2y_c \sum_{l=1}^{M} y_l &= d^2 \cos^2(\frac{\gamma}{2})\frac{(M^2-1)}{2M}\sum_{l=1}^{M}|l-k| \\ &= d^2 \cos^2(\frac{\gamma}{2})\frac{(M-1)^2(M+1)^2}{8M}. \end{aligned} \tag{A.9}$$

Therefore if we combine the expressions in, (A.7), (A.8) and (A.9), with (A.6), we get P_{yy} as,

$$P_{yy} = d^2 \cos^2(\frac{\gamma}{2})\frac{(M^2-1)}{8}\frac{M^2+3}{6M}. \tag{A.10}$$

Using the equations (A.5) and (A.10) in order to satisfy (3.13), V-angle is found as,

$$\gamma_{iso_M} = 2 \times \arctan(\sqrt{\frac{M^2+3}{4M^2}}). \tag{A.11}$$

APPENDIX B

Isotropic V-angle for Nonuniform V-shaped Arrays

In this part, the derivation of (3.20) and (3.21) for nonuniform V-shaped isotropic planar array is presented.

$$x_c = \frac{1}{M}\sin(\gamma/2)\left(\sum_{l=M_1+2}^{M} d_l - \sum_{l=1}^{M_1} d_l\right) \tag{B.1}$$

$$y_c = \frac{1}{M}\cos(\gamma/2)\left(\sum_{l=1}^{M_1} d_l + \sum_{l=M_1+2}^{M} d_l\right) \tag{B.2}$$

P_{xy} must be zero for isotropic response.

$$\begin{aligned} P_{xy} &= \sum_{l=1}^{M}(x_l - x_c)(y_l - y_c) = 0 \\ &= \sum_{l=1}^{M} x_l y_l - M x_c y_c = 0 \\ \sum_{l=1}^{M} x_l y_l &= M x_c y_c \end{aligned} \tag{B.3}$$

The above equation is satisfied only if

$$\sum_{l=1}^{M_1} d_l = \sum_{l=M_1+2}^{M} d_l \quad \text{and} \quad \sum_{l=1}^{M_1} d_l^2 = \sum_{l=M_1+2}^{M} d_l^2. \tag{B.4}$$

So x_c becomes zero and $\mathrm{P}_{xy} = 0$. We need to equate P_{xx} to P_{yy} in order to get isotropic response.

$$\begin{aligned} P_{xx} &= \sum_{l=1}^{M}(x_l - x_c)^2 = \sum_{l=1}^{M} x_l^2 \\ &= \sin^2(\frac{\gamma}{2})\left(\sum_{l=1}^{M_1} d_l^2 + \sum_{l=M_1+2}^{M} d_l^2\right) \end{aligned} \tag{B.5}$$

If (B.4) is satisfied, P_{xx} and P_{yy} can be written as,

$$P_{xx} = 2\sin^2(\frac{\gamma}{2})\sum_{l=1}^{M_1} d_l^2 \tag{B.6}$$

$$P_{yy} = \sum_{l=1}^{M}(y_l - y_c)^2 = \sum_{l=1}^{M} y_l^2 - My_c^2$$

$$= 2\cos^2(\frac{\gamma}{2})\sum_{l=1}^{M_1} d_l^2 - My_c^2 \tag{B.7}$$

where

$$My_c^2 = \frac{4}{M}\cos^2(\frac{\gamma}{2})\left(\sum_{l=1}^{M_1} d_l\right)^2 . \tag{B.8}$$

Therefore if we substitute (B.8), into (B.7), we get P_{yy} as,

$$P_{yy} = 2\cos^2(\frac{\gamma}{2})\left(\sum_{l=1}^{M_1} d_l^2 - \frac{2}{M}\left(\sum_{l=1}^{M_1} d_l\right)^2\right). \tag{B.9}$$

If we equate (B.6) and (B.9) in order to satisfy isotropy condition (P_{xx}=P_{yy}), we get γ_{iso} as in (3.21).

APPENDIX C

The MCM Structure of PULA

In this part, the structure of the mutual coupling matrix (MCM) of the PULA is given. The sub-matrices $\mathbf{C}_1$ and $\mathbf{C}_2$ in (5.7), are composed as,

$$\mathbf{C}_1 = \begin{bmatrix} 1 & x & y & 0 & 0 & 0 & \cdots & 0 \\ x & 1 & x & y & 0 & 0 & \cdots & 0 \\ c_2 & c_1 & 1 & c_1 & c_2 & 0 & \cdots & 0 \\ 0 & c_2 & c_1 & 1 & c_1 & c_2 & \cdots & 0 \\ & & \ddots & \ddots & \ddots & \ddots & \ddots & \\ 0 & \cdots & 0 & c_2 & c_1 & 1 & c_1 & c_2 \\ 0 & \cdots & 0 & 0 & y & x & 1 & x \\ 0 & \cdots & 0 & 0 & 0 & y & x & 1 \end{bmatrix}_{\frac{\tilde{M}}{2}\times\frac{\tilde{M}}{2}} \tag{C.1}$$

$$\mathbf{C}_2 = \begin{bmatrix} w & z & 0 & 0 & 0 & 0 & \cdots & 0 \\ z & w & z & 0 & 0 & 0 & \cdots & 0 \\ 0 & c_3 & c_4 & c_3 & 0 & 0 & \cdots & 0 \\ 0 & 0 & c_3 & c_4 & c_3 & 0 & \cdots & 0 \\ & & & \ddots & \ddots & \ddots & & \\ 0 & \cdots & 0 & 0 & c_3 & c_4 & c_3 & 0 \\ 0 & \cdots & 0 & 0 & 0 & z & w & z \\ 0 & \cdots & 0 & 0 & 0 & 0 & z & w \end{bmatrix}_{\frac{\tilde{M}}{2}\times\frac{\tilde{M}}{2}} \tag{C.2}$$

where x, y, w, z are the coupling coefficients for auxiliary sensors. c_1 and c_2 are the coupling coefficients in the nearest neighborhood of the sensors and c_3 and c_4 are the cross terms for the parallel ULA. As it is seen, the MCM structure for the PULA is in the block banded Toeplitz structure.

The sub-matrices, $\mathbf{C}_{(k),m}$ in (5.16) for $m = 1, 2, 3$ are in the form of

$$\mathbf{C}_{(k),1} = \begin{bmatrix} \mathbf{0}_{M\times(k-1)} & \mathbf{C}^L_{M\times M} & \mathbf{C}^R_{M\times M} & \mathbf{0}_{M\times(\bar{M}-2M-k+1)} \end{bmatrix}_{M\times\bar{M}} \tag{C.3}$$

$$\mathbf{C}_{(k),2} = \begin{bmatrix} \mathbf{0}_{M\times k} & \mathbf{C}^L_{M\times M} & \mathbf{C}^R_{M\times M} & \mathbf{0}_{M\times(\bar{M}-2M-k)} \end{bmatrix}_{M\times\bar{M}} \tag{C.4}$$

$$\mathbf{C}_{(k),3} = \begin{bmatrix} \mathbf{0}_{M\times(k-1)} & \mathbf{C}^R_{M\times M} & \mathbf{C}^L_{M\times M} & \mathbf{0}_{M\times(\bar{M}-2M-k+1)} \end{bmatrix}_{M\times\bar{M}} \tag{C.5}$$

where $\mathbf{C}^L$ is the left coupling matrix and defined as,

$$\mathbf{C}^L = \begin{bmatrix} c_2 & c_1 & 1 & c_1 & c_2 & 0 & \cdots & 0 \\ 0 & c_2 & c_1 & 1 & c_1 & c_2 & \cdots & 0 \\ & & \ddots & \ddots & \ddots & \ddots & \ddots & \\ 0 & \cdots & 0 & c_2 & c_1 & 1 & c_1 & c_2 \end{bmatrix}_{M\times M} \tag{C.6}$$

and $\mathbf{C}^R$ is the right coupling matrix and defined as,

$$\mathbf{C}^R = \begin{bmatrix} 0 & c_3 & c_4 & c_3 & 0 & 0 & \cdots & 0 \\ 0 & 0 & c_3 & c_4 & c_3 & 0 & \cdots & 0 \\ & & & \ddots & \ddots & \ddots & \ddots & \\ 0 & \cdots & 0 & 0 & c_3 & c_4 & c_3 & 0 \end{bmatrix}_{M\times M} . \tag{C.7}$$

As we can see, $\mathbf{C}_{(k),2}$ is the shifted version of the $\mathbf{C}_{(k),1}$ and in $\mathbf{C}_{(k),3}$, $\mathbf{C}^L$ and $\mathbf{C}^R$ matrices are swapped according to the $\mathbf{C}_{(k),1}$. These relations are formulated in (5.17) and (5.18). The $\mathbf{U}$ and $\mathbf{L}$ matrices in these relations are defined as,

$$\mathbf{U} = \begin{bmatrix} 0 & 1 & 0 & 0 & \cdots & 0 \\ 0 & 0 & 1 & 0 & \cdots & 0 \\ & & & \ddots & & \\ 0 & 0 & 0 & \cdots & 0 & 1 \\ 1 & 0 & 0 & \cdots & 0 & 0 \end{bmatrix}_{\bar{M}\times\bar{M}} \quad \mathbf{L} = \begin{bmatrix} 0 & \cdots & 0 & 0 & 1 \\ 0 & \cdots & 0 & 1 & 0 \\ \vdots & & & & \\ 0 & 1 & 0 & \cdots & 0 \\ 1 & 0 & 0 & \cdots & 0 \end{bmatrix}_{\bar{M}\times\bar{M}} . \tag{C.8}$$

The k^{th} power of the $\mathbf{U}$ matrix is represented as,

$$\mathbf{U}^k = \underbrace{\mathbf{U}\ldots\mathbf{U}}_{k\ time} \tag{C.9}$$

CURRICULUM VITAE

PERSONAL INFORMATION

Surname, Name: Filik, Tansu
Nationality: Turkish (TC)
Date and Place of Birth: 1979 , Eskişehir
Phone: +90 505 427 04 88
email: tfilik@metu.edu.tr

EDUCATION

Degree	Institution	Year of Graduation
Integrated MS and PhD	METU, Electrical and Electronics Engineering, Ankara	2010
BS	Anadolu University, Electrical and Electronics Engineering, Eskişehir	2002
High School	Hoca Ahmed Yesevi, Eskişehir	1997

WORK EXPERIENCE

Year	Place	Enrollment
2002-	METU, Electrical and Electronic Eng. Dep.	Research and Teaching Assistant

FOREIGN LANGUAGES

Advanced English

PUBLICATIONS

1. Tansu Filik and T. Engin Tuncer, *A Fast and Automatically Paired 2-D Direction-of-Arrival Estimation With and Without Estimating The Mutual Coupling Coefficients*, Radio Science, (14 Pages), to be published in Radio Science, 2010.

2. Tansu Filik and T. Engin Tuncer, *Uniform and Nonuniform V-Shaped Planar Arrays for 2-D Direction-of-Arrival Estimation*, Radio Science, Vol.44, pp.1-12, Sept.22, 2009.

3. Tansu Filik and T. Engin Tuncer, *2-D Paired Direction-of-Arrival Angle Estimation with Two Parallel Uniform Linear Arrays*, Submitted to International Journal of Innovative Computing, Information and Control

4. Tansu Filik and T. Engin Tuncer, *Fast and Paired 2-D DOA Estimation in case of Unknown Mutual Coupling for Multipath Signals*, IEEE Transactions on Signal Processing, in Preparation.

5. Tansu Filik, T. Engin Tuncer, *Closed-Form Automatically Paired 2-D Direction-of-Arrival Estimation with Arbitrary Arrays*, European Signal Processing Conference (EUSIPCO), Glasgow, Scotland, Aug. 24, 2009.

6. Tansu Filik, T Engin Tuncer, *A Novel Approach for Fast and Paired 2-D Direction-of-Arrival Estimation Using Two Parallel Uniform Linear Arrays*, ICIC-Express Letters, Vol.3, No.4(B), pp.1275–1281, December 2009.

7. Tansu Filik, T. Engin Tuncer, *Uniform and Nonuniform V-shaped Isotropic Planar Arrays*, The fifth IEEE Sensor Array and Multichannel Signal Processing Workshop, SAM-2008, Darmstadt, Germany, July 21 2008.

8. Tansu Filik, T. Engin Tuncer, *Design and evaluation of V-shaped arrays for 2-D DOA estimation*, Int. Conf. on Acoustics Speech and Signal Proc., ICASSP-2008, Las Vegas, Nevada, USA, March 30, 2008.

9. Tansu Filik, T. Engin Tuncer, *A fast and automatically paired 2-dimensional direction-of-arrival estimation using arbitrary array geometry*, Signal Processing and Communication Applications, 2009. SIU 2009, pp. 556–559, April 2009.

10. Tansu Filik, T. Engin Tuncer, T. K. Yasar *Uniform and non-uniform V-shaped arrays for 2-D DOA estimation*, Signal Processing and Communication Applications, 2008. SIU 2008, pp. 1–4, April 2008.

11. T. K. Yasar, T. Engin Tuncer, Tansu Filik *Direction of arrival estimation in non-uniform linear arrays for wide band signals with colored noise*, Signal Processing and Communication Applications, 2008. SIU 2008, pp. 1–4, April 2008.

12. Tansu Filik, T. Engin Tuncer, T. K. Yasar *Design of V-shaped Array Geometry*, Signal Processing and Communication Applications, 2007. SIU 2007, pp. 1–4, April 2007.

13. T. K. Yasar, T. Engin Tuncer, Tansu Filik *Direction of Arrival Estimation in Non-Uniform Linear Arrays for Wide Band Signals*, Signal Processing and Communication Applications, 2007. SIU 2007, pp. 1–4, April 2007.